



CRISPR-BASED SCREENING & FUNCTIONAL CHARACTERIZATION OF LONG NON-CODING RNAs IN MELANOMA

Dissertation

Zur Erlangung des akademischen Grades eines

Doktors der Naturwissenschaften

(Dr. rer. nat.)

der Fakultät Chemie und Chemische Biologie

der Technischen Universität Dortmund

Vorgelegt von Stavroula Petroulia, M. Sc.

Geboren am 31.12.1978 in Athen

Matrikelnummer 223795

Dortmund, 2024

The work presented in this thesis was performed under the supervision of Dr. Jochen Imig and the formal supervision of Prof. Dr. Dr. h.c. Herbert Waldmann, from August 2019 until August 2022, at the Chemical Genomics Centre of the Max Planck Society, the Max Planck Institute of Molecular Physiology, and the Faculty of Chemistry and Chemical Biology at TU Dortmund University in Dortmund.

Erstgutachter: Prof. Dr. Dr. h.c. Herbert Waldmann

Zweitgutachter: Prof. Dr. Carsten Watzl

Betreuer: Dr. Jochen Imig

For my Mother, my Sister and in loving memory of my Father

1. Acknowledgements

My academic journey has been far from conventional, with many achievements coming later than expected. Nevertheless, the paramount importance lies in successfully reaching these milestones. Among these achievements was the pursuit of a PhD, and I owe immense gratitude to my mentor, Dr. Jochen Imig, for believing in me and allowing me to fulfill my dream. Under his continuous guidance, I was fortunate to engage in diverse research projects that deeply captured my interest and heightened my appreciation for basic research. Moreover, I was given the opportunity to reside in a foreign country, engage in an interdisciplinary environment, and collaborate with charismatic people, even amidst the challenges posed by a global pandemic. Undoubtedly, this experience has greatly influenced my personal and professional growth, fostering my development as both a person and a scientist.

I wish to express my appreciation to Professor Herbert Waldmann for his profound influence on my academic path and for his pivotal contribution to the establishment of the Chemical Genomics Centre, which has played a crucial role in shaping my PhD experience. Additionally, I am honoured to have had him as my primary examiner and for his insightful perspective and evaluation of my dissertation.

I would like to express my profound gratitude to Professor Carsten Watzl for accepting my request to be my second examiner for my doctoral defense. I highly value his expertise and knowledge to evaluate my research.

This expression of thankfulness is dedicated to the members of the MPI Institute and TU Dortmund University, whose invaluable support and guidance over the course of three years enabled me to successfully conduct numerous experiments. I express my thankfulness to Professor Philippe Bastiaens, whose gracious permission allowed me to benefit from the expertise of his scientific team and utilize the resources within Department II. I must also extend my deepest appreciation to Dr. Sven A. H. Müller, whose expertise in microscopy enabled me to confidently operate the wide-field fluorescence microscope, offering invaluable assistance and guidance whenever required. The completion of countless experiments would have been impossible without his support. I would also like to thank Dr. Christian Schröter and his doctoral student Max Fernkorn for our scientific discussions, and their generosity to share valuable protocols and reagents. Last but not least, from Department II, I would like to thank Dr. Michael Schulz for his patience, guidance in many flow cytometry experiments required in my research and for his kindness in providing his support even in short notice.

I am thankful to Dr. Daniel Prumbaum from Department III for granting me access to utilize their S2 lab for conducting a multitude of experiments. His unfailing assistance whenever I faced challenges, was greatly appreciated. Additionally, I extend my appreciation to Nathalie Bleimling, for her support and kind assistance each time I visited her lab. I would like to acknowledge Dr. Matias Hernandez for allowing me to utilize the flow cytometer in his laboratory. Furthermore, I am grateful to Dr. Angela Hagemeyer and Dr.

Anson Shek for their constant support, valuable guidance, and warm reception, which created a welcoming environment for me.

I would like to extend my appreciation to Professor Daniel Summerer for allowing me to utilize the flow cytometer in his laboratory. Additionally, I am deeply appreciative of Dr. Tzu-Chen Lin's unwavering kindness, generosity, and support, as she always came to my rescue whenever I needed to conduct a flow cytometry experiment.

I would like to thank Dr. Malte Gersch and Dr. Peng Wu, with whom I had the privilege of collaborating. I am appreciative of the opportunity to work with them, and hope that my efforts have met their expectations and made a meaningful contribution to their research.

I would like to convey my sincere appreciation to Christa Hornemann, our Administrative Coordinator, for the tremendous guidance she has offered, even in the absence of my association with the IMPRS program. I would like to thank Debora Bruzzese, our CGC Coordinator, for her remarkable skills in organization and support, even across the vast distance of the Atlantic Ocean.

I would like to thank the CGC funding companies and in particular *Pfizer* for their generous support. Their contribution has been instrumental in advancing our research.

I would like to express my gratitude to Dr. Sama Shamloo for generously providing her expertise, guidance and valuable training, which allowed me to achieve independence within a short timeframe. I want to express my thankfulness to Dr. Alejandro Ulloa-Morales for all his guidance. He had a unique ability to make you feel his unwavering support, even when it went unspoken.

I wish to express my deep appreciation to Kim Fischer, Lin Qiu, Shashank Tiwari, Katja Schamrin, Sanat Mishra, Rajeha Perinbarajah and Boris Simeonov for their irreplaceable presence and meaningful contributions throughout my three-year tenure in the Imig lab. The moments we shared, the conversations, and the laughter we enjoyed together added immense joy to my daily life, leaving an indelible mark that I will forever treasure.

I would like to thank Stefan Schmeing, Joseph Openy, Lydia Borgelt, Kai Gallant, Rachel O'Dea, Ilja Gordijenko, Daniel Esposito, Pascal Hommen, Niko Klink, Kim Wendrich, Oguz Hastürk, Fubao Huang, Yang Liu and Mao Jiang. You all had an impact on my life and thank you for all the moments we shared.

At last, I would like to thank my family, my mother, my sister and my stepfather.

Especially my mother; *Everything has happened because of You.*

Table of Contents

1. Acknowledgements	1
2. Abstract	6
3. Introduction	12
3.1 Melanoma	12
3.1.1 Epidemiology	12
3.1.2 Risk Factors to Melanoma Development	13
3.1.3 Melanoma Tumour Formation and Progression	14
3.1.4 Overview of Melanoma Therapy Treatments	16
3.1.4.1 Surgical Treatment	16
3.1.4.2 Immuno-based Melanoma Therapeutical Approaches	16
3.1.4.3 Molecular Targeted Melanoma Therapeutical Approaches	18
3.2 Long non-coding RNAs (lncRNAs)	19
3.2.1 Introduction to long non-coding RNAs	19
3.2.2 Structural Classification	19
3.2.3 Functional Characterization	21
3.2.3.1 lncRNAs as Key Players in cis-Regulatory Mechanisms	22
3.2.3.2 Trans-Regulatory Mechanisms Mediated by lncRNAs	23
3.2.4 Significance of lncRNAs in Oncogenesis and Tumour Progression	24
3.2.5 Functional Interplay of lncRNAs in Melanoma	25
3.3 Modulation of lncRNA Expression for Functional and Therapeutical Studies	29
3.4 Perturbation of lncRNA Expression utilizing CRISPR-based Technology	29
3.4.1 Introduction to CRISPR-Cas9 System	29
3.4.2 Engineered CRISPR Methods for Transcriptional Regulation of lncRNA Expression	30
3.4.3 Introduction to CRISPR Screens	31
3.4.4 Design and Analysis of pooled CRISPR Screens	32
4. Study Objectives	34
5. Materials and Methods	35
5.1 Materials	35
5.1.1 Chemicals and Reagents	35
5.1.2 Buffers and Solutions	37
5.1.3 Antibodies	37
5.1.4 Enzymes	38
5.1.5 Kits	38
5.1.6 Bacterial Strains	38
5.1.7 Cell Lines	39
5.1.8 Plasmids	39

5.1.9 Oligonucleotides.....	39
5.1.10 Primers	40
5.1.11 NGS Primers lncRNA KRAB Library	42
5.1.12 Consumables.....	43
5.1.13 Lab Equipment	44
5.1.14 Software	45
5.2 Methods	46
5.2.1 sgRNA Cloning	46
5.2.1.1 Vector Preparation	46
5.2.1.2 Oligonucleotide sgRNA Design and Preparation	46
5.2.1.3 Ligation and Chemical Transformation	47
5.2.2 Transformation of Chemical Competent Stb13 <i>Escherichia coli</i> Cells	47
5.2.3 Plasmid DNA Purification.....	47
5.2.4 Cell Culture Methods.....	48
5.2.4.1 Cultivation of Mammalian Cells.....	48
5.2.4.2 Production of Conditioned Medium - TU 2 %.....	49
5.2.4.3 Subculturing and Seeding of Mammalian Cells	49
5.2.4.4 Cryopreservation of Mammalian Cells	50
5.2.4.5 Lentivirus Production	50
5.2.4.6 Lentivirus Transduction	50
5.2.4.7 Apoptosis Assay by Immunoblotting	51
5.2.4.8 Cell Cycle Analysis by Flow Cytometry	52
5.2.4.9.1 Transwell Invasion Assay	53
5.2.4.9.2 Quantification of Invading Cells.....	54
5.2.4.10 RNA-Fluorescence <i>in situ</i> Hybridization [FISH]	55
5.2.4.11 Lentivirus Titration by Flow Cytometry.....	56
5.2.4.12 CRISPRi Proliferation lncRNA Screen.....	57
5.2.4.13 Preparation of CRISPRi sgRNA Library for Next Generation Sequencing Analysis	58
5.2.4.14 Transcriptome profiling of XLOC030781 Knock-Down.....	60
5.2.4.15 Preparation of RNA Samples for Next Generation Sequencing Analysis.....	61
5.2.5 RNA Isolation using TRIzol Reagent.....	63
5.2.6 Reverse Transcription-Quantitative PCR (RT-qPCR).....	63
5.2.7 Agarose Gel Electrophoresis	64
5.2.8 Immunoblotting	64
5.2.8.1 Cell Lysate Preparation.....	64
5.2.8.2 Protein Concentration Quantification (DC Protein Assay)	65

5.2.8.3 SDS-PAGE Electrophoresis	65
5.2.8.4 Blotting	65
5.2.9 Bioinformatic Analysis	66
6. Results.....	67
6.1 Preliminary Experimental Research.....	67
6.2 CRISPRi Proliferation Screen 2.0.....	71
6.2.1 Design and Evaluation of sgRNA Positive Controls.....	71
6.2.2 Preparation for CRISPRi Proliferation Screen 2.0.....	72
6.2.3 Conduction of CRISPRi Proliferation Screen 2.0	77
6.3 Functional Characterization of Top Depleted lncRNA Candidates	82
6.3.1 Investigation of Apoptosis Induction in a CRISPRi Environment.....	82
6.3.2 Role of lncRNA Candidates in Cell Cycle Regulation.....	85
6.3.3 Exploring the Invasive Aptitude of Top lncRNA Candidates	88
6.3.4 Subcellular Localization utilizing Fluorescence <i>in situ</i> Hybridization	94
6.3.5 Transcriptome Profiling of <i>XLOC030781</i> Knock-Down	98
7. Discussion – Conclusions	102
7.1 Evaluation of CRISPRi Proliferation Screen 2.0	102
7.2 Evaluation of Functional Characterization Studies on <i>BDNF-AS</i> , <i>GMDS-AS1</i> and <i>XLOC030781</i>	106
8. Supplementary Figures.....	110
9. Bibliography.....	113

2. Abstract

Melanoma manifests as the primary cause of skin cancer-induced fatalities, with a prominent inclination towards metastasis and a substantial upsurge in prevalence within Western populations. This form of cutaneous cancer is distinguished by the accumulation of multiple somatic mutations resulting from UV-induced mutagenesis, with an elevated base mutation rate that surpasses that of nearly all other solid tumours. The advancement of melanoma is represented by the unregulated proliferation and dissemination of malignant melanocytes. The identification of disruptions within the MAPK-ERK and PI3K-AKT-mTOR pathways during the onset of melanoma has contributed to the discovery of advanced therapeutic modalities. However, the pronounced capacity of melanoma tumours to generate drug resistance and propagate through metastasis remains a daunting challenge for the scientific community.

The well-known, yet elusive, dark matter of the genome, previously dismissed as "junk DNA", has recently emerged as a focal point for its confirmed regulatory capabilities independent of protein coding. Notably, the extensive class of long non-coding RNAs, typically longer than 200 nucleotides, is widely regarded as playing a critical role in cellular development, differentiation, and the progression of cancer. Numerous scientific studies have consistently demonstrated the association between lncRNAs and the growth and advancement of melanoma. An elevation in lncRNA expression levels has been repeatedly detected in cutaneous melanoma, underscoring their potential contribution to the disease's pathogenesis through a range of molecular pathways and interactions with various molecular targets. The functional aspects of lncRNAs have been unraveled through the utilization of CRISPRi methodology, which involves the suppression of their expression and subsequent observation of the resulting phenotype.

Herein, this study attempted to elucidate the involvement of a specific set of lncRNAs in mechanisms underlying cell growth and proliferation. These lncRNAs, which had been observed to exhibit increased expression in melanoma cell lines and in short-term cultures derived from brain and lymph node metastasis, are examined by employing CRISPRi screening. Furthermore, functional characterization analyses were conducted on the most promising lncRNA candidates, including *BDNF-AS*, *GMDS-AS1*, and a novel, non-annotated lncRNA named *XLOC030781* based on preliminary data that validate their importance in melanoma. Our CRISPRi screening results were in complete agreement with the preliminary data and reflected their statistical significance. Furthermore, we successfully demonstrated that the aforementioned lncRNAs, when suppressed, initiated apoptotic mechanisms and inhibited cell cycle processes. *XLOC030781* exhibited a remarkable role in melanoma migration, broadening its functional scope in relation to this malignancy. Finally, the implementation of fluorescence *in situ* hybridization technique provided data on their subcellular localization, offering complementary information on their functionality.

Melanom manifestiert sich als primäre Ursache für durch Hautkrebs verursachte Todesfälle, mit einer deutlichen Neigung zur Metastasierung und einem erheblichen Anstieg der Prävalenz innerhalb westlicher Populationen. Diese Form von Hautkrebs zeichnet sich durch die Ansammlung mehrerer somatischer Mutationen aus, die durch UV-induzierte Mutagenese verursacht werden und eine erhöhte Basenmutationsrate aufweisen, die die fast aller anderen soliden Tumoren übertrifft. Die Entwicklung von Melanomen wird durch die unkontrollierte Proliferation und Ausbreitung von bösartigen Melanozyten gekennzeichnet. Die Identifizierung von Störungen in den MAPK-ERK und PI3K-AKT-mTOR Signalwegen während des Beginns von Melanomen hat zur Entdeckung von fortgeschrittenen therapeutischen Möglichkeiten beigetragen. Die ausgeprägte Fähigkeit von Melanom Tumoren, Resistenz gegen Medikamente zu entwickeln und durch Metastasen zu propagieren, bleibt jedoch eine beunruhigende Herausforderung für die wissenschaftliche Gemeinschaft.

Die bekannte, aber schwer fassbare Dunkle Materie des Genoms, früher als "Junk-DNA" abgetan, ist in jüngerer Zeit aufgrund ihrer bestätigten regulatorischen Fähigkeiten unabhängig von der Protein-Codierung in den Mittelpunkt gerückt. Insbesondere die umfangreiche Klasse der langen nicht-kodierenden RNAs, die in der Regel länger als 200 Nukleotide sind, wird weithin als entscheidende Rolle bei der Zellentwicklung, Differenzierung und Fortschreiten von Krebs angesehen. Zahlreiche wissenschaftliche Studien haben die Assoziation zwischen lncRNAs und der Entwicklung und dem Wachstum von Melanomen konsequent nachgewiesen. Eine Erhöhung der lncRNA-Expressionsniveaus wurde wiederholt bei kutanem Melanom nachgewiesen, was ihr potenzieller Beitrag zur Pathogenese der Krankheit durch eine Reihe von molekularen Wegen und Wechselwirkungen mit verschiedenen molekularen Zielen unterstreicht. Die funktionellen Aspekte von lncRNAs wurden durch die Verwendung der CRISPRi-Methode entschlüsselt, die die Unterdrückung ihrer Expression und die anschließende Beobachtung des resultierenden Phänotyps beinhaltet.

Hierin versuchte diese Studie, die Beteiligung einer spezifischen Gruppe von lncRNAs an dem Mechanismus des Zellwachstums und der Zellproliferation zu erläutern. Diese lncRNAs, bei denen eine erhöhte Expression in Melanom Zelllinien und in aus Hirn- und Lymphknotenmetastasen abgeleiteten Kurzzeitkulturen festgestellt wurde, wurden durch den Einsatz von CRISPRi-Screening untersucht. Darüber hinaus wurden funktionelle Charakterisierungsanalysen an den vielversprechendsten lncRNA-Kandidaten, einschließlich *BDNF-AS*, *GMDS-AS1* und einer neuartigen, nicht-annotierten lncRNA namens *XLOC030781*, auf der Grundlage von vorläufigen Daten durchgeführt, die ihre Bedeutung bei Melanomen bestätigen. Unsere CRISPRi-Screening-Ergebnisse waren in voller Übereinstimmung mit den vorläufigen Daten und spiegelten ihre statistische Signifikanz wider. Darüber hinaus konnten wir erfolgreich nachweisen, dass die oben genannten lncRNAs, wenn sie unterdrückt werden, apoptotische Mechanismen in Gang setzen und Zellzyklusprozesse hemmen. *XLOC030781* zeigte eine bemerkenswerte Rolle bei der Wanderung von Melanomen, was seinen funktionellen Bereich in Bezug auf diese Krebserkrankung erweitert. Schließlich lieferte die Implementierung der in-situ-Fluoreszenz-Hybridisierungstechnik Daten zu ihrer subzellulären Lokalisierung und bot ergänzende Informationen zu ihrer Funktionalität.

Abbreviations

Abbreviation	Analytical Term
7-AAD	7-Aminoactinomycin D
aa	Amino Acid
AF-546	Alexa Fluor 546
AF-647	Alexa Fluor 647
Airn	Antisense IGFR2 RNA non-coding
ANRIL	Antisense non-coding RNA at the INK4 locus
APEX1	Apurinic/Apyrimidinic Endodeoxyribonuclease 1
ASO	Antisense Single-Stranded Oligonucleotide
BANCR	BRAF-activated non-coding RNA
BBB	Blood-Brain Barrier
BDNF-AS	Brain-Derived Neurotrophic Factor Antisense Strand RNA
BM	Brain Metastasis
BRAF	V-Raf Murine Sarcoma Viral Oncogene Homolog B
BSA	Bovine Serum Albumin
CASC15	Cancer Susceptibility Candidate 15
CBX7	Chromobox Homolog 7
CDK4	Cyclin Dependent Kinase 4
CDKN1B	Cyclin Dependent Kinase Inhibitor 1B
CDKN2A	Cyclin Dependent Kinase Inhibitor 2A
ChIP-Seq	Chromatin Immunoprecipitation Sequencing
circRNA	Circular Intronic RNA
c-KIT	KIT Proto-Oncogene, Receptor Tyrosine Kinase
c-Met	MET Proto-Oncogene, Receptor Tyrosine Kinase
CNA	Copy Number Amplification
CPM	Counts per Million
CRISPR	Clustered Regularly Interspaced Short Palindromic Repeats
CRISPRa	CRISPR Transcriptional Activation
CRISPRi	CRISPR Interference
CRISPR-KO	CRISPR Knock-Out
crRNA	CRISPR RNA
CTLA-4	Cytotoxic T-Lymphocyte Antigen-4
CXCL11	C-X-C Motif Chemokine Ligand 11
DAG	Diacylglycerol
dCas9	Catalytically dead Cas9
DGE	Differential Gene Expression
DMEM	Gibco Dulbecco's Modified Eagle's Medium
DPBS	Dulbecco's Phosphate Buffered Saline
DSB	Double Strand Break
dsRNA	Double Stranded RNA
DTT	Dithiothreitol
E2F3	E2 Transcription Factor 3
EdU	5-ethynyl-2'-deoxyuridine
EMT	Epithelial to Mesenchymal Transition
eRNA	enhancer RNA
EZH2	Enhancer of Zeste Homolog
FAMMM	Familial Atypical Multiple Mole Melanoma
FBS	Fetal Bovine Serum
FBXW7	F-Box And WD Repeat Domain Containing 7, E3 Ubiquitin Protein Ligase
FC	Fold Change
FDA	Food and Drug Administration
FDR	False Discovery Rate
FER1L4	Fer-1 Like Family Member 4
FOXM1	Forkhead Box M1

Abbreviation	Analytical Term
FWD	Forward
GAPDH	Glyceraldehyde 3-phosphate Dehydrogenase
GAS5	Growth Arrest Specific Transcript 5
GFP	Green Fluorescent Protein
GLOBOCAN	Global Cancer Observatory
GLUT	Glucose Transporter
GMDS-AS1	GDP-mannose 4,6-dehydratase Antisense 1
GSEA	Gene Set Enrichment Analysis
H3K27ac	Acetylated Lysine 27 of Histone H3
H3K27me3	Trimethylated Lysine 27 of Histone H3
H3K4me3	Trimethylated Lysine 4 of Histone H3
HCC	Hepatocellular Carcinoma
HDAC8	Histone Deacetylase 8
HOTAIR	HOX Transcript Antisense Intergenic RNA
HOXB3	Homeobox B3
HOXC11	Homeobox C11
HOXC12	Homeobox C12
HOXD	Homeobox D Cluster
HSF1	Heat Shock Factor 1
ICB	Immune Checkpoint Blockade
ICI	Immune Checkpoint Inhibitor
IFN-alpha-2b	Interferon-alpha-2b
IGFR2	Insulin like Growth Factor 2 Receptor
IL-2	Interleukin-2
ITGB1	Integrin Subunit Beta 1
KRAB	Kruppel-associated Box
LDHA	Lactate Dehydrogenase A
lincRNA	Long Intergenic non-coding RNA
lincRNA-EPS	Long Intergenic non-coding RNA-Erythroid Prosurvival
LINK-A	Long Intergenic non-coding RNA for Kinase Activation
LN	Lymph Node
lncRNA	Long non-coding RNA
Lockd	LncRNA Downstream of CDKN1B
LPA	Lysophosphatidic Acid
m7G	7-methyl Guanosine
MALAT1	Metastasis-associated Lung Adenocarcinoma Transcript 1
MAPK	Mitogen-activated Protein Kinase
MC1R	Melanocortin-1 Receptor
MEG3	Maternally Expressed Genes 3
MITF	Microphthalmia-associated Transcription Factor
MMP	Matrix Metalloproteinase
MMP2	Matrix Metalloproteinase 2
MMP9	Matrix Metalloproteinase 9
MMP14	Matrix Metalloproteinase 14
MOI	Multiplicity of Infection
mRNA	Messenger RNA
mTOR	Mechanistic Target of Rapamycin
MEN	Multiple Endocrine Neoplasia
NATs	Natural Antisense Transcripts
ncRNA	Non-coding RNA
NEAT1	Nuclear Enriched Abundant Transcript 1
NEXT	Nuclear Exosome Targeting Complex
NGS	Next Generation Sequencing
NHEJ	Non-homologous End Joining
NONO	Non-POU Domain-Containing Octamer-Binding Protein

Abbreviation	Analytical Term
NORAD	Non-coding RNA Activated by DNA Damage
Notch2	Neurogenic Locus Notch Homolog Protein 2
NRAS	Neuroblastoma RAS Viral Oncogene Homolog
ORF	Open Reading Frame
p14ARF	Tumour Suppressor Gene Encoded by the CDKN2A Locus
p15INK4b	Cyclin-dependent Kinase 4 Inhibitor B
p16INK4a	Tumour Suppressor Gene Encoded by the CDKN2A Locus
p32	Tumour Suppressor Protein 32
p53	Tumour Suppressor Protein 53
PA	Phosphatidic Acid
PAM	Protospacer Adjacent Motif
PARP1	Poly [ADP-ribose] Polymerase 1
PBS	Phosphate Buffered Saline
PCR	Polymerase Chain Reaction
PCR1	Polycomb Repressive Complex 1
PCR2	Polycomb Repressive Complex 2
PD-1	Programmed Cell Death-1
PDCD4	Programmed Cell Death 4
PEG	Polyethylene Glycol
PI3K	Phosphoinositid-3-Kinase
Pol II	Polymerase II
polyA	Polyadenylation
PPIB	Peptidylprolyl Isomerase B
PROMPTs	Promoter Upstream Transcripts
PSF	Polypyrimidine Tract Binding Protein-associated Splicing Factor
PSPC1	Paraspeckle Component 1
PTB	Polypyrimidine tract Binding Protein
PTEN	Phosphatase and Tensin Homolog
PUM1	Pumilio RNA Binding Family Member 1
PUM2	Pumilio RNA Binding Family Member 2
PVDF	Polyvinylidene Difluoride
PVT1	Human Plasmacytoma Variant Translocation 1
Rab23	Ras-related GTP Binding Protein 23
RAP	RNA Antisense Purification
RBP	RNA Binding Protein
REV	Reverse
RISC	RNA-induced Silencing Complex
RNAi	RNA Interference
RNase P	Ribonuclease P
RNA-Seq	RNA Sequencing
RT	Reverse Transcription
SAM	Synergistic Activation Mediator System
SAMMSON	Survival-associated Mitochondrial Melanoma Specific Oncogenic non-coding RNA
SDS-PAGE	Sodium Dodecyl Sulfate Polyacrylamide Gel Electrophoresis
SEER	Surveillance, Epidemiology, and End Results Program
SEM	Standard Error of Mean
SFPQ	Splicing Factor Proline And Glutamine Rich
sgRNA	Single Guide RNA
siRNA	Single Stranded Small Interfering RNA
SNAIL	Snail Family Transcriptional Repressor 1
snoRNA	Small Nucleolar RNA
SOC	Super Optimal Broth
SPRY4	Sprouty4
SPRY4-IT1	SPRY4 Intronic Transcript 1
SSC	Saline Sodium Citrate

Abbreviation	Analytical Term
STC	Short Term Culture
Suz12	SUZ12 Polycomb Repressive Complex 2 Subunit
TBS	Tris Buffered Saline
TCGA	The Cancer Genome Atlas
TEMED	Tetramethylethylenediamine
TERT	Telomerase Reverse Transcriptase
Tet	Tetracycline
tracrRNA	Trans-activating crRNA
Tris	Tris(hydroxymethyl)aminomethane
TSG	Tumour Suppressor Gene
TSS	Transcription Start Site
TYR	Tyrosinase
TYRP1	Tyrosinase-related Protein 1
UCA1	Urothelial Carcinoma Associated 1
UV	Ultra Violet
Xist	X-inactive Specific Transcript
YB1	YBox-binding Protein 1
YUSAC	Melanoma Cell Line CVCL_A746

3. Introduction

3.1 Melanoma

3.1.1 Epidemiology

Cutaneous malignant melanoma is the most aggressive and potentially lethal skin cancer. In the 20th century, cutaneous melanoma was considered infrequent; the prospect of developing the disease in a person's lifetime was one in 500. However, in Western populations, this has altered considerably, with the probability being one in 50 now¹⁻³. Melanoma accounts for 1.7 % of all cancer diagnoses worldwide, with 325,000 reported cases in 2020 as specified by GLOBOCAN (Global Cancer Observatory) data. While the incidence of many types of malignancy has been declining, melanoma incidence steadily increases. The incidence rates vary greatly by country; with the highest rates being observed in Australia (36.6 per 100,000 person-years) and New Zealand (31.6 per 100,000 person-years). In Europe, the Scandinavian countries, The Netherlands, and Switzerland are ranked as the top countries with the highest incidence of melanoma. Similarly, fair-skinned populations in North America are also predominantly affected by melanoma. Race plays a significant role in the occurrence of melanoma, with populations of European ancestry having a risk approximately 10 times higher compared to Black, Asian, or Hispanic populations. Numerous studies have established a correlation between melanoma occurrence, sex, and age⁴⁻⁶. Interestingly, the most common sites for melanoma lesions differ between genders, with men more likely to develop melanoma on the upper back and women on the arms and legs. Melanoma is more prevalent among older populations, but it remains the third most common cancer among individuals aged 15-39^{3,7}.

In 2020 around 57,000 people died of melanoma; the age-standardized mortality was 0.7/100,000 for men and 0.4/100,000 for women worldwide, according to GLOBOCAN. Despite being broadly avertible, the elevated mortality rates reflect its high metastatic potential, making it untreatable. The most recent 5-year survival rate (2011-2017) according to SEER (Surveillance, Epidemiology, and End Results Program) is 93.3 % for melanoma, up from 81.9 % in 1975, the earliest recorded. The survival rate significantly decreases as melanoma progresses. Various factors affect the prognosis and thus the life expectancy. Foremost, early diagnosis, age and overall health contribute highly. Inversely, the mutation burden impacts the disease's development and response to clinical treatments⁶.

3.1.2 Risk Factors to Melanoma Development

The transformation of cutaneous melanocytes, the melanin pigment producing skin cells into melanoma is a greatly perplexing process, that emerges from the reciprocity between a wide variety of genetic deviations and specific patterns of environmental exposure. Therefore, hereby it is attempted a more condensed overview, highlighting the most important risk elements. In respect to environmental mediators, the influence of natural ultraviolet (UV) radiation has been extensively inspected, not only because it is regarded as the predominant contributor to cutaneous melanoma development, but also due to the convoluted mechanisms involved. Sunlight exposure is divided into three classes based on human behavioral patterns: intermittent, chronic, and total. Intermittent exposure describes sporadic but intense sun exposure (i.e., outdoor sports, vacations), chronic exposure refers to continuous occupational exposure; and finally, total exposure is a combination of all sun exposure types. Interestingly enough, extensive meta-analyses of published epidemiological studies on malignant melanoma, show that intermittent exposure is overall the most carcinogenic. A possible explanation is that melanocytes are more susceptible due to irregular exposure intervals, the epidermis is less thick and less pigmented, and thus DNA damage is highly probable to occur^{1,2,7,8}. Artificial UV exposure is also evaluated, since the UVA radiation emitted during an indoor tanning session has been asserted to be up to three times than the UVA in natural light⁹.

Melanocytic or dysplastic nevi, both classified as benign melanocytic tumours, have an immediate association with melanoma incidence. 25 % of melanoma cases are histologically linked to a pre-existing nevus¹⁰. Their clinical significance is directly proportional to their number. Individuals with >100 nevi have a 7-fold increased risk of developing invasive melanoma in comparison to those with <15⁸.

A small fraction of 10 % of malignant tumours have a distinct hereditary background. High-penetrance germline mutations at chromosome 9 and 12 are detected in the patients' genetic expression profiling. These mutations are missense or silent and affect *CDKN2A* (Cyclin-Dependent Kinase Inhibitor 2A) or *CDK4* (Cyclin-Dependent Kinase 4) genes respectively, that are involved in cell cycle regulation and are associated with familial atypical multiple mole-melanoma (FAMMM) syndrome and its variant, melanoma-astrocytoma syndrome^{3,11}. Moreover, there is supporting evidence that aberrations in DNA-repair-related genes and pigmentation-related genes increase the risk of hereditary melanoma. The former gene group includes defects of tumour suppressor genes *TP53* (Tumour Suppressor Protein p53 Gene), *TERT* (Telomerase Reverse Transcriptase) and *APEX1* (Apurinic/Apyrimidinic Endodeoxyribonuclease 1) and whereas the latter encompasses alterations of the gene pairs *MITF* (Microphthalmia-associated Transcription Factor), *MC1R* (Melanocortin-1 Receptor) and *TYR* (Tyrosinase), *TYRP1* (TYROSINASE-related Protein 1)¹²⁻¹⁵.

Data acquired from The Cancer Genome Atlas (TCGA) project, illustrate that cutaneous melanoma isn't the consequence of a single genetic event but rather the accumulation of multiple somatic mutations due to

UV mutagenesis¹⁶. It is characterized by the highest median number of mutations amongst 22 cancer types and also exhibits inflated base mutation rates compared to almost all solid tumours^{17,18}.

Mutations in the *BRAF* (V-Raf Murine Sarcoma Viral Oncogene Homolog B) and *NRAS* (Neuroblastoma RAS Viral Oncogene Homolog) oncogenes, which induce constitutive signaling of the mitogen-activated protein kinase (MAPK) pathway, are quite prevalent. Notably, mutations in either *BRAF* or *NRAS* genes appear in a mutually exclusive manner^{19,20}. In contrast, 44 % of melanomas with *BRAF* mutations also possess a *PTEN* (Phosphatase and Tensin Homolog) mutation. Melanoma tumours with loss of *PTEN* generally demonstrate elevated levels of activation of the PI3K-AKT-mTOR pathway. Regarding *BRAF*, ~60 % of patients carry the gain-of-function mutation *BRAF*^{V600E}, where there is a substitution from valine to glutamic acid at amino acid (aa) 600. Less frequently, other activating mutations such as *BRAF*^{V600K} and *BRAF*^{V600R} are observed^{21,22}. *c-KIT* (*KIT* Proto-Oncogene, Receptor Tyrosine Kinase) mutations appear at lower frequency in comparison to *BRAF* and *NRAS* mutations. Quite interestingly, *c-KIT* mutations in a similar manner, seldom occur in conjunction with *BRAF* and *NRAS* mutations, depicting an epistatic interaction. *c-KIT* is a type III transmembrane receptor tyrosine kinase, encoded by a proto-oncogene on chromosome 4 and is highly involved in melanocyte development²³⁻²⁷. Almost all mutations in the *c-KIT* gene, found in melanoma, are missense substitutions that alter the structure of the juxtamembrane domain of the protein, resulting in continuous activation of the receptor, regardless of the presence and/or binding of a ligand^{25,28}. The constitutive activation of MAPK-ERK and PI3K-AKT-mTOR pathways during melanoma occurrence originating from such somatic mutations, allows the upregulation of cell proliferation and anti-apoptotic mechanisms, crucial for the survival and expansion of tumour cells.

3.1.3 Melanoma Tumour Formation and Progression

An extensive comprehension of the underlying mechanisms of melanoma tumorigenesis is imperative for the development of innovative diagnostic protocols and therapeutic approaches. Melanoma progression represents a prolonged and multilateral phenomenon characterized by the uncontrolled proliferation and dissemination of malignant melanocytes. Normal melanocytes are highly differentiated cells of neural crest origin, generally located in the skin epidermal basal layer that produce a pigment called melanin in melanosomes²⁹.

The Clark model describes analytically in a consecutive order, the histological alterations that melanocytes acquire until they present metastatic potency. The first step includes the formation of benign nevi; these benign precursor lesions result as non-malignant accumulations of melanocytes or nevus cells and appear to be flat or slightly elevated. Their aberrant proliferation is constrained by oncogene-induced cell senescence^{30,31}. During the next step, uncontrolled cell growth is established within the pre-existing benign nevus or in a new area, and is identified by the presence of distinctive architectural and cytological

characteristics such as asymmetry, abnormal borders, and heterogenous pigmentation. These formations are termed dysplastic or atypical nevi. In the third step of Clark’s model, cells enter the radial-growth phase, where they proliferate within the epidermis, a few might also spread in the papillary dermis (microinvasive melanoma), and display continuous atypia. The fourth step is critical for melanoma metastasis; the lesions that continue to vertical-growth phase have the ability to trespass the epidermal basement membrane and proliferate vertically in the dermis, where they create tumour nodules. During the final step, cells disassociate from the primary tumour, travel through the lymph or blood circulation, to distant locations such as the brain, lungs, and lymph nodes where they proliferate and establish their metastatic potential (Figure 1)^{31–34}.

It is apparent that in Clark’s model the formation of the primary tumour and metastasis manifestation have been described as a multistep yet linear process. Acquisition of scientific data over the last decades provide additional evidence that melanoma progression isn’t as simple as depicted, non-linearity in the process is also probable such that different steps can be bypassed. Inevitably, these discrepancies increase the tumour aggressiveness and decrease the duration of establishment of malignancy³⁵.

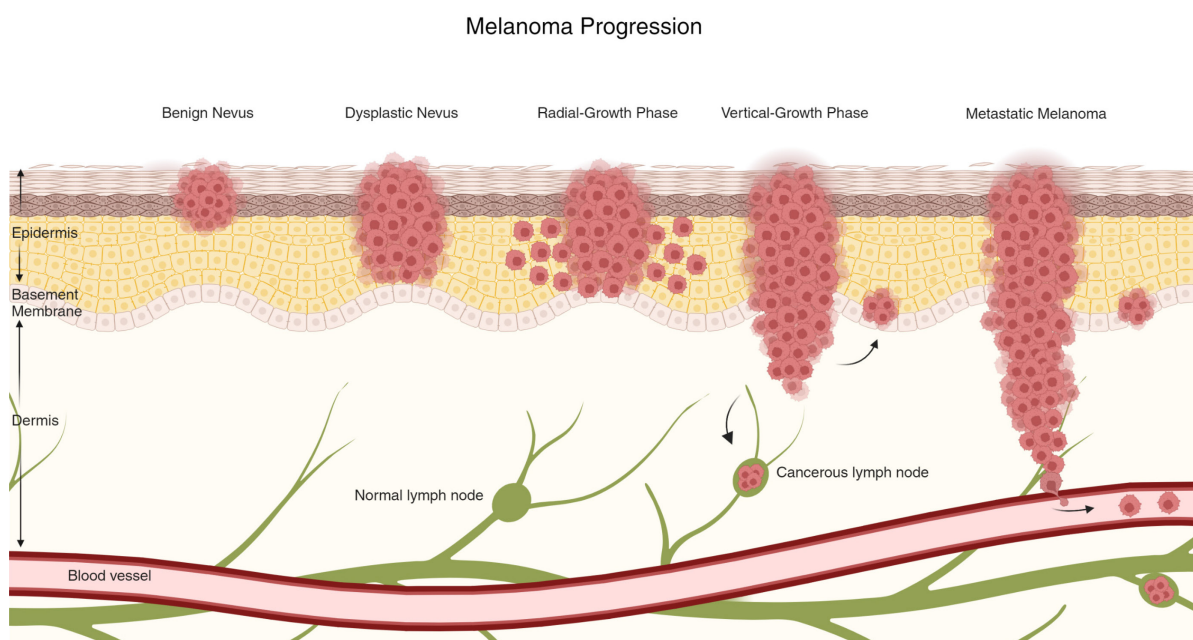


Figure 1. Schematic overview of the Clark model. The histopathological alterations that occur in melanocytes during the multifaceted linear progression towards malignancy are illustrated. Generated from “Melanoma Staging”, by BioRender.com (2023). Retrieved from <https://app.biorender.com/biorender-templates>

3.1.4 Overview of Melanoma Therapy Treatments

Owing to its strong invasive nature, high genetic heterogeneity and steadily increasing incidence rates, malignant melanoma has been a significant challenge to battle in public health care. In recent years, however, substantial advancements have been made in treatment approaches to improve living standards and increase survival expectancy. For Stage 0-II or alternatively early diagnosed melanoma cases, a precise and complete surgical excision of the localized tumour is the first-line treatment. This treatment strategy is sufficient in 90 % of cases, and no adjuvant therapy is required given a favorable prognosis. For advanced neoplasms of late-stage II-IV, a surgical operation is advised where allowed, and is supported by radiation therapy, chemotherapy but also newly developed immunotherapies and mutation-specific targeted therapies^{36,37}.

3.1.4.1 Surgical Treatment

Surgical intervention is critical in the effective treatment of melanoma. The primary aim of surgery is to completely eradicate the tumour, ensuring that both the primary lesion and any associated proximate or distant metastatic regions are fully excised³⁸. The extent of surgical removal differs depending on factors such as tumour thickness, presence of ulceration, mitotic rate, and depth of invasion³⁹. Consequently, treatment guidelines recommend wide local excision within a margin of healthy tissue, typically ranging from 1 to 2 cm for primary melanomas to reduce the possibility of cancer recurrence⁴⁰. If lymph node involvement is suspected, a biopsy of the lymph nodes is performed to assess the presence of metastasis. The least invasive approach to determine the spreading to adjacent lymph nodes is called sentinel lymph node biopsy. This established method requires the administration of a dye or a radioactive solution in close proximity to the tumour, facilitating the identification of the sentinel lymph node, which serves as the primary site for potential cancer cell migration. In the absence of cancer cells within this sentinel node, patients can avoid unnecessary lymph node dissection. Nevertheless, it is important to address that surgical treatment alone may not always be curative, and adjuvant therapies may be necessary to improve overall survival rates^{41,42}.

3.1.4.2 Immuno-based Melanoma Therapeutical Approaches

The recruitment of the immune system in the fight against most cancer types, including cutaneous melanoma, has emerged as a promising treatment approach. Hereby, the ability of different cells of the immune system to recognize, target, and eliminate melanoma cells, is being successfully utilized. In essence, the majority of immunotherapeutic reagents act as immune checkpoint inhibitors that hinder the inhibitory signals that cancer cells employ to bypass immune surveillance. The first established

immunotherapies for high-risk melanoma patients were the independent administration of the cytokines, interleukin-2 (IL-2) and interferon-alpha-2b (IFN-alpha-2b). In more detail, interleukin-2 acts by stimulating cytotoxic T-cells whereas Interferon-alpha-2b acts by upregulating antigen presentation to T lymphocytes, both of them contributing to the attack and elimination of melanoma cells. The most important downside of their dispensation is the high toxicity side effects that patients experience⁴³⁻⁴⁷. To control the intensity of the side effects from interferon-alpha-2b in particular, the protein was modified by adding polyethylene glycol (PEG) to its structure. This modification increased the drug's half-life in the body, subsequently decreasing the dosage frequency. Despite the efforts, the side effects are difficult to tolerate, especially for long-term therapy^{47,48}.

The newer classes of immunotherapeutic agents exhibit higher efficacy by targeting specific pathways of the adaptive immune system. The checkpoint regulatory proteins CTLA-4 (Cytotoxic T-Lymphocyte Antigen-4) and PD-1 (Programmed Cell Death-1) are transmembrane proteins, expressed predominantly on the cell surface of T cells, that act towards preventing hyperactivation of immune cells and controlling inflammatory responses in normal tissues. In further detail, CTLA-4 receptor interacts with its B7 ligand expressed on antigen-presenting cells and subsequently downregulates T cell activation; PD-1 receptor binds to its ligand PD-L1 and promotes the apoptosis of T cells. In the context of malignancy, it is advantageous to limit the activity of CTLA-4 and PD-1, not only due to the obtainable acceleration of an anti-tumour immune response, but also because melanoma cells have developed the ability to express these receptors as well, thereby exploiting this mechanism⁴⁹⁻⁵². Consequently, monoclonal antibodies that target CTLA-4 and PD-1 as immune checkpoint inhibitors (ICI) have been developed. Ipilimumab, an FDA-approved (Food and Drug Administration) monoclonal antibody against CTLA-4 since 2011, was used for the treatment of advanced, inoperable melanoma. Similarly, nivolumab and pembrolizumab are FDA-approved antibodies blocking PD-1⁵³⁻⁵⁸. Administration of nivolumab or pembrolizumab was attempted as an alternative approach when treatment with ipilimumab reached a plateau and cancer relapsed. Anti-PD-1 treatment demonstrates overall higher response rates^{57,59}. Dual immune checkpoint blockade (ICB) with ipilimumab-nivolumab is selected for patients that do not respond to any other ICI therapy. Notably, such treatment has a high probability of being terminated due to significant and intolerable toxicity side effects^{57,60}. Conclusively, the decision on which type of anti-PD-1 and/or anti-CTLA-4 treatment should be used depends on patient-related factors such age, mutation profile and other present medical conditions⁵⁷.

3.1.4.3 Molecular Targeted Melanoma Therapeutical Approaches

The identification of perturbations in the MAPK-ERK pathway during melanoma formation, has played a significant role in the discovery of advanced therapies. The MAPK-ERK pathway has been reported to be constitutively active in many melanoma cases due to *BRAF*, *NRAS*, and *c-KIT* mutations, resulting in aberrant cell growth, proliferation and differentiation. Most mutations are observed in *BRAF* and less frequently in *NRAS* (17 %) and *c-KIT* (11 %) genes. The lesions where *BRAF* mutations are present, are located at sites after intermittent sun exposure, whereas for *NRAS* and *c-KIT* the mutations are discovered at areas after chronic sun damage or at acral and mucosal sites respectively⁶¹. *BRAF* is a serine-threonine protein kinase and a downstream target of RAS with a distinctive role in regulating the MAPK-ERK pathway. *BRAF* proto-oncogene is altered in approximately 50 % of melanomas with mutations *BRAF*^{V600E/K} being the most prominent^{57,62}. FDA-approved *BRAF* inhibitors such as vemurafenib (2011), dabrafenib (2013) and encorafenib (2018), when administered separately as monotherapy, showed notable improvement in treating patients with late-stage melanoma. Disappointingly, resistance against *BRAF* inhibitors developed after about 5-7 months⁶³⁻⁶⁵.

MEK inhibitors, aiming for the downstream target of *BRAF* in the MAPK-ERK pathway, delayed the occurrence of resistance. FDA-approved MEK inhibitors trametinib (2013), cobimetinib (2015) and binimetinib (2018) have been used either separately or in combination with *BRAF* inhibitors for better efficiency and have depicted a longer durable response⁴⁹.

Finally, constant *c-KIT* expression causes uncontrolled activation of the MAPK-ERK and PI3K-AKT-mTOR cascades. Therefore, *c-KIT* has been used as a therapeutic target and inhibitors have been developed to suppress its function. The first FDA-approved *c-KIT* inhibitor was imatinib. Treatment with imatinib as monotherapy in *c-KIT*-mutated melanoma patients initially revealed promising results, but its potency soon drastically decreased⁶⁶⁻⁶⁹. Newer generation *c-KIT* inhibitors such as sorafenib, sunitinib, dasatinib and nilotinib, have had limited success. A possible explanation for the lack of efficacy could be the localization of metastases in advanced melanoma to the brain or central nervous system, where these small molecules fail to penetrate the blood-brain barrier (BBB)²⁷.

Choosing the most beneficial treatment approach for metastatic melanoma is not a simple decision. Many complex factors, such as the high mutational burden, the frequently acquired resistance to therapeutic agents and the inevitable toxicity that accompanies their administration, must be considered. Personalized therapy based on the patient's multi-level profiling has proven to be the best treatment strategy. Typically, such a treatment approach involves the combinatorial administration of more than one therapeutic reagent belonging to different categories.

3.2 Long non-coding RNAs (lncRNAs)

3.2.1 Introduction to long non-coding RNAs

Owing to the discovery and accelerated development of next-generation sequencing technologies, the comprehensive transcriptome exploration, provided adequate knowledge to quickly become apparent that less than 2 % of the human genome comprises of protein-coding genes⁷⁰. DNA transcription occurs pervasively and confers to the formulation of a multiplex network of protein-coding transcripts (mRNAs) and non-coding RNAs (ncRNAs)⁷¹⁻⁷³. There is sufficient scientific evidence to support that, these non-coding entities could facilitate noteworthy roles in the regulation of numerous biological operations including development, differentiation, proliferation, and metabolism^{70,74-76}.

Amongst the variety of non-coding transcripts, a heterogeneous and expanding class that has gathered increasing interest is the long non-coding RNAs (lncRNAs). lncRNAs are defined as transcripts with an arbitrary length cut-off of >200 nucleotides with none to limited observable protein coding capacity^{77,78}. Mainly transcribed by RNA polymerase II (Pol II) but also by other RNA polymerases, frequently appear capped by 7-methyl guanosine (m⁷G) at their 5' ends, polyadenylated at their 3' ends and spliced similarly to mRNAs^{73,79}. Predominantly localize in the nucleus compartment, are characterized by a cell type-specific expression at significantly lower levels than standard protein-coding genes and are poorly conserved^{71,78,80,81}. Most lncRNAs acquire stability through polyadenylation, for the non-polyadenylated lncRNAs secondary structures such as triple-helical structures in the 3' ends are the key stabilization factor^{70,82,83}.

3.2.2 Structural Classification

With the aim to unfold the biological significance of lncRNAs, it is efficacious to categorize them into different groups. Classification methods based on their positional relationship to protein-coding genes and the divergent processing mechanisms, contributes to enhanced investigation of their operating principles, and confers the opportunity for new insights and functional discoveries⁸⁴. New emerging scientific data has accumulated to distinguish lncRNAs into nine classes. lncRNAs which are generated from a genomic locus between two independent coding genes, and that show no overlap with any annotated protein-coding sequences are called long intergenic ncRNAs (lincRNAs)⁸⁵. Another class includes natural antisense transcripts (NATs) whose sequence overlaps with one or more exons of a coding gene in the opposite direction⁸⁶. Moreover, there are new lncRNA species which are derived from primary transcripts utilizing unconventional RNA processing pathways. Maturation isn't achieved through canonical 5' end m⁷G capping or 3' end poly (A) tailing. These lncRNAs (*MALAT1*, *NEAT1-2*) possess alternatively processed 3'

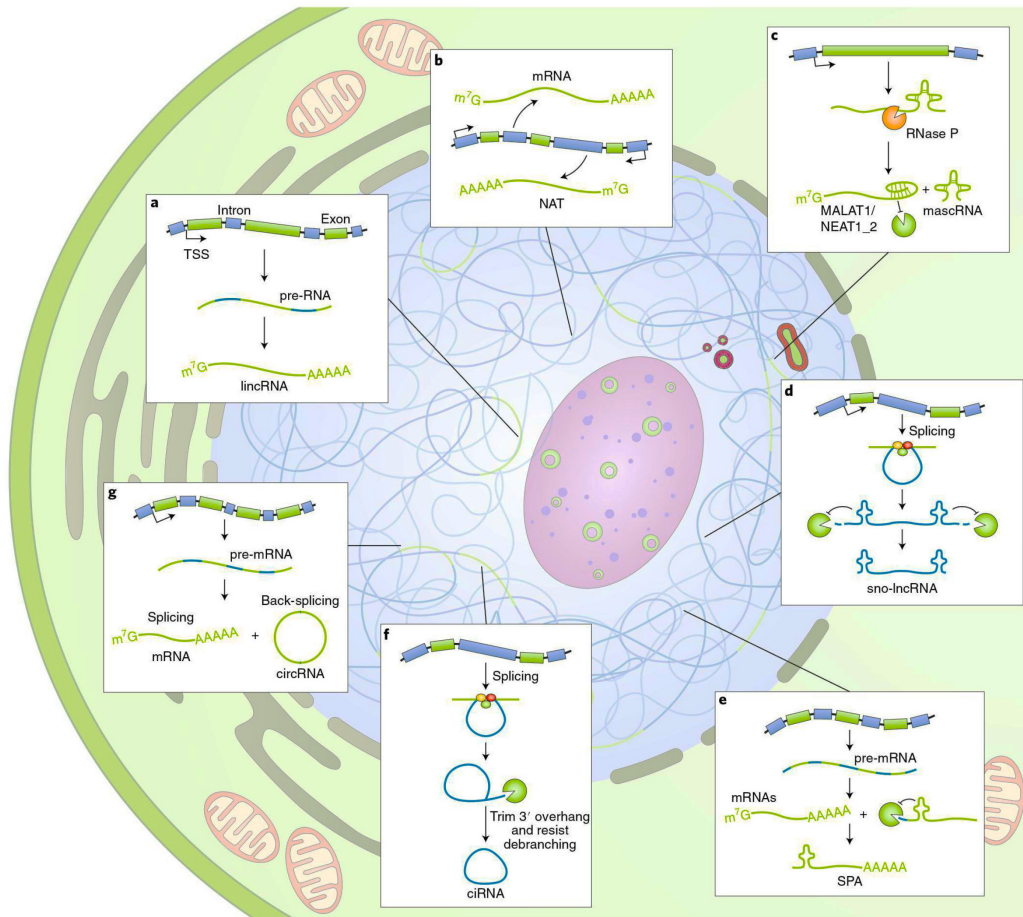


Figure 2. Structural Classification of lncRNAs: **a.** lincRNAs are transcribed by Pol II from intergenic regions, which are expected to undergo capping, splicing, and polyadenylation, **b.** NATs, transcribed from the opposite strands of protein-coding genes by Pol II, resemble mRNA-like lncRNAs, **c.** RNase P processes *MALAT1* and *NEAT1-2*, and their stability is increased by U-A-U triple helix structures at their 3' ends, **d.** Excised introns give rise to snoRNA-ended lncRNAs (sno-lncRNAs), which are protected from degradation by a snoRNP complex formed during splicing. These sno-lncRNAs are flanked by snoRNAs and lack a 5' m⁷G cap and 3' poly(A) tail, **e.** SPAs (5' snoRNA-ended and 3'-polyadenylated lncRNAs) are generated from readthrough transcripts and have their 5' ends safeguarded by co-transcriptionally assembled snoRNPs, **f.** ciRNAs result from excised introns and rely on consensus RNA sequences to prevent debranching of the lariat introns, and **g.** circRNAs are produced from pre-mRNAs through back-splicing circularization of exons during splicing, wherein pre-mRNAs can either be spliced into mRNAs or back-spliced into circRNAs. eRNAs and PROMPTs are not depicted²³⁰.

ends by Ribonuclease P (RNase P) or by Microprocessor complex cleavage. The RNase P cleavage generates a specific 3' triple helix (U-A-U) RNA structure that provides protection to the 3' end, whereas the Microprocessor generates lncRNAs without 3' end poly (A) tails^{73,87,88}. There are two additional classes of lncRNAs that are encoded by upstream regions of genes or by regions where transcriptional enhancers are located, and are characterized by a brief life span^{73,89}. In more detail, the former are called promoter upstream transcripts (PROMPTs), are transcribed in the antisense orientation, approximately 0.5-2.5 kb upstream of the active transcription start sites (TSSs) of most protein-coding genes in mammals and are subject to degradation by the RNA nuclear exosome targeting (NEXT) complex^{73,89-93}. The latter are known as enhancer RNAs (eRNAs), usually being less than 2000 nucleotides in length and are bidirectionally

transcribed from enhancers. It is proposed that these lncRNAs exhibit enhancer-like function and thus could be considered essential regulatory elements^{73,89,92,94–96}. Furthermore, there are lncRNAs which are generated when one intron contains two small nucleolar RNA (snoRNA) genes, known as sno-lncRNAs. During splicing the sequences between the snoRNAs are not degraded, leading to the accumulation of lncRNAs flanked by snoRNA sequences lacking 5' caps and 3' poly(A) tails^{73,97}. Moreover, in relation to snoRNAs, there has been discovered a class of unusually processed lncRNAs that originate from polycistronic transcripts, capped at the 5' end by snoRNAs and appear polyadenylated at the 3' end. These lncRNA species mediate transcription regulation through sequestration of RNA binding proteins (RBPs)^{73,98,99}. Finally, there are two classes that comprise of circular lncRNAs. The circular intronic RNAs (ciRNAs) are produced from excised intron lariats which don't debranch after splicing, producing a covalent circle with a 2',5'- phosphodiester bond between the 5' splice donor site and the branch point site. And the circular RNAs (circRNAs) that are derived from back-sliced exons of pre-mRNAs, undergoing a non-canonical splicing which connects a downstream 5' splice site with an upstream 3' splice site to yield a circRNA with a 3',5'- phosphodiester bond^{73,89,100}.

3.2.3 Functional Characterization

The indisputable heterogeneity that characterizes these non-protein-coding transcripts provides an indication of the wide range of their functionality in complex biological networks. A convenient way to classify lncRNAs based on their function, is whether they operate in a cis or trans manner, regulating the expression and/ or the chromatin formation of adjacent or distant genes respectively. In more detail, regarding cis-acting lncRNAs, three different operating mechanisms have been suggested: a. the mature lncRNA molecule itself influences positively or negatively the expression of nearby genes by gathering regulatory elements to the specific genomic locus, b. the functionality is independent of the lncRNA sequence and stems from the combinatorial effect of transcription and splicing from which the lncRNA is generated, and c. the presence of DNA regulatory elements that reside within the lncRNA promoter or the entire lncRNA genomic locus, is exclusively responsible for the alteration of expression of proximate genes. Finally, the trans-acting lncRNAs perform a. by migrating far away from their transcription location site, where they interfere in chromatin configurations and gene expression, b. by affecting nuclear structure and arrangement and c. by interplaying with RNAs and/or proteins to modulate their localization and subsequently their mechanism of action^{71,101,102}.

3.2.3.1 LncRNAs as Key Players in cis-Regulatory Mechanisms

In accordance with earlier statements, lncRNAs possess the ability to function as cis-regulatory elements through three distinct modalities. Of particular significance within a cis framework is the prevalent mechanism in which the lncRNA molecule itself mediates the activation or repression of the genetic locus situated in close proximity. The extensively studied lncRNA *Xist* (X-inactive Specific Transcript) performs a fundamental function in regulating genes located in close proximity (cis regulation). Particularly during the initial stages of embryonic development in female mammals, one of the X chromosomes undergoes transcriptional repression to maintain balanced gene expression. The activation of *Xist* on one of the X chromosomes brings about the formation of an inactive chromosome (Xi). Post-expression, the *Xist* transcripts diffuse across the inactive X chromosome, initiating a cascade of events resulting in the modification of chromatin structure and eventual suppression of gene activity over the majority of the chromosome¹⁰².

Concerning the second mechanism, the modulation of local gene expression derives from the activity of the genomic locus containing the lncRNA encoding region, thereby establishing independence from the corresponding lncRNA transcript, its nucleotide sequence, or its spatial positioning. The regulation observed at the imprinted *IGF2R* gene serves as an illustration of this particular type. Key to this process is the antisense lncRNA known as *Airn* (Antisense IGF2R RNA Non-coding), that overlaps with both the *IGF2R* gene body and promoter. By systematically introducing polyadenylation (polyA) cassettes that truncated the *Airn* transcript at distinct locations in relation to the *IGF2R* (Insulin like Growth Factor 2 Receptor) promoter, it was depicted that the *IGF2R* silencing is independent of the spliced or unspliced *Airn* transcripts. The repression of the *IGF2R* promoter results from transcriptional interference which reduces the on-site occupancy of RNA polymerase II^{102,103}.

Finally, the erythroid-enriched lncRNA *Lockd* (lncRNA downstream of *CDKN1B*) locus stands as a noteworthy example of the third mechanism, wherein cis-DNA regulatory elements are found within the lncRNA genomic locus, effectively regulating the expression of genes in proximity. *Lockd* locus localizes downstream of the *CDKN1B* (Cyclin Dependent Kinase Inhibitor 1B) gene locus. *Lockd* originates from a regulatory element exhibiting promoter-associated histone mark signatures of active transcription, that also physically interacts with the *CDKN1B* promoter. While transcription and the presence of *Lockd* transcript are not essential, the regulatory element within the *Lockd* locus appears to act as an enhancer, modulating the expression of *CDKN1B*^{104,105}.

3.2.3.2 Trans-Regulatory Mechanisms Mediated by lncRNAs

In contrast to cis-regulatory mechanisms, which may involve the participation of the lncRNA transcript, or its genetic locus, or other DNA regulatory elements located within its locus, in governing the transcriptional levels of adjacent genes, trans-regulation is specifically reliant on the lncRNA, its binding capacities, and subcellular distribution.

lincRNA-EP5 (Long Intergenic Non-coding RNA-Erythroid Prosurvival) has been identified as a crucial trans-regulator of inflammatory gene expression in immune cells, specifically macrophages and dendritic cells. However, when exposed to microbial ligands like lipopolysaccharide (LPS), the transcription of *lincRNA-EP5* is significantly reduced. Deletion of *lincRNA-EP5* does not result in any alteration of proximate gene expression, thus dismissing the possibility of cis-regulatory properties. Furthermore, *lincRNA-EP5* lentiviral transduction of knock-out macrophages successfully reverses the downregulation of immune response genes caused by *lincRNA-EP5* loss. In addition, RNA antisense purification (RAP) experiments reveal that *lincRNA-EP5* directly interacts with distantly located promoters of the repressed genes^{102,106}.

Certain lncRNAs facilitate modifications in nuclear architecture, leading to changes in gene expression and contributing to the progression of various diseases. One noteworthy example is *NEAT1*, a nuclear transcript characterized by its single-exon composition and overexpression in paraspeckles. It is considered a major structural component of these subnuclear ribonucleoprotein complexes^{102,107,108}. Paraspeckles actively participate in the regulation of critical cellular processes, including transcription and RNA processing. The functionality of *NEAT1* relies on its interaction with several proteins found within paraspeckles, such as p54nrb/NONO, PSP1/PSP1, and PSF/SFPQ, as it plays an indispensable role in both the establishment and maintenance of these nuclear domains^{102,109}.

Finally, the last trans-regulatory mechanism involves lncRNAs that interact with proteins or RNA molecules interfering with their function. Non-coding RNA activated by DNA damage (*NORAD*) is a highly abundant, conserved lncRNA. It is an unspliced polyadenylated transcript that is enriched in the cytoplasm. It has been suggested that *NORAD* acts as molecular decoy for RNA-binding proteins (RBPs) *PUMILIO1* (PUM1) and *PUMILIO2* (PUM2). These proteins belong to a conserved family of RBPs that bind to the sequence UGUANAUA (PUMILIO response element), located at the 3' UTR of selected mRNAs. *NORAD* upon binding to PUM1/PUM2 initiates mRNA degradation and subsequently inhibition of translation of the targeted mRNA molecules^{102,110,111}. Additionally, *NORAD* functions as a miRNA sponge, post-transcriptionally regulating gene expression. In neuroblastoma, for instance, *NORAD* suppresses apoptosis and autophagy by downregulating miR-144-3p and thus inducing overexpression of HDAC8 (Histone Deacetylase 8) through miR-144-3p/HDAC8 axis^{102,112,113}.

3.2.4 Significance of lncRNAs in Oncogenesis and Tumour Progression

Unraveling the mechanisms promoting carcinogenesis is of fundamental importance towards impactful therapeutic approaches. Annotation of the cancer genome is a difficult and continuous research convention. Genome-wide cancer mutation analyses have disclosed a broad repertoire of mutations stemming from the non-coding genome. Several genomic locations that are recurrently altered in cancer, encode lncRNA transcripts. Differentially expressed lncRNAs involved in cancer occurrence, promote malignancy through interactions with nucleic acids and proteins, thus controlling various biological processes including cell growth, differentiation, metabolism, and inflammation^{71,114}.

There are notable examples, where it is reported that many lncRNAs showcase direct oncogenic properties. *HOTAIR* (HOX Transcript Antisense Intergenic RNA) has been characterized as a formidable oncogenic lncRNA, linked to cancer escalation in twenty-six cancer types^{115,116}. It is overexpressed in breast cancer and is a credible biomarker for metastasis and poor prognosis¹¹⁷. lncRNAs can also hold an indirect oncogenic role by acting synergistically with oncogenic drivers. For the oncogene *MYC*, plentiful lncRNAs have been identified as upstream or downstream modulators affecting its expression. For example, *PVT1* (Human Plasmacytoma Variant Translocation 1) acts post-translationally to stabilize *MYC*¹¹⁸. Moreover, it is not surprising that there are lncRNAs which either exert a straightforward tumour-suppressor role or facilitate the function of protein-coding tumour-suppressor genes (TSGs). In hepatocellular carcinoma (HCC), the expression of the lncRNA *FER1L4* (Fer-1 Like Family Member 4) is downregulated, and in addition its knock-down in HCC cells induces aberrant proliferation and migration, which reflects its function in a tumour-suppressive manner^{116,119}. Finally, maternally expressed genes 3 (*MEG3*) lncRNA is a modulator of the well-known tumour-suppressor gene *TP53*. It has been established in many studies that *MEG3* activates *p53* (Tumour Suppressor Protein p53), and therefore downregulated expression of *MEG3* interferes with the downstream target activity of *p53*¹²⁰⁻¹²².

Comprehensive differential expression lncRNA analyses have shown that lncRNAs can exhibit both oncogenic and tumour-suppressing properties in a completely cancer-specific manner. This differential expression fluidity makes the understanding of their functionality even more complicated. There is evidence that some lncRNAs promote carcinogenesis by participating in the regulation of metabolic pathways¹²². Metabolic reprogramming is one of the main characteristics of malignant cells, and it is crucial for supporting their accelerated energy requirements. Aerobic glycolysis is the preferred rapid metabolic process for cancer cells to acquire energy in the form of glucose. One way in which lncRNAs modulate glycolytic steps is by binding to glucose transporters (GLUTs), thus increasing overall glucose uptake. For example, antisense non-coding RNA at the *INK4* locus (*ANRIL*) is overexpressed in nasopharyngeal carcinoma. PI3K-AKT-mTOR signaling pathway is being activated, leading to upregulation of *GLUT1* and *LDHA* (Lactate Dehydrogenase A) expression and therefore increase in the intracellular glucose levels¹²³.

Lastly, recent studies have revealed that some lncRNAs can induce tumorigenesis by regulating cellular immune response. This is considered a drawback, especially since immunotherapy is at the forefront of cancer treatment. T cells are involved in diverse antigen recognition and in the maintenance of immunological memory and self-tolerance. lncRNAs *MALAT1* and *LINK-A* (Long Intergenic Non-coding RNA for Kinase Activation) have been described to inhibit T cell activity, consequently resulting in attenuation of the immune system's arsenal and allowing cancer progression^{122,124}.

3.2.5 Functional Interplay of lncRNAs in Melanoma

The involvement of lncRNAs in many cancer types has been supported by continuously growing evidence, and malignant melanoma is not an exception. Various studies elucidate the functional role of lncRNAs in melanoma development and progression, thus illustrating their potential clinical importance. Hereby, the most well-studied lncRNAs, corresponding to melanoma, are mentioned and their molecular mechanisms are analyzed.

ANRIL was initially discovered in patients with hereditary cutaneous melanoma carrying a large germline deletion in the *p15^{INK4b}-p16^{INK4a}-p14ARF* gene cluster. *ANRIL*, in the presence of a bidirectional promoter, is transcribed in the opposite direction in relation to *p15^{INK4b}-p16^{INK4a}-p14ARF* locus¹²⁵. The locus encodes three tumour suppressor genes that mediate oncogene-induced senescence. Under normal conditions *ANRIL* represses their expression in cis by recruiting PCR1 (Polycomb Repressive Complex 1) and PCR2 (Polycomb Repressive Complex 2) complexes through CBX7 (Chromobox Homolog 7) protein and Suz12 protein respectively on *p15^{INK4b}-p16^{INK4a}-p14ARF* locus. *ANRIL* is upregulated in cutaneous melanoma compared to normal melanocytes, where it contributes to aberrant cell proliferation^{126,127}. Lastly, *ANRIL* has been reported to undergo alternative splicing that results in many linear and circular isoform variants. The subcellular localization and stability of *ANRIL* isoforms differ, reflecting higher complexity in its regulatory network; linear isoforms appear enriched in the nucleus compartment, whereas the circular isoforms reside in the cytoplasm¹²⁸.

BRAF-activated non-coding RNA (*BANCR*) has been associated with the prominent activating *BRAF^{V600E}* mutation. Upregulation of *BANCR* was observed in *BRAF^{V600E}*-mutated melanomas, with its expression levels showing a positive correlation with staging progression and metastasis^{127,129}. *BANCR* knock-down in BRAF-mutated melanoma cell lines impacted transcription levels of 88 genes. Most downregulated genes promoted cell migration. C-X-C motif chemokine ligand 11 (*CXCL11*) being one of them, when overexpressed, was able to reverse the effect of *BANCR* depletion and induce cell motility in a rescue experiment in *BANCR*-depleted cells^{127,128}. Lastly, the expression of miR-204 is downregulated in melanoma cells compared to melanocytes. The significant decrease in the expression of miR-204 has been connected

with low survival rates and linked to the sponging ability of *BANCR*. In the absence of miR-204, *Notch2* is induced which plays an oncogenic role in melanoma^{127,130,131}.

Cancer susceptibility candidate 15 (*CASC15*) is a long intergenic non-coding RNA located on chromosome 6. *CASC15* transcription levels increase consistently during melanoma progression. Accordingly, *CASC15* is overexpressed in metastatic melanoma tumours compared to normal tissues. Mechanistically, *CASC15* silences the expression of tumour suppressor programmed cell death 4 (*PDCD4*) by increasing the histone methylation (H3K27me3) levels at its promoter's region. This epigenetic mechanism is mediated by the recruitment of enhancer of zeste homolog 2 (EZH2) which is a component of PCR2 and acts as a histone methyltransferase^{132,133}. Knock-down experiments using siRNA molecules depicted that *CASC15* silencing inhibited melanoma cell clonogenic growth, and thus showcasing that it modulates phenotype switching between proliferative and invasive phases^{133,134}.

Growth arrest-specific transcript 5 (*GAS5*) is a lncRNA located on chromosome 1. Comparing to the vast majority of lncRNAs that are involved in melanoma and are overexpressed, *GAS5* is downregulated and acts as a tumour suppressor^{133,135}. As stated before, melanoma cells exert their metastatic potential in a multistep process. Initially, cell invasiveness requires degradation of the extracellular matrix, which is modulated by matrix metallopeptidases (MMPs). Matrix metallopeptidase 2 (MMP2) mediates type IV collagen degradation and its expression levels are elevated in many melanoma cells^{136,137}. In transwell invasion assays using modified melanoma cell lines stably overexpressing *GAS5*, there was a significant decrease in the migratory ability; melanoma cells couldn't penetrate the extracellular matrix. It was observed that *MMP2* expression was downregulated when *GAS5* was overexpressed which illustrated a negative correlation between them and a possible mechanism by which *GAS5* inhibits melanoma migration and invasion¹³⁷. Finally, another study depicted a positive relationship on a transcriptional level between *GAS5* and miR-137. miR-137 was also shown to be a tumour suppressor in melanoma by downregulating oncogenes in melanoma such as *MITF*, *c-Met*, *YB1* (YBox-binding protein 1), and *EZH2*. *GAS5* induces the expression of miR-137. Low levels of *GAS5* are correlated with low survival rates^{133,138}.

HOTAIR is a long intervening non-coding RNA located between *HOXC11* (Homeobox C11) and *HOCX12* (Homeobox C12) genes on chromosome 12q13.13^{127,139}. Upregulation of *HOTAIR* was detected in primary and metastatic melanoma samples. Similar to other lncRNAs, *HOTAIR* initiates epigenetic modifications by facilitating the relocalization of PCR2 complex to the *HOXD* (Homeobox D Cluster) locus and regulating its silencing by H3K27 methylation¹³⁹. Knock-down of *HOTAIR* confirmed inhibition of cell proliferation and migration. Epithelial-to-mesenchymal transition (EMT) is considered a histological signature for melanoma metastasis^{140,141}. In experiments using si-*HOTAIR* transfected melanoma cell lines, it was shown that the protein expression levels of E-cadherin (essential epithelial marker) were increased while those of N-cadherin (mesenchymal marker) were decreased. Furthermore, transwell migration assays using si-*HOTAIR* transfected melanoma cell lines demonstrated a decrease in cell invasiveness. These findings support the

hypothesis that *HOTAIR* plays a significant role in melanoma metastasis by modulating EMT phenomenon. Lastly, *HOTAIR* acts as a competing endogenous RNA (ceRNA) by sponging the tumour suppressor miR-152-3p. miR-152-3p exerts its function by binding to oncogene *c-MET* and disrupting its tumorigenic potential. miR-152-3p expression levels are decreased in melanoma cells while *c-MET* appears upregulated. *HOTAIR* binds directly to miR-152-3p, and thus promotes metastasis through upregulation of c-MET pathway¹⁴¹.

Llme23 is a lncRNA located on chromosome 6, which is exclusively upregulated in human melanoma cells, and therefore it could be used as a diagnostic and prognostic biomarker¹⁴². *Llme23* is able to specifically bind to polypyrimidine tract-binding (PTB) protein-associated splicing factor (PSF). PSF showed tumour suppressor properties when binding to oncogene *Rab23* (Ras-related GTP Binding Protein 23), by repressing its expression. This interaction is reversed by *Llme23* binding to PSF, promoting melanoma progression. Experimentally, the oncogenic role of *Llme23* was confirmed with knock-down experiments on YUSAC metastatic melanoma cells, where a significant decrease in their malignancy potential was observed^{133,142,143}.

Metastasis-associated lung adenocarcinoma transcript 1 (*MALAT1*) is a highly evolutionarily conserved and abundant lncRNA, linked to many human cancers¹²⁷. *MALAT1* is overexpressed in melanoma tissues compared to adjacent healthy melanocytes and functions as competing endogenous RNA for numerous miRNAs such as miR-22^{133,144}, miR-34a^{133,145}, or miR-183^{133,146} which showcase tumour suppressing properties. In more detail, miR-22 negatively regulates the expression of *MMP14* (Matrix Metalloproteinase 14) and *SNAIL* (Zinc Finger transcription factor) that mediates EMT, an essential step for metastasis^{133,144}. miR-34a being a tumour suppressor miRNA, binds to the 3' UTR region of many oncogenes such as *c-MYC* and *MET* repressing their transcription, thus prohibiting cell invasion to nearby locations^{133,145}. Finally, miR-183 binds to targets integrin subunit beta 1 (ITGB1) which is associated with tumour growth. *MALAT1* halts their anti-tumour potential by sponging these miRNAs and promotes activation of the above-named oncogenes leading to metastasis in melanoma^{133,146}.

Nuclear-enriched abundant transcript 1 (*NEAT1*) is a lncRNA encoded by the familial tumour syndrome multiple endocrine neoplasia (MEN) type 1 locus on chromosome 11 and is transcribed into two variants *NEAT1* and *NEAT2*^{147,148}. *NEAT1* is upregulated in melanoma tissues and acts like a sponge for miR-495-3p. miR-495-3p targets *E2F3* (E2 Transcription Factor 3) gene that discloses carcinogenic properties by causing cell cycle disturbances in malignant melanoma¹⁴⁹. Overexpression of *E2F3* is positively correlated with extensive copy number amplification (CNA) and results in decreases in overall survival¹⁵⁰. *NEAT1* binds directly to miR-495-3p and reverses inhibition of *E2F3*, thus promoting cell proliferation and migration¹⁴⁹.

Survival-associated mitochondrial melanoma specific oncogenic non-coding RNA (*SAMMSON*) is a lncRNA frequently overexpressed in melanoma, located on chromosome 3p13–3p14 in close proximity to *MITF*, a transcription factor that regulates genes associated with the pigmentation of melanocytes. *SAMMSON* and

MITF are co-amplified in 10 % of all melanoma cases, which reveals an indirect association even if they are transcribed independently under the control of different promoters^{133,151}. Moreover, *SAMMSON* overexpression is not indicative of the tumour mutational profile (*BRAF*, *NRAS*, or *TP53* mutations)^{127,152}. *SAMMSON* knock-down suppressed MMP2 and MMP9 expression levels, which indicates that *SAMMSON* promotes melanoma cell migration by modulating epithelial-mesenchymal transition (EMT). Induction of MMPs transcription is required for the establishment of EMT¹⁵². *SAMMSON* mainly localizes in the cytoplasm where it regulates in trans p32 (Tumour Suppressor Protein p32). p32 is a protein important for mitochondrial function and metabolism. p32 expression levels are upregulated in many cancers including melanoma. Highly functional mitochondria are of significant importance to tumour cells to maintain elevated proliferative and invasive potential. Silencing of *SAMMSON* reduces p32 levels that cause mitochondrial dysfunctionalities which result in mitochondrial-dependent apoptosis of melanoma cells^{127,151}.

SPRY4 intronic transcript 1 (*SPRY4-IT1* or *SPRIGHLY*) is a lncRNA that originates from the second intron of *SPRY4* (*Sprouty4*) gene. *SPRY4-IT1* and *SPRY4* are both functional genes and transcribed independently. Their expression profiles across various tissues are comparable, suggesting that *SPRY4-IT1* likely participate in the biological pathway of *SPRY4*^{127,153}. *SPRY4-IT1* transcripts undergo processing in the nucleus and are transferred to the cytoplasm where they are present in polysomes. *SPRY4-IT1* is highly expressed in melanoma tissues and is involved in lipid metabolism by binding to lipid phosphatase Lipin 2 which catalyzes the conversion of phosphatidic acid (PA) to diacylglycerol (DAG). The functional relationship between *SPRY4-IT1* and Lipin 2 was investigated with knock-down experiments using siRNA technology. Silencing of *SPRY4-IT1* upregulates Lipin 2 both on mRNA and protein level, whereas silencing of Lipin 2 leads to suppression of *SPRY4-IT1* as well. Based on these discoveries potential *SPRY4-IT1* knock-down can cause cellular lipotoxicity and result to apoptosis due to accumulation of Lipin 2^{127,154}.

Urothelial carcinoma-associated 1 (*UCA1*) is a lncRNA that exhibits oncogenic properties in melanoma and other cancer types. *UCA1* expression increases as melanoma progresses to advanced stages and metastasis is established. *UCA1* functions as a ceRNA for miR-28-5p and miR-507. Direct binding sites on both miRNAs were identified for *UCA1*. miR-28-5p and miR-507 regulate the expression of *HOXB3* (*Homeobox B3*) and *FOXM1* (*Forkhead Box M1*) respectively. *UCA1* induces cell proliferation, cell cycle progression and migration by inhibiting the aforementioned interactions leading to *HOXB3* and *FOXM1* overexpression^{155,156}.

3.3 Modulation of lncRNA Expression for Functional and Therapeutic Studies

Combination of the increasing number of identified lncRNAs along with their miscellaneous functions in developmental processes, affecting proliferation, differentiation, and programmed death, makes them undoubtedly a significant player in human diseases like cancer or neurodegenerative disorders. Therefore, to untangle the association of these non-coding regulatory transcripts with the initiation and progression of many complex human diseases, innovative molecular tools and model systems should be established.

RNA interference (RNAi) has predominantly been the approach to regulate gene expression post-transcriptionally¹⁵⁷⁻¹⁵⁹. This method utilizes a synthetically designed double-stranded RNA (dsRNA) which is cleaved into a single-stranded small interfering RNA (siRNA). The siRNA molecule directs the multiprotein complex RNA-induced silencing complex (RISC) to the target RNA causing its degradation. Alternative to RNAi, short (12-20 nucleotides) synthetic antisense single-stranded oligonucleotides (ASOs) have been utilized for the depletion of RNA transcripts. These oligonucleotides bind via base complementarity to RNA sequences with high specificity, their degradation is induced by RNase-H activity^{160,161}.

RNAi and ASOs approaches are characterized by a few constrictions; Firstly, both promote *transient* and incomplete depletion of the target RNA sequences. RNAi suffers from limited efficiency due to the fact that most lncRNAs are nuclear and expressed at low levels, although the RNAi machinery has been reported to function also inside the nucleus. Implementation of ASOs comes also with challenges because of their enzymatic instability in biological fluids and potential cytotoxicity¹⁵⁹. To overcome these limitations, especially towards the direction of achieving long-term results and fine-tuning lncRNAs' expression, revolutionary CRISPR approaches were developed.

3.4 Perturbation of lncRNA Expression utilizing CRISPR-based Technology

3.4.1 Introduction to CRISPR-Cas9 System

Prokaryotic organisms acquire adaptive immunity towards invading genetic material like plasmids and viruses by using the clustered, regularly interspaced, short palindromic repeats (CRISPR)-CRISPR-associated protein (Cas) systems. The functionality of CRISPR-Cas loci is modulated by a variable CRISPR array of identical repeats interspersed with genome targeting sequences called spacers, and *cas* genes arranged in operons^{162,163}. Six types of CRISPR-Cas systems have been discovered¹⁶⁴. Type II system, which was found in *Streptococcus pyogenes*, is considered the most broadly studied and modified system for genomic engineering in mammalian cells. Cas9 protein is a large multifunctional protein with two putative nuclease domains, HNH and RuvC-like. Cas9 endonuclease is guided by two RNAs called CRISPR RNA (crRNA) and trans-activating crRNA (tracrRNA) and upon sequence-specificity cleaves foreign genetic sequences for

host protection creating double strand breaks (DSBs) in the target DNA. Site-specific cleavage relies on a. base pairing complementarity between the crRNA (17-20 nucleotide sequence) and the protospacer sequence intergraded into the host genome and b. a short motif (3 nucleotide sequence) called protospacer adjacent motif (PAM) located on the opposite DNA strand. This three-component system was converted for simplicity and higher efficiency in a two-component system by fusing crRNA and tracrRNA sequences of the Cas9-RNA complex into a chimeric single-guide RNA (sgRNA) forming the sgRNA-Cas9 complex^{165,166}.

3.4.2 Engineered CRISPR Methods for Transcriptional Regulation of of lncRNA Expression

Initially, CRISPR-cas9 system was adopted as a gene editing tool for the knock-out (CRISPR-KO) and knock-in of protein-coding genes. In mammalian cells, the double strand breaks (DBS) which are generated by the endonuclease activity of Cas9 immediately initiate the DNA repair mechanisms these cells behold¹⁶⁶. In more detail, Cas9 is guided to the genomic location where the open reading frame (ORF) of the gene of interest is situated, where it creates blunt ends. Non-homologous end joining (NHEJ) is the primary cellular repair pathways that restores the DBS, usually through insertion or deletion of 1-3 nucleotides (inDels). These inDels create a frameshift leading to a premature stop codon and thereby inevitably to mRNA degradation. It is apparent that the original CRISPR-Cas9 system lacks applicability to effectively manipulate the expression of long non-coding RNA because these genes are missing an open reading frame, thus requiring a modified CRISPR-Cas9 system¹⁶⁷⁻¹⁶⁹. For this reason, Cas9 protein has been genetically engineered. The D10A and H840a mutations in the RuvC and HNH domains respectively, the domains that are responsible for its nuclease activity, safeguard Cas9 as a functional protein, that no longer creates DNA cleavage but instead acts as a transcription regulator. This Cas9 mutant called catalytically dead Cas9 (dCas9) when targeted by the guide RNA before the promoter region, prevents the binding of RNA polymerase, and thus inhibits transcription initiation¹⁷⁰⁻¹⁷². The regulatory efficiency of the dCas9 variant is amplified through its fusion with transcription effectors either towards repression or activation of transcription. When fused with transcriptional repressor domains as Kruppel-associated box (KRAB) repressor or SID domains, dCas9 inhibits the expression of the target site known as CRISPR transcriptional interference (CRISPRi), whereas fused with transcriptional activation domains (such as VP16, VP64, p65AD domains) activates the target site defined as CRISPR transcriptional activation (CRISPRa). These systems can regulate transcription in a reversible manner when dCas9 is under the control of a tetracycline-inducible promoter¹⁷³⁻¹⁷⁵.

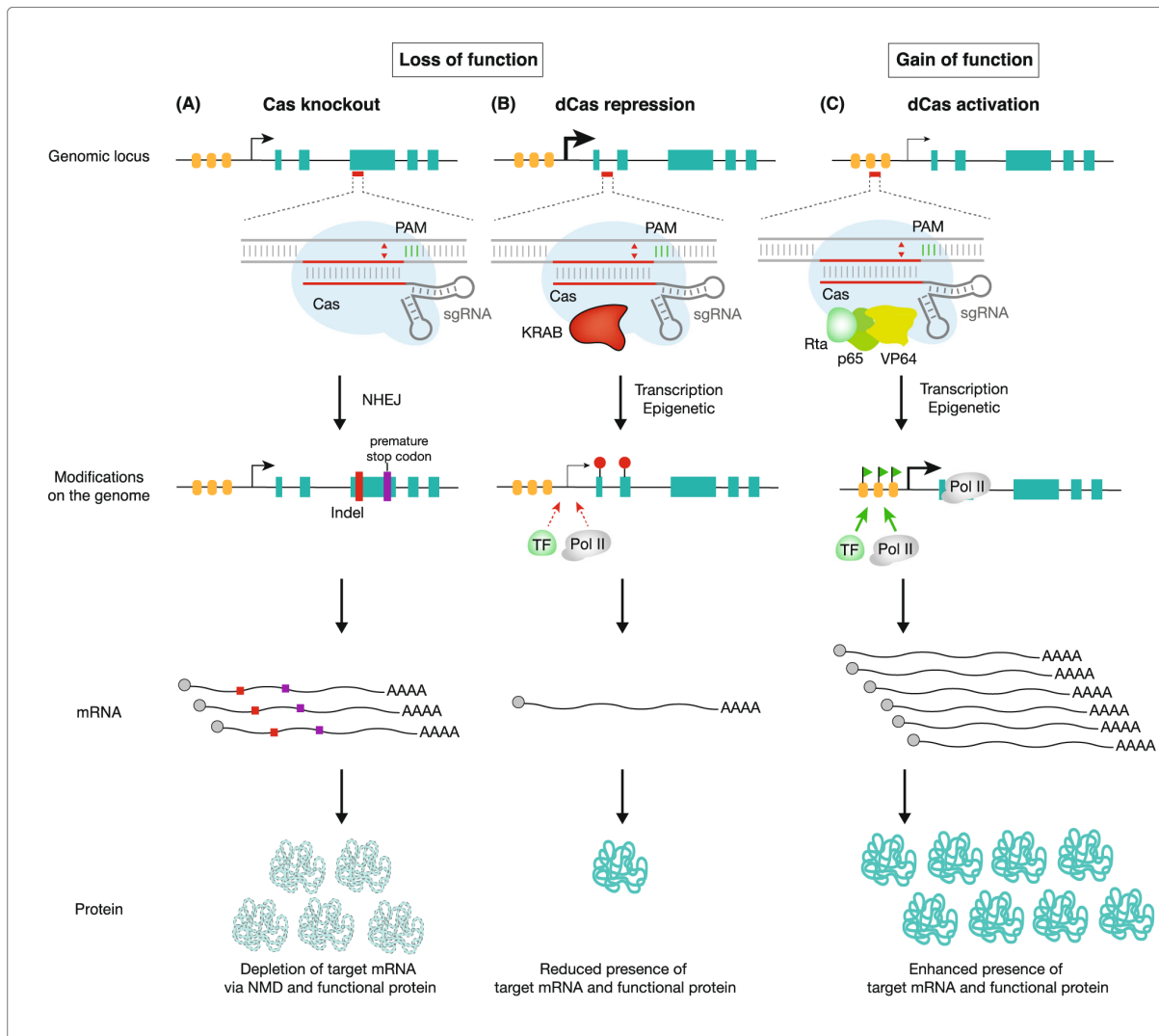


Figure 3. Schematic representation of the CRISPR-Cas system and its gene editing applications. **A.** The CRISPR-Cas system consists of Cas9 protein and a guide RNA, which can be programmed to target specific DNA sequences for gene editing. **B.** CRISPRi (CRISPR interference) and **C.** CRISPRa (CRISPR activation) systems utilize modified Cas proteins to repress or activate gene expression, respectively, providing versatile tools for precise control of gene function²³¹.

3.4.3 Introduction to CRISPR Screens

CRISPR-Cas9 system (CRISPR-KO) and its derivatives systems (CRISPRi, CRISPRa) are utilized for conducting large-scale screens with high throughput performance in mammalian cells. CRISPR screens are a powerful tool for elucidating the function of genes of interest and for establishing correlations between the cellular phenotypes resulting from the genetic perturbations analyzed. There are two types of genetic regulation used in screens: the loss-of-function or negative selection (CRISPR-KO or CRISPRi) and the gain-of-function or positive selection (CRISPRa) which negatively and positively affect gene expression levels, respectively. In more detail, negative selection screens acquire important information by systematically causing permanent gene expression excision (CRISPR-KO) or reversible expression deficiency (CRISPRi). Genes that

are getting depleted over time are profiled as essential for cell viability and proliferation. Conversely, positive selection screens rely on the enrichment of specific genes by upregulating their expression and these screens usually identify genetic alternations that lead to drug resistance. Additionally, the format in which CRISPR screenings are implemented, determines whether they are pooled or arrayed. In pooled CRISPR screens the single-guide RNA (sgRNA) library, is introduced in bulk in the cell population, such that each cell is transduced with one sgRNA that is integrated into its genome, and thus the resulting phenotype corresponds directly to the genetic perturbation. However, arrayed CRISPR screens are performed in multi-well cell culture formats (i.e., 96-well or 384-well culture plates), which inevitably ensures a more precise and defined cell transduction approach. There are different experimental designs for arrayed CRISPR screens, the most prevalent are either one sgRNA per well or multiple sgRNAs per gene pooled in a well, such that in all setups the result is the regulation of a specific gene in each well^{176–178}.

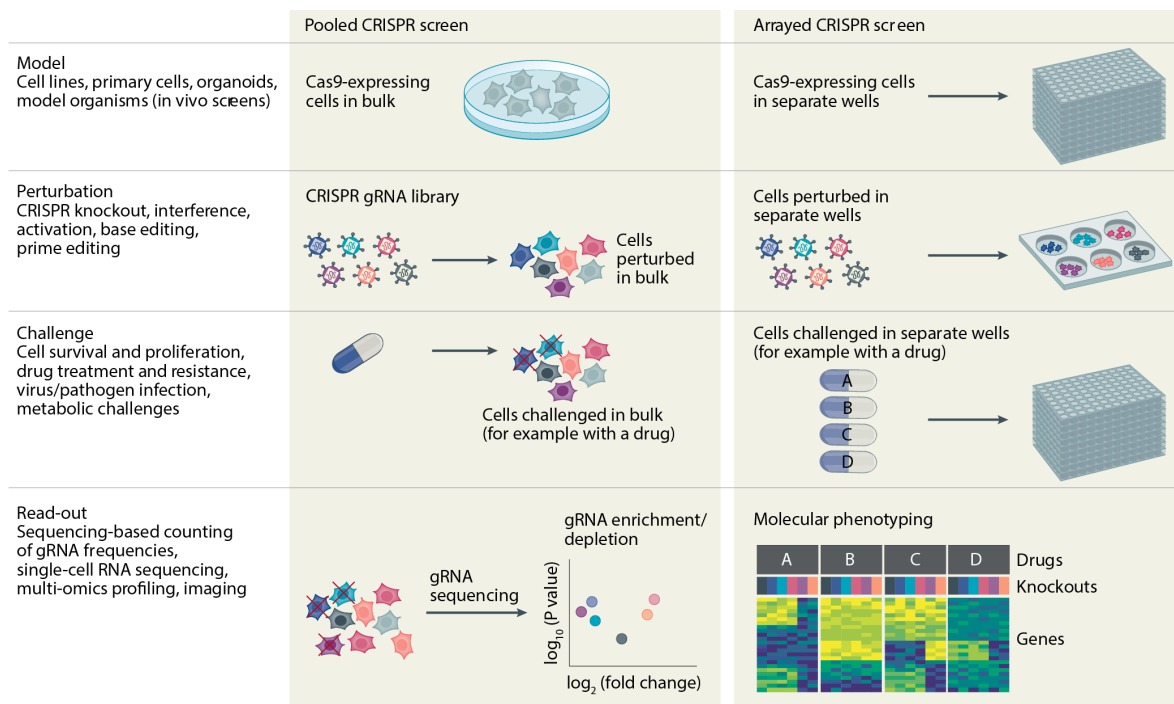


Figure 4. Visual representation of the experimental setup for CRISPR screening in a pooled or arrayed format, outlining the biological model, the CRISPR-induced perturbations, the cellular challenges, and the methods for measuring molecular or cellular effects¹⁷⁸.

3.4.4 Design and Analysis of pooled CRISPR Screens

To conduct a pooled CRISPR screen, a library of single guide RNAs (sgRNA) that targets specific genes of interest is initially designed *in silico*. The goal of the CRISPR screen dictates the target window in relation to the transcription start site (TSS) of each gene from where the sgRNA sequences will be generated. High CRISPRi efficacy is achieved when targeting dCas9-KRAB to a window of DNA from +25 to +75 bp downstream of the TSS of the gene. For CRISPRa, the optimal window to target dCas9-VP64 is situated at

-150 to -75 bp upstream from the TSS¹⁷⁹. Typically, around 4-10 sgRNAs per gene are designed for enhanced potency and avoiding off-target hits and increase reproducibility. Several online tools are available to detect on-target and off-target predictions and calculate their scores. Based on these scores the sgRNAs are ranked and their efficiency can be predicted¹⁷⁹⁻¹⁸¹. Each library contains negative controls which are scrambled guide RNA sequences that don't target any genomic locus and if available, also positive controls which can validate the biological effect that is being studied. The sgRNA library is cloned into a lentiviral vector and the cells are transduced at a low multiplicity of infection (MOI) between 0.3 and 0.5, such that the probability of two or more different types of sgRNA to enter the same cell is relatively low. The MOI determination is crucial not only to prevent multiple sgRNA integration but also to prohibit really low transduction levels. The MOI is dependent on the titer of the lentivirus and the transduction efficiency of the selected cell line¹⁸². The size of a sgRNA library varies widely; large libraries can be technically and economically demanding thus smaller sized libraries are preferred for better screening quality and performance. Genome-scale screens require a large numbers of cells for sufficient coverage, whereas focused screens moderate this necessity. The nature of the screen determines the level of coverage required; for positive screens a coverage of 100-200X per target gene is aimed, while for negative screens a higher coverage of 500-1000X per target gene is intended. The coverage refers to the number of cells transduced with one sgRNA¹⁷⁸.

The most common read-out for CRISPR screen is performed by guide RNA sequencing. DNA samples are collected at different timepoints throughout the screen, to be evaluated and compared to early reference or mock control samples. Next generation sequencing (NGS)-ready libraries are produced by PCR amplification of the integrated sgRNAs. Thus, sgRNA vector-specific primers are used for the library preparation, to amplify only the part of the lentiviral backbone that includes the sgRNA. It is apparent that each sgRNA acts as its own barcode since the sequence is unique and therefore can be backtracked and mapped to the genome and to the gene that it alters. However it is frequent that additional adapters are attached to the PCR primers to label the samples. The PCR cycling conditions are critical to avoid PCR-introduced sequence errors and amplification bias. The sequencing results are in the form of raw read counts, where the level of abundance of each sgRNA is depicted for all screen samples. The sgRNA read counts are the basis for data analysis, as they provide information on the statistical significance of depleted or enriched sgRNAs and thus on the essentiality or no-non essentiality of the perturbed genes^{183,184}.

4. Study Objectives

Melanoma constitutes an engaging research subject, given the intricate interdependence of genetic and environmental factors. What distinguishes this malignancy is its compelling combination of a significant mutational burden and a pronounced propensity for metastasis, rendering it a captivating domain for delving into the genetic foundations and mechanisms underlying cancer dissemination. Furthermore, lncRNAs have been implicated in multiple aspects of melanoma biology, including cell proliferation, invasion, and metastasis, highlighting their potential as valuable targets for elucidating the molecular mechanisms underlying melanoma pathogenesis. Furthermore, the dysregulation of lncRNAs in melanoma has been linked to treatment resistance and poor patient outcomes, highlighting their clinical significance. Investigating the interplay of lncRNAs in melanoma may offer valuable insights into the complex gene regulatory networks driving this aggressive form of skin cancer, with potential implications for the development of novel diagnostic and therapeutic strategies.

The present research endeavors to shed light on the role of pre-defined upregulated lncRNAs in melanoma. To accomplish this objective, the study is structured into two primary components:

- a. A pre-determined range CRISPRi proliferation screen is conducted on one melanoma cell line to validate existing data and discover novel lncRNA targets that are integral to melanoma development.
- b. Functional characterization studies are carried out for the three most promising lncRNA candidates (*BDNF-AS*, *GMDS-AS1*, and *XLOC030781*) identified through preliminary data analysis. These studies examine their impact on cell growth, proliferation, invasion, and subcellular localization. To broaden the scope of understanding, two melanoma cell lines with distinct mutational profiles and metastatic dynamics are employed.

5. Materials and Methods

5.1 Materials

5.1.1 Chemicals and Reagents

Commercial Name	Catalog Number	Supplier
Actinomycin D 93 %	294940010	Acros Orga
Agencourt AMPure XP	A63880	Beckman Coulter™
DNA Ladder 1 kb	N3232S	New England Biolabs
DNA Ladder 100 bp	N3231S	New England Biolabs
30 % Acrylamide/Bis Solution, 37.5:1	1610158	Bio-Rad
7-AAD Solution	61410-00	BioGems
Agarose Powder	A9539	Sigma Aldrich
Ammonium Persulfate	A3678	Sigma Aldrich
Ampicillin Sodium Salt	K029.4	Carl Roth GmbH
Blasticidine S Hydrochloride	15205	Sigma Aldrich
Bovine Serum Albumin, Lyophilized Powder	SAB4200541	Sigma Aldrich
BSA Molecular Biology Grade	B9000S	New England Biolabs
Calcein Am, Fluorescent Dye	ab141420	Abcam
Calcium Chloride Solution	C-34006	Sigma Aldrich
Chloroform	288306	Sigma Aldrich
Chloroform: Isoamyl Alcohol 24:1 Biotech	C0549	Sigma Aldrich
Clarity™ Western ECL Substrate	1705060	Bio-Rad
cOmplete™, Mini, EDTA-free Protease Inhibitor Cocktail	4693159001	Sigma Aldrich
Corning® Matrigel®	356234	Corning BV
DAPI For Molecular Biology	A4099,0010	PanReac Ap
Denhardt's Reagent Solution 50X, DNase Free	BP515-5	Fisher Bio
Dextran Sulphate 500 Sodium Salt for Biology	5956.3	Carl Roth GmbH & Co. KG
Dimethyl Sulfoxide (DMSO), Cell Culture	sc-358801	Santa Cruz Biotechnology Inc
Disinfectant Rapid Bacillo AF	9802143	Bode Local/VWR
Doxycycline Hydrochloride	10224633	Thermo Fisher Scientific
DMEM, High Glucose, Pyruvate	11594486	Gibco
Ethanol, 70 %, For Molecular Biology	BP8201	Sigma Aldrich
EDTA, Molecular Biology Reagent	E5134	Sigma Aldrich
Ethanol, 99.8 %	10644795	Thermo Fisher Scientific
Ethidium Bromide	E1510	Sigma Aldrich
Etoposide	E1383	Sigma Aldrich
Formaldehyde Solution, Molecular Biology	F8775	Sigma Aldrich
Formamide, Deionized, Molecular Biology	F9037	Sigma Aldrich
Gel Loading Dye, Purple 6X	B7025S	New England Biolabs
GlutaMAX Supplement	35050038	Thermo Fisher Scientific
Glycerol Gelatin, Aqueous Slide Mounting	GG1	Sigma Aldrich
Glycerol, 99+%	G/0650/08	Thermo Fisher Scientific
Glycine	G8898	Sigma Aldrich
GlycoBlue™ Coprecipitant	AM9515	Thermo Fisher Scientific

Commercial Name	Catalog Number	Supplier
HBSS, Calcium, Magnesium, No Phenol Red	14025050	Thermo Fisher Scientific
Heparin Sodium Salt	sc-203075	Santa Cruz Biotechnology Inc
HyClone™ Water	SH30538.02	Thermo Fisher Scientific
Hygromycin B Solution	sc-29067	Santa Cruz Biotechnology Inc
Immobilon® -P PVDF	IPVH00005	Merck Millipore
Insulin Solution from Bovine Pancreas 1+	I0516-5ML	Sigma Aldrich
Isopropanol	11398461	Thermo Fisher Scientific
Leibovitz's L-15 Medium	11415049	Thermo Fisher Scientific
MCDB 153 Medium Complete	M7403	Sigma Aldrich
Methanol	176840010	Thermo Fisher Scientific
Molecular Bio Quality Water	SH30538.02	Thermo Fisher Scientific
NEBuffer™ r3.1 10X	B6003S	New England Biolabs
Non-fat Milk Powder	54650	Biomol GmbH
NuPAGE™ LDS Sample Buffer 4X	NP0007	Thermo Fisher Scientific
Oleoyl-L-Alpha lysophosphatidic Acid	L7260	Sigma Aldrich
Opti-MEM™	31985062	Thermo Fisher Scientific
PageRuler™ Prestained Protein Ladder, 10 to 180 kDa	26617	Thermo Fisher Scientific
Paraformaldehyde Fixative Solution	J61984	Alfa Aesar
Penicillin-Streptomycin	P4333	Sigma Aldrich
Phosphate-Buffered Saline (PBS)	45000-446	Corning
Phusion Flash High-Fidelity PCR Master Mix	F548S	Thermo Fisher Scientific
Polybrene	TR-1003-G	Sigma Aldrich
Polyethyleneimine (PEI)	408727	Sigma Aldrich
Polymount Mounting Medium	KHH001	Rockland
Ponceau S	33427.01	Serva
Propidium Iodide Solution	60910-00	BioGems
Proteinase K, Recombinant, PCR Grade	3115828001	Sigma Aldrich
Puromycin Dihydrochloride	sc-108071A	Santa Cruz Biotechnology Inc
RNase AWAY	11952385	Thermo Fisher Scientific
RNasin® Ribonuclease Inhibitor	N2615	Promega
Sodium Acetate 3 M, pH 5.5	AM9740	Thermo Fisher Scientific
Sodium chloride, 5 M Aqua Solution, RNase Free	J60434.AE	Alfa Aesar
Sodium Dodecyl Sulfate (SDS)	L3771	Sigma Aldrich
Sodium Bicarbonate	S6014	Sigma Aldrich
Sodium Hydroxide Solution, Molecular Biology, 10 M	2068	Sigma Aldrich
Sodium Phosphate Dibasic, Molecular Biology	S3264	Sigma Aldrich
SSC Buffer Molecular Biology Grade	42555.01	SERVA Electrophoresis GmbH
TEMED	T7024	Sigma Aldrich
Transfer Membrane Immobilon® - P PVDF	IPVH00005	Merck Millipore
Tris Base 10708976001 Roche	10708976001	Roche
Tris base, DNase RNase Protease Free	10103203	Thermo Fisher Scientific
TRIzol Reagent	T9424	Sigma Aldrich
Trypsin-EDTA (0.05 %)	25300054	Thermo Fisher Scientific
Tween® 20	P9416	Sigma Aldrich
UltraPure™ TAE Buffer 10X	15558042	Thermo Fisher Scientific
Water For Cell Culture	H20CC0501	Millipore

5.1.2 Buffers and Solutions

Name	Components	Method
30 % Probe Hybridization Buffer	30 % Formamide, 5X Sodium Chloride Sodium Citrate (SSC), 9 mM Citric Acid pH 6.0, 0,1 % Tween 20, 60 µg/mL Heparin, 1X Denhardt's Solution, 10 % Dextran Sulfate	FISH
30 % Probe Wash Buffer	30 % Formamide, 5X Sodium Chloride Sodium Citrate (SSC), 9 mM Citric Acid pH 6.0, 0,1 % Tween 20, 60 µg/mL Heparin	FISH
50 % Dextran Sulfate	20 g Dextran Sulfate Powder, fill up to 40 mL with ddH ₂ O	FISH
Amplification Buffer	5X Sodium Chloride Sodium Citrate (SSC), 0,1 % Tween 20, 10 % Dextran Sulfate	FISH
Blocking Buffer	5 % (w/v) Non-fat Dry Milk in TBST Buffer	Immunoblotting
Coating Buffer	0.01 M Tris-HCl pH 8.0, 0.7 % NaCl	Invasion Assay
DPBS, no Calcium, no Magnesium	2.67 mM KCl, 1.47 mM KH ₂ PO ₄ , 136.9 mM NaCl, 8.1 mM Na ₂ HPO ₄ , pH 7.4 in ddH ₂ O	FISH
Fixing Solution	4 % Paraformaldehyde 1X PBS	Flow Cytometry
Flow Buffer	1X PBS/FBS 2 %, 2 mM EDTA (1:250)	Flow Cytometry
Radioimmunoprecipitation assay buffer (RIPA Buffer)	25 mM Tris-base, 150 mM NaCl 1 M, 1 % NP-40, 0.5 % Sodium Deoxycholate (DOC), 0.1 % SDS	Immunoblotting
Resuspension Buffer	Tris 1 M pH 8.0, EDTA 0.5 M pH 8.0, NaCl 5 M, Triton X-100 (10 %, w/v)	Genomic DNA Isolation
SDS Extraction Buffer	Tris-HCl 1 M pH 7.5, EDTA 0.5 M pH 8.0, SDS (10 %, w/v)	Genomic DNA Isolation
SDS Running Buffer	25 mM Tris-base, 192 mM Glycine, 1 % SDS	Immunoblotting
SDS Separation Gel	8-10 % Acrylamide, 0.1 % SDS, 1.5 M Tris-HCl pH 8.8, 0.1 % APS, 0.004 % TEMED in ddH ₂ O	Immunoblotting
SDS Stacking Gel	5 % Acrylamide, 1 M Tris-HCl pH 6.8, 0.1 % SDS, 0.1 % APS, 0.01 % TEMED in ddH ₂ O	Immunoblotting
SSCT 5X	10 mL of 20X SSC, 400 µL of 10 % Tween 20, 29.6 mL ddH ₂ O	Immunoblotting
TAE Buffer	0.4 M Tris-base, 0.01 M EDTA-Na ₂ , 0.2 M Glacial Acetic Acid	Gel Electrophoresis
TBS Buffer	20 mM Tris-base, 150 mM NaCl, pH 7.6	Immunoblotting
TBST Buffer	20 mM Tris-base, 150 mM NaCl, pH 7.6, 0.1 % Tween 20	Immunoblotting
Transfer Buffer	25 mM Tris-base, 192 mM Glycine, pH 8.3, 10 % Methanol	Immunoblotting

5.1.3 Antibodies

Name	Catalog Number	Supplier
Anti-GAPDH Antibody, Mouse Monoclonal	G8795	Sigma Aldrich
Anti-S.P.-Cas9 Antibody, Mouse Monoclonal	14697	Cell Signaling Technology
Anti-Mouse IGG – HRP	A9044	Sigma Aldrich
Anti-Rabbit IGG – HRP	10545	Sigma Aldrich
Anti-PARP1 Antibody, Goat Monoclonal	9542S	Cell Signaling Technology

5.1.4 Enzymes

Commercial Name	Type	Catalog Number	Supplier
DNase I recombinant, RNase-free	DNase	4716728001	Sigma Aldrich
Esp3I (BsmBI)	Restriction Endonuclease	ER0451	Thermo Fisher Scientific
GoTaq® DNA Polymerase	Polymerase	A6001	Promega
JumpStart™ Taq DNA Polymerase	Polymerase	D9307	Sigma Aldrich
Phusion Hot Start II DNA Polymerase	Polymerase	F549S	Sigma Aldrich
Phusion® Hot Start Flex DNA Polymerase	Polymerase	M0535S	New England Biolabs
Rapid Alkaline Phosphatase	Phosphatase	4898133001	Sigma Aldrich
RNase I	RNase	AM2294	Life Technologies
T4 DNA Ligase	Ligase	M0202S	New England Biolabs
T4 Polynucleotide Kinase	Kinase	EK0032	Thermo Fisher Scientific

5.1.5 Kits

Commercial Name	Catalog Number	Supplier
DC(tm) Protein Assay Kit I	5000111	Bio-Rad
DNA Clean & Concentrator-5	D4013	Zymo Research
EdU Click FC-647 ROTI® kit for Flow Cytometry	7783.1	Carl Roth
GoTaq® qPCR Master Mix	A6001	Promega
High-Capacity cDNA Reverse Transcription Kit	4368814	Thermo Fisher Scientific
KAPA Hyper Prep Kit	KR0961	KAPABIOSYSTEMS
Lookout Mycoplasma PCR Detection Kit	MP0035	Sigma Aldrich
OneStep™ PCR Inhibitor Removal Kit	D6030	Zymo Research
QIAGEN Plasmid Midi Kit	12143	Qiagen
QIAprep Spin Miniprep Kit	27104	Qiagen
QIAquick Gel Extraction Kit	28704	Qiagen
QIAquick PCR Purification Kit	28104	Qiagen
QIAseq FastSelect RNA Removal Kit	333390	Qiagen
QIAseq Stranded Total RNA Library Kit	180450	Qiagen

5.1.6 Bacterial Strains

Bacterial Strains	Description	Catalog Number
Stbl3™ <i>E. coli</i>	Chemical Competent Cells	C737303

5.1.7 Cell Lines

Cell Lines	Description	Supplier
501-mel	Metastatic Melanoma Cell Line	CVCL_4633
Lenti-X™ 293T Cell Line	HEK 293T Cell Line	Takara Cat. No. 632180
501-mel SAM	Modified Melanoma Cell Line	Aifantis Lab, NYUMC
501-mel-tetON dCas9 KRAB	Modified Melanoma Cell Line	Aifantis Lab, NYUMC
WM1361A	Modified Melanoma Cell Line	CVCL_6788
WM1361A-tetON dCas9 KRAB	Modified Melanoma Cell Line	Aifantis Lab, NYUMC

5.1.8 Plasmids

Plasmid	Description	Resistance	Addgene
pMD2.G	VSV-G Envelope Expressing Plasmid	Ampicillin	#12259
psPAX2	2nd Generation Lentiviral Packaging Plasmid	Ampicillin	#12260
pLVx-U6se-EF1a-sfPac	Lentiviral sgRNA Expression Vector with Modified Stem Loop driven by U6 Promoter, Puro Resistance and Reporter gene GFP by EF-1alpha Promoter	Amp, Puro	Unknown
Lenti_tetON-dCas9-KRAB	Lentiviral and tet-inducible Expressing Vector Encoding dCas9-KRAB for CRISPRi. Contains mCherry as Fluorescent Protein	Amp, Blast	Unknown
Lenti_sgRNA-(MS2)-puro backbone	Optimized Lenti sgRNA Cloning Backbone with MS2 Loops at Tetraloop and Stem Loop ()	Amp, Puro	#73797

5.1.9 Oligonucleotides

Oligo Name	sgRNA Target Sequence	Purpose	sgRNA 'Cut' Site TSS Offset
sgRNA 1_KRAB_BRAF_F	GCCTGGGCCACCTCAGGTAC	Cloning - BsmBI site	+42
sgRNA 1_KRAB_BRAF_R	GCCTGGGCCACCTCAGGTAC	Cloning - BsmBI site	
sgRNA 2_KRAB_BRAF_F	CCACCTCAGGTACCGGCCCG	Cloning - BsmBI site	+35
sgRNA 2_KRAB_BRAF_R	CCACCTCAGGTACCGGCCCG	Cloning - BsmBI site	
sgRNA 3_KRAB_BRAF_F	GCCATCTTATAACCGAGAGC	Cloning - BsmBI site	+66
sgRNA 3_KRAB_BRAF_R	GCCATCTTATAACCGAGAGC	Cloning - BsmBI site	
sgRNA 1_KRAB_EGFR_F	GGGCGCTCACACCGTGC GGG	Cloning - BsmBI site	+52
sgRNA 1_KRAB_EGFR_R	GGGCGCTCACACCGTGC GGG	Cloning - BsmBI site	
sgRNA 2_KRAB_EGFR_F	GGGCAGCCCCCGGCAGCG	Cloning - BsmBI site	+25
sgRNA 2_KRAB_EGFR_R	GGGCAGCCCCCGGCAGCG	Cloning - BsmBI site	
sgRNA 3_KRAB_EGFR_F	CACGGTGTGAGCGCCCGACG	Cloning - BsmBI site	+38
sgRNA 3_KRAB_EGFR_R	CACGGTGTGAGCGCCCGACG	Cloning - BsmBI site	
sgRNA 1_KRAB_MITF_F	AAAGTGAGAACAGAGCCCGG	Cloning - BsmBI site	+69
sgRNA 1_KRAB_MITF_R	AAAGTGAGAACAGAGCCCGG	Cloning - BsmBI site	
sgRNA 2_KRAB_MITF_F	GCAGAGCTCGGCACTGCGCC	Cloning - BsmBI site	+45
sgRNA 2_KRAB_MITF_R	GCAGAGCTCGGCACTGCGCC	Cloning - BsmBI site	

Oligo Name	sgRNA Target Sequence	Purpose	sgRNA 'Cut' Site TSS Offset
sgRNA 3_KRAB_MITF_F	GTGAGAACAGAGCCCGGGGG	Cloning - BsmBI site	+66
sgRNA 3_KRAB_MITF_R	CCCCCGGGCTCTGTTCTCAC	Cloning - BsmBI site	
sgRNA 1_SAM_BDNF-AS_F	TGAGTGCAGCCGAGGCTCGG	Cloning - BsmBI Site	-142
sgRNA 1_SAM_BDNF-AS_R	TGAGTGCAGCCGAGGCTCGG	Cloning - BsmBI Site	
sgRNA 2_SAM_BDNF-AS_F	CGGCGCTAGGGGAACCCGTG	Cloning - BsmBI Site	-108
sgRNA 2_SAM_BDNF-AS_R	CGGCGCTAGGGGAACCCGTG	Cloning - BsmBI Site	
sgRNA 3_SAM_BDNF-AS_F	CCACAGGAAATGACGACAGA	Cloning - BsmBI Site	-63
sgRNA 3_SAM_BDNF-AS_R	CCACAGGAAATGACGACAGA	Cloning - BsmBI Site	
sgRNA 1_SAM_GMDS-AS1_F	CCGGCCGCCACAGTCTGACAG	Cloning - BsmBI Site	-175
sgRNA 1_SAM_GMDS-AS1_R	CCGGCCGCCACAGTCTGACAG	Cloning - BsmBI Site	
sgRNA 2_SAM_GMDS-AS1_F	GCGCCCCTGTCAGACTGTGG	Cloning - BsmBI Site	-169
sgRNA 2_SAM_GMDS-AS1_R	GCGCCCCTGTCAGACTGTGG	Cloning - BsmBI Site	
sgRNA 3_SAM_GMDS-AS1_F	CCGTGCGCCCCTGTCAGACTG	Cloning - BsmBI Site	-166
sgRNA 3_SAM_GMDS-AS1_R	CCGTGCGCCCCTGTCAGACTG	Cloning - BsmBI Site	
sgRNA 1_SAM_XLOC030781_F	GGCAGCAAAAAGTTGCATCCG	Cloning - BsmBI Site	-24
sgRNA 1_SAM_XLOC030781_R	GGCAGCAAAAAGTTGCATCCG	Cloning - BsmBI Site	
sgRNA 2_SAM_XLOC030781_F	CGGCGGGCGCAAAAATCCGCG	Cloning - BsmBI Site	-110
sgRNA 2_SAM_XLOC030781_R	CGGCGGGCGCAAAAATCCGCG	Cloning - BsmBI Site	
sgRNA 3_SAM_XLOC030781_F	GGCTTTTTGCCCTTGCCACGG	Cloning - BsmBI Site	-177
sgRNA 3_SAM_XLOC030781_R	GGCTTTTTGCCCTTGCCACGG	Cloning - BsmBI Site	
sgRNA 1_SAM_PVT1_F	GGTTGCCCGTGACGTCACGG	Cloning - BsmBI Site	-43
sgRNA 1_SAM_PVT1_R	GGTTGCCCGTGACGTCACGG	Cloning - BsmBI Site	
sgRNA 2_SAM_PVT1_F	GCCGGGACCGAGGACGCACG	Cloning - BsmBI Site	-118
sgRNA 2_SAM_PVT1_R	GCCGGGACCGAGGACGCACG	Cloning - BsmBI Site	
sgRNA 3_SAM_PVT1_F	GCGGGTTGCCCGTGACGTCA	Cloning - BsmBI Site	-40
sgRNA 3_SAM_PVT1_R	GCGGGTTGCCCGTGACGTCA	Cloning - BsmBI Site	

5.1.10 Primers

Primer Name	Sequence 5'→3'	Purpose
BRAF_F	ATCCCAGAGTGCTGTGCTG	RT-qPCR
BRAF_R	GGAAATATCAGTGCCCAACCA	RT-qPCR
EGFR_F	GGCACTTTTGAAGATCATTCTC	RT-qPCR
EGFR_R	CTGTGTTGAGGGCAATGAG	RT-qPCR
MITF_F	CAAAAGTCAACCGCTGAAGA	RT-qPCR
MITF_R	AGGAGCTTATCGGAGGCTTG	RT-qPCR
GAPDH_F	AGCCACATCGCTCAGACAC	RT-qPCR
GAPDH_R	GCCCAATACGACCAAATCC	RT-qPCR
RPA3_F	GACTCTGGGGAGGTGAACTG	RT-qPCR
RPA3_R	GGAGTACTTCTGCAGGATCTGG	RT-qPCR
MS2-P65-HSF1_F	CCATCGCCGCTAACTCAGGTAT	RT-qPCR

Primer Name	Sequence 5'->3'	Purpose
MS2-P65-HSF1_R	TGGTTGCTGATCTGCCCTGAAG	RT-qPCR
CAS9_F	CAGAGAGAACCAGACCACCCAG	RT-qPCR
CAS9_R	TACAGCTTCTCGTTCTGCAGCT	RT-qPCR
XLOC030781_F	TAATTTACGGGCAACCGAAG	RT-qPCR
XLOC030781_R	GGCCAGAAGGTATCCTGTCA	RT-qPCR
BDNF-AS_F1	GGTCCTCATCCAACAGCTCT	RT-qPCR
BDNF-AS_R1	GCAGGTTCAAGAGGCTTGAC	RT-qPCR
BDNF-AS_F2	TGTAGAGATGAGCCCAAGGAG	RT-qPCR
BDNF-AS_R2	CATGTTTGTAGGGAGCCAACA	RT-qPCR
GMDS-AS1_F1	GCACTGCCGAATGTCTAAGA	RT-qPCR
GMDS-AS1_R1	CGTATCTGCGAGACCTGGAT	RT-qPCR
GMDS-AS1_F1	GGTCCATGGAATTGTACGGC	RT-qPCR
GMDS-AS1_R1	TCAATGTGAGCCTGGGGATT	RT-qPCR
BDNF-AS1_F1	CCGCCATGCAATTTCCACTA	RT-qPCR
BDNF-AS1_R1	TTGGTGCCCGGTATGTACT	RT-qPCR
BDNF-AS1_F2	TTAATGAGACACCCACCGCT	RT-qPCR
BDNF-AS1_R2	GGTCCGATTCTGGCTCCA	RT-qPCR
XLOC030781_F1	TAGTGCCCATCAAAGGCTCA	RT-qPCR
XLOC030781_R1	GCTGCCCAGGAACAAAGAAA	RT-qPCR
XLOC030781_F2	TCTGGGCCATTTGAGGGTAG	RT-qPCR
XLOC030781_R2	GGTTGGCTGATGAGAAGCTG	RT-qPCR
BDNF-AS_F1	GGAAGAGGGAAGGAGGTAAAG	RT-qPCR
BDNF-AS_R1	AGAATGAGGGAGGGATGGAG	RT-qPCR
BDNF-AS_F2	GGAAGAGGGAAGGAGGTAAAG	RT-qPCR
BDNF-AS_R2	GGAAGAGATAGAATGAGGGAGG	RT-qPCR
GMDS-AS1_F1	AGTGCCGGAAGGGAAAAG	RT-qPCR
GMDS-AS1_R1	TGATAGGGGACGAAACCAG	RT-qPCR
GMDS-AS1_F2	GCCGAAAGGGAAAAGAAC	RT-qPCR
GMDS-AS1_R2	TGATAGGGGACGAAACCAG	RT-qPCR
PVT1_F	TTACAGGCGTGTGCCACAAAGC	RT-qPCR
PVT1_R	GCCTGTAATCCCAGCACGTTGA	RT-qPCR
EGFR_F	GGCACTTTTGAAGATCATTTTCTC	RT-qPCR
EGFR_R	CTGTGTTGAGGGCAATGAG	RT-qPCR
EF1a_R Seq	TTCTTTTTCGCAACGGGTTTG	RT-qPCR

5.1.11 NGS Primers IncRNA KRAB Library

Primer Name	Sequence 5'->3'
NGS_LIB_KRAB_R1	CAAGCAGAAGACGGCATAACGAGATTCGCCTTGGTGACTGGAGTTCAGACGTGTGCTCTCCGATCTCCGACTCGGTGCCACTTTTTCAA
NGS_LIB_KRAB_R2	CAAGCAGAAGACGGCATAACGAGATATAGCGTCGTGACTGGAGTTCAGACGTGTGCTCTCCGATCTCCGACTCGGTGCCACTTTTTCAA
NGS_LIB_KRAB_R3	CAAGCAGAAGACGGCATAACGAGATGAAGAAGTGTGACTGGAGTTCAGACGTGTGCTCTCCGATCTCCGACTCGGTGCCACTTTTTCAA
NGS_LIB_KRAB_R4	CAAGCAGAAGACGGCATAACGAGATATTCTAGGGTGACTGGAGTTCAGACGTGTGCTCTCCGATCTCCGACTCGGTGCCACTTTTTCAA
NGS_LIB_KRAB_R5	CAAGCAGAAGACGGCATAACGAGATCGTTACCACTGACTGGAGTTCAGACGTGTGCTCTCCGATCTCCGACTCGGTGCCACTTTTTCAA
NGS_LIB_KRAB_R6	CAAGCAGAAGACGGCATAACGAGATGTCTGATGGTGACTGGAGTTCAGACGTGTGCTCTCCGATCTCCGACTCGGTGCCACTTTTTCAA
NGS_LIB_KRAB_R7	CAAGCAGAAGACGGCATAACGAGATTTACGCACGTGACTGGAGTTCAGACGTGTGCTCTCCGATCTCCGACTCGGTGCCACTTTTTCAA
NGS_LIB_KRAB_R8	CAAGCAGAAGACGGCATAACGAGATTTGAATAGGTGACTGGAGTTCAGACGTGTGCTCTCCGATCTCCGACTCGGTGCCACTTTTTCAA
NGS_LIB_KRAB_R9	CAAGCAGAAGACGGCATAACGAGATATCACGGTGACTGGAGTTCAGACGTGTGCTCTCCGATCTCCGACTCGGTGCCACTTTTTCAA
NGS_LIB_KRAB_R10	CAAGCAGAAGACGGCATAACGAGATCGATGTGTGACTGGAGTTCAGACGTGTGCTCTCCGATCTCCGACTCGGTGCCACTTTTTCAA
NGS_LIB_KRAB_R11	CAAGCAGAAGACGGCATAACGAGATCTAGCTTGGTGACTGGAGTTCAGACGTGTGCTCTCCGATCTCCGACTCGGTGCCACTTTTTCAA
NGS_LIB_KRAB_R12	CAAGCAGAAGACGGCATAACGAGATGACGAGAGGTGACTGGAGTTCAGACGTGTGCTCTCCGATCTCCGACTCGGTGCCACTTTTTCAA
NGS_LIB_KRAB_F1	AATGATACGGCGACCACCGAGATCTACACTCTTTCCCTACACGACGCTCTCCGATCTTAAGTAGGCTTTATATATCTTGTGGAAAGGACCTTAAACACC
NGS_LIB_KRAB_F2	AATGATACGGCGACCACCGAGATCTACACTCTTTCCCTACACGACGCTCTCCGATCTATCATGCGCTTTATATATCTTGTGGAAAGGACCTTAAACACC
NGS_LIB_KRAB_F3	AATGATACGGCGACCACCGAGATCTACACTCTTTCCCTACACGACGCTCTCCGATCTGATGCACGCTTTATATATCTTGTGGAAAGGACCTTAAACACC
NGS_LIB_KRAB_F4	AATGATACGGCGACCACCGAGATCTACACTCTTTCCCTACACGACGCTCTCCGATCTCGATTGCGCTTTATATATCTTGTGGAAAGGACCTTAAACACC
NGS_LIB_KRAB_F5	AATGATACGGCGACCACCGAGATCTACACTCTTTCCCTACACGACGCTCTCCGATCTTCGATAGGCTTTATATATCTTGTGGAAAGGACCTTAAACACC
NGS_LIB_KRAB_F6	AATGATACGGCGACCACCGAGATCTACACTCTTTCCCTACACGACGCTCTCCGATCTATCGATAGCTTTATATATCTTGTGGAAAGGACCTTAAACACC
NGS_LIB_KRAB_F7	AATGATACGGCGACCACCGAGATCTACACTCTTTCCCTACACGACGCTCTCCGATCTGATCGATGCTTTATATATCTTGTGGAAAGGACCTTAAACACC
NGS_LIB_KRAB_F8	AATGATACGGCGACCACCGAGATCTACACTCTTTCCCTACACGACGCTCTCCGATCTCGATCGAGCTTTATATATCTTGTGGAAAGGACCTTAAACACC
NGS_LIB_KRAB_F9	AATGATACGGCGACCACCGAGATCTACACTCTTTCCCTACACGACGCTCTCCGATCTACGATCGGCTTTATATATCTTGTGGAAAGGACCTTAAACACC
NGS_LIB_KRAB_F10	AATGATACGGCGACCACCGAGATCTACACTCTTTCCCTACACGACGCTCTCCGATCTTACGATCGCTTTATATATCTTGTGGAAAGGACCTTAAACACC
NGS_LIB_KRAB_F11	AATGATACGGCGACCACCGAGATCTACACTCTTTCCCTACACGACGCTCTCCGATCTACATAGCGCTTTATATATCTTGTGGAAAGGACCTTAAACACC
NGS_LIB_KRAB_F12	AATGATACGGCGACCACCGAGATCTACACTCTTTCCCTACACGACGCTCTCCGATCTTATAACCTGCTTTATATATCTTGTGGAAAGGACCTTAAACACC

5.1.12 Consumables

Commercial Name	Model	Supplier
Amicon® Ultra-15 Centrifugal Filter Unit	UFC910024	Millipore
Aspiration Pipette 2 mL	86.1252.011	Sarstedt AG
BioLite Cell Culture Treated Dishes	11815275	Thermo Fisher Scientific
BioLite™ 96-Well, Cell Culture-Treated, Flat-Bottom Microplate	11835275	Thermo Fisher Scientific
Cell Strainer, 40 µm, Blue, CS50	431750	Corning BV
Cryotube™ 1.8 mL	479-6843	VWR International
CytoOne® Bottle Top Filtration Unit	CC6032-8233	Starlab
Dish TC 15.0 cm Cell ATT TR	734-2818	VWR International
Disposal Bags	HEB-3020	Kisker Biotech
DNA LoBind Tubes, 1.5 mL, PCR Clean	30108051	Eppendorf
Falcon Round Bottom Tubes	C-3082	Neo Lab
Falcon® 10 mL Serological Pipet	356551	Corning
Falcon® 14 mL High Clarity PP Test Tube	352059	Corning
Falcon® 25 mL Serological Pipet	357525	Corning
Falcon® 5 mL Serological Pipet	356543	Corning
Falcon® 5mL Round	352054	Corning BV
Fisherbrand Comfort Nitril Gloves	15642367	Thermo Fisher Scientific
Fisherbrand™ Cell Lifters	11577692	Thermo Fisher Scientific
Fisherbrand™ Easy Reader™ Conical Polypropylene Centrifuge Tubes, 15 mL	05-539-12	Thermo Fisher Scientific
Fisherbrand™ Easy Reader™ Conical Polypropylene Centrifuge Tubes, 50 mL	05-539-9	Thermo Fisher Scientific
Fisherbrand™ Filter Tips 1-200 µL	10102512	Thermo Fisher Scientific
Fisherbrand™ Top-Line Pipette Filter Tips 0.1-10 µL	10366242	Thermo Fisher Scientific
FluoroBlok™ Insert, 24-well Inserts, 8µm Pore	351152	Corning BV
Hard-Shell® 96-Well PCR Plates	HSP9601	Bio-Rad
Inoculation Spreader	86.1569.005	Sarstedt AG
Microseal 'B' PCR Plate Sealing Film	MSB1001	Bio-Rad
PCR Tubes 0.5 mL (Flat Cap)	732-3207	VWR International
Protein LoBind Tubes 1.5 mL, PCR Clean	30108116	Eppendorf
SafeSeal Microcentrifuge Tube 1.5 mL	72.706	Sarstedt AG
SafeSeal Microcentrifuge Tube 2 mL	72.695.500	Sarstedt AG
Single-Use Syringes, 2-Piece, HENKE-JECT®	613-2009	VWR International
Slide Cell Counting Eve	734-2676	VWR International
Stericup Receiver 1000 mL	S200B10RE	Millipore
Syringe Filter PES 33mm 0.2 µM	15206869	Thermo Fisher Scientific
TC Dish 100, Standard	83.3902	Sarstedt AG
TC Flask T25, Stand. Vent. Cap	83.3910.002	Sarstedt AG

Commercial Name	Model	Supplier
TC Flask T75, Stand. Vent. Cap	83.3911.002	Sarstedt AG
TC Plate 6-Well, Standard, F	83.3920.005	Sarstedt AG
Tip Filter 1000 µL Micropoint Graduated	613-0992	VWR International
Tip Filter 20 µL Beveled Graduated	613-0988	VWR International
Tip Filter 200 µL Genomic LR RACK	613-0996	VWR International
Tube Strips 0.2 mL Flat Cap	732-3229	VWR International
µ-Slide 8-Well ibiTreat	80826	Ibidi GmbH

5.1.13 Lab Equipment

Type	Model	Manufacturer
Biological Safety Cabinet	Thermo Heraeus HERAsafe HS12	Thermo Fisher Scientific
Centrifuge	5415R	Eppendorf
Centrifuge	5804R	Eppendorf
Centrifuge	Fisherbrand™ Mini-Centrifuge	Thermo Fisher Scientific
Electrophoresis Chamber	Wide Mini-Sub Cell GT System 1704405	Bio-Rad
Electrophoresis Chamber	Mini-Sub Cell GT Cell 1664400	Bio-Rad
Wide-Field Fluorescence Microscope	Olympus Cell^R	Olympus Live Science
Fluorescence-activated Cell Sorting	BD Accuri C6 Flow Cytometer	BD Biosciences
Fluorescence-activated Cell Sorting	BD FACSCanto II Clinical Flow Cytometry System	BD Biosciences
Fluorescence-activated Cell Sorting	SH800S Cell Sorter	Sony
Gel Visualization System	ChemiDoc™ MP Imaging System	Bio-Rad
Incubator	CO ₂ Incubator Model CB 170	Binder
Microplate Reader	Spark® Multimode Microplate Reader	Tecan
PCR Cycler	Master Cycler EP Gradient 5341	Eppendorf
Pipette	0.5-10 µL Single Channel Microliter Pipettes LLG-proMLP	LLG Labware
Pipette	2-20 µL Single Channel Microliter Pipettes LLG-proMLP	LLG Labware
Pipette	20-200 µL Single Channel Microliter	LLG Labware
Pipette	Pipettes LLG-proMLP 100-1000 µL Single Channel Microliter Pipettes LLG-pomp	LLG Labware
Power Supply	PowerPac™ Basic Power Supply	Bio-Rad
qPCR Cycler	CFX Connect™ Real-Time System	Bio-Rad
Shaking Incubator	Incubator Shaking Series I26	New Brunswick Scientific
Spectrophotometer	Nanodrop™ 2000c	Thermo Fisher Scientific
Vortexer	Scientific Industries SI™ Vortex- Genie™ 2	Thermo Fisher Scientific
Wet/Tank Blotting System	Mini Trans-Blot Electrophoretic Transfer Cell 1703930	Bio-Rad

5.1.14 Software

Name	Description	Supplier
Bio Render	Tool for Scientific Images	Bio Render
Fiji	Image Analysis Software	Open Source
Illustrator	Tool for Figures	Adobe
Image Lab	FACS Analysis Software	TreeStar Inc.
Microsoft Office	Excel, PowerPoint and Word Processor	Microsoft, USA
Photoshop	Image Analysis Software	Adobe
Prism 8.0	Data Analysis Software	GraphPad Software, USA
qPCR Analysis	CFX Maestro	BioRad
Python	Programming Language	R Core Team

5.2 Methods

5.2.1 sgRNA Cloning

5.2.1.1 Vector Preparation

The circular pLVx U6se EF1a sfPac and Lenti-sgRNA-(MS2)-puro-backbone vectors served as an empty backbone to incorporate the synthesized oligo sgRNAs, for a CRISPRi and CRISPRa system correspondingly. Both plasmids contained an antibiotic selection marker for puromycin resistance, and a single BsmBI cloning site which was utilized for the stuffer removal and subsequently the sgRNA integration. Only the pLVx U6se EF1a sfPac vector carried the green fluorescent marker GFP for intracellular detection. At last, both plasmids were compatible with 2nd and 3rd generation lentiviral packaging vectors which were required for sgRNA lentivirus production. 10 µg of each vector were digested with 2 µL BsmBI restriction enzyme in 5 µL NE Buffer 3.1 in a reaction of 50 µL final volume for 3 hours at 55 °C. For self-ligation prevention, the digested vectors were incubated with 1 µL rAPid Alkaline Phosphatase for 1 hour at 37 °C. Thereafter, the open-vector fragments were purified by gel electrophoresis in a 1 % agarose gel at constant 110 V for 1.5 hours. The correct band was excised from the gel and was purified using QIAquick Gel Extraction Kit.

5.2.1.2 Oligonucleotide sgRNA Design and Preparation

The sgRNA sequences for the CRISPR interference system were generated using the web design tool provided by the Broad Institute (~100 nt window downstream of TSS), whereas those for the CRISPR activation system were designed using the online tool Benchling R & D Cloud (~200 nt window upstream of TSS), keeping in both cases in consideration the site recommendations regarding the highest on-target and lowest off-target matches. The oligos were of 20-21 bp length and designed in a formation where 2 overhangs (forward oligo: 5'CACC, reverse oligo: 5'AAAC) were created after the forward and reverse strands matched upon complementarity. The transcription start site was depicted by the addition of a 'G/C' before the oligo sequence, in the cases where the forward oligo didn't begin with G. Firstly, the oligos were phosphorylated at the 5'-end, by mixing 1 µL of each pair of forward and reverse oligo (100 µM) with 0.5 µL T4 polynucleotide kinase (PNK) in 1 µL T4 PNK buffer 10X and 6.5 µL ddH₂O, for 30 minutes at 37 °C. Afterwards, the phosphorylated oligos were annealed by incubation for 5 minutes at 95 °C forming oligo duplexes, and were left on the heatblock to cool down to room temperature.

5.2.1.3 Ligation and Chemical Transformation

25 ng purified digested pLVx U6se EF1a sfPac/ Lenti-sgRNA-(MS2)-puro-backbone vector were ligated with 1 μ L diluted 1:200 oligo duplexes in 6.5 μ L ddH₂O supplemented with 1 μ L T4 DNA Ligase and 1 μ L T4 DNA Ligase buffer 10X for 1 hour at room temperature. Thereafter, the whole ligation reaction was used for chemical transformation of Stb13 competent cells as described in section 5.2.2. With respect to the CRISPRi system, three separate sgRNA sequences were devised for the protein coding genes *BRAF*, *EGFR*, and *MITF*. The CRISPRi IncRNA screen utilized the most efficient sgRNA for each gene as a positive control. Conversely, for the CRISPRa system, three sgRNA sequences were designed specifically for the IncRNAs *BDNF-AS*, *GMDS-AS1*, *XLOC030781*, and *PVT1*. The invasion assay employed the sgRNA sequence that resulted in the highest overexpression.

5.2.2 Transformation of Chemical Competent Stb13 *Escherichia coli* Cells

The Stb13™ *E. coli* strain originates from the HB101 *E. coli* strain, is ideal for high-efficiency chemical transformation and reduces the probability of recombination especially for challenging cloning experiments that involve plasmid vectors prone to DNA recombination. One vial of One Shot® Stb13™ cells was thawed on ice. 10 μ L of the ligation reaction described at section 5.2.1.3, were added to the vial containing the competent cells and were mixed gently. The mixture was incubated on ice for 30 minutes. Thereafter, cells went through heat-shock for approximately 45 seconds at 42 °C on a heatblock without shaking and then were placed on ice for 2 minutes. 250 μ L of pre-warmed Super Optimal Broth (S.O.C) bacterial medium were added to the vial and cells were incubated for 1 hour at 37 °C on a heatblock under continuous agitation. 100 μ L of the mixture were spread on a pre-warmed LB agar plate and were incubated overnight at 37 °C. On the following day, distinct colonies were selected for plasmid isolation.

5.2.3 Plasmid DNA Purification

To obtain significant amounts of DNA plasmids, which have been integrated and amplified using chemically competent Stb13 cells through transformation, distinct single colonies were carefully chosen from the LB agar plates with a pipette tip in the presence of a Bunsen burner. 5 mL liquid LB cultures supplemented with 100 μ g/mL ampicillin in sterile plastic tubes were inoculated separately with the pipette tips carrying the bacterial colonies and were incubated overnight in a bacterial incubator at 37 °C with continuous agitation. The specific requirements for further experiments on each plasmid determined whether a mini/midi or max preparation method was used to isolate the plasmid DNA. For a mini prep, the 5 mL liquid LB culture was centrifuged at 3,000 $\times g$ for 5 minutes and the cell pellet was handled following the

standard protocol included in the QIAGEN Plasmid Mini Kit. For a midi or maxi prep, an additional step was required, a larger volume of LB bacterial culture had to be produced. The 5 mL liquid LB culture after 8 hours incubation at 37 °C with continuous agitation, were used for inoculation of 95 mL or 495 mL liquid LB, always enriched with 100 µg/mL ampicillin for a midi or a maxi prep respectively. The cultures were incubated overnight at 37 °C with vigorous shaking and on the following day were centrifuged at 3,000 *x g* for 5 minutes. Subsequently, the cell pellet was used for plasmid DNA isolation following standard procedure protocol described in QIAGEN Plasmid Midi and Maxi Kits. The DNA plasmids were redissolved in TE buffer pH 8.0, their concentration was measured using Nanodrop™ 2000c and were stored at -20 °C till further use. The correct plasmid isolation was confirmed by Sanger Sequencing.

5.2.4 Cell Culture Methods

5.2.4.1 Cultivation of Mammalian Cells

Human melanoma cell lines 501-mel, its CRISPRa and CRISPRi stable cell lines 501-mel SAM and 501-mel-tetON dCas9 KRAB respectively and WM316A were provided by Aifantis Lab, NYU. WM1361A-tetON dCas9 KRAB cell line was produced specifically for the purposes of this doctoral research. Human embryonic kidney Lenti-X 293T cells were purchased from Takara Bio. The cancer cell lines were maintained in the recommended growth medium according to ATTC protocols. 501-mel, 501-mel SAM, 501-mel-tetON dCas9 KRAB and Lenti-X 293T were grown as monolayer adherent cultures in Gibco Dulbecco's modified Eagle's medium (DMEM), high glucose with pyruvate supplemented with 10 % (v/v) fetal bovine serum (FBS) and 1 % (v/v) penicillin/streptomycin. WM1361A and WM1361A-tetON dCas9 KRAB were cultured in medium containing 80 % (v/v) MCD B153 with trace elements, L-glutamine and 28 mM HEPES, 20 % (v/v) Leibovitz L-15, and supplemented with 1.2 g/L NaHCO₃, 2 % heat inactivated FBS, 1.68 mM CaCl₂, 5 µg/mL insulin from bovine pancreas and 1 % (v/v) penicillin/streptomycin. All cell lines were cultivated in a humidified incubator at 37 °C and 5 % CO₂. Cells were tested negative for Mycoplasma contamination.

5.2.4.2 Production of Conditioned Medium - TU 2 %

The composition of TU 2 % was as follows: 80 % (v/v) MCDB 153, 20 % (v/v) Leibovitz's L-15, 2 % (v/v) FBS, 5 µg/mL bovine insulin, 1.68 mM CaCl₂ and 1 % (v/v) penicillin/streptomycin. All the ingredients were available, except for MCDB 153, which required preparation. In a clean 1 L Schott bottle, 900 mL ddH₂O, the powder content of a vial of MCDB 153 growth medium and a stirring magnet were added, and it was allowed to dissolve on a magnetic-stirrer device for 15 minutes at room temperature. Subsequently 1.2 g sodium bicarbonate were added, and the pH of the solution was adjusted to 7.5 by adding NaOH 5 M slowly, using a pH meter. The volume was adjusted to 1 L by adding ddH₂O. In order to produce the complete growth medium appropriate for the WM1361A melanoma cell line, the solution was sterile filtered using CytoOne® Bottle Top Filtration Unit to become suitable for cell culture use. For the production of 500 mL TU 2 %, 400 mL MCDB 153 were mixed with 100 mL Leibovitz's L-15, 10.2 mL FBS, 5 mL penicillin/streptomycin, 250 µL insulin 10 mg/mL and 345 µL CaCl₂ 2.5 M.

5.2.4.3 Subculturing and Seeding of Mammalian Cells

Cells were cultured in their respective growth medium until they reached 80 % confluency. Grown medium was aspirated from the cell vessel and the formed monolayer was gently washed once with PBS 1X to prevent cell disturbance. Pre-warmed Trypsin-EDTA solution was added, and the cell vessel was incubated for 2-4 minutes at 37 °C, until signs of cell detachment were noticeable. The cell vessel was lightly tapped, when necessary, to dislodge cells further. For trypsin neutralization, a sufficient pre-warmed amount of growth medium (equivalent of 2 volumes used for the dissociation agent) was added, and the cells were pipetted up and down until a homogenous single cell suspension was obtained. The cell suspension was transferred in a 50 mL Falcon tube and was centrifuged at 500 x *g* for 5 minutes. Pre-warmed medium was added to guarantee complete resuspension of the cell pellet and cell number determination was acquired with the automated cell counter Countness II and Trypan Blue staining. The desired number of cells was transferred into a new cell culture vessel containing the appropriate type and volume of growing medium.

5.2.4.4 Cryopreservation of Mammalian Cells

Cell lines in continuous long-term culture are susceptible to senescence, microbial contamination and genetic alterations. Cryopreservation was used to assure the successful maintenance of established cell lines. Cells were harvested by trypsinization, centrifuged at $500 \times g$ for 5 minutes. The cell pellet was washed once with PBS 1X. After centrifugation, cells were resuspended in freezing medium which contained 90 % FBS and 10 % cryoprotective agent such as dimethyl sulfoxide (DMSO), aliquoted into cryovials, transferred to a Mr. Frosty™ Freezing Container and stored at $-80 \text{ }^{\circ}\text{C}$. The following day the vials were transferred in a liquid nitrogen cell tank until further required.

5.2.4.5 Lentivirus Production

Lentiviral particles were produced by a standardized three-plasmid transfection protocol. One day before transfection, 10^7 Lenti-X 293T cells were plated in a 150 mm cell culture dish in 10 mL complete DMEM culture medium. 24 hours later the medium was changed, and the transfection was performed with the following mixed cocktail of two sterilized 1.5 mL Eppendorf tubes. One tube contained 1.2 mL of Opti-MEM I Reduced Medium with 22.5 μg of transfer plasmid, 16.5 μg of psPAX2 (viral packaging plasmid) and 11 μg of pMD2.G (viral envelope plasmid), while the other tube contained 1.2 mL of Opti-MEM and 75 μL of PEI transfecting reagent. The mixed solution was incubated for 15 minutes at room temperature, and was added drop wise to the cells. After 24 hours, the growth medium was replaced. On the three following days, virus supernatants were harvested in 50 mL falcon tubes and stored at $4 \text{ }^{\circ}\text{C}$. Supernatants were centrifuged for 5 minutes at $500 \times g$ and subsequently cleared of any cell debris through a $0.2 \text{ }\mu\text{m}$ filter. The filtered supernatant was concentrated using concentrating filter units for 30 minutes to 1 hour at $2,000 \times g$, then aliquoted 50 μL in 1.5 mL Eppendorf tubes and stored at $-80 \text{ }^{\circ}\text{C}$.

5.2.4.6 Lentivirus Transduction

Target cell lines were plated each in 6-well culture plates using a seeding density (2.5×10^5 cells/well for 501-mel SAM and 501-mel-tetON dCas9 KRAB, 2×10^5 cells/well for WM1361A-tetON dCas9 KRAB) that guaranteed $\sim 80 \%$ confluency on the following day, on which the virus infection was performed. The cell growth medium was changed to fresh culture medium containing 8.0 $\mu\text{g}/\text{mL}$ of polybrene and 50 to 100 μL of concentrated sgRNA lentivirus was added drop wise. 24 hours post infection, the virus-containing medium was changed to fresh growth medium appropriate for each cell line and cells were left to recover. 48 hours post infection, 2.0 $\mu\text{g}/\text{mL}$ puromycin was added to the cells in order to select stable modified cell

lines. The duration of the antibiotic selection varied amongst the cell lines from 2-5 days, until all cells in the negative control wells died.

5.2.4.7 Apoptosis Assay by Immunoblotting

Apoptosis is a type of programmed cell death, which is enforced by a class of cysteine proteases called caspases. Caspases are synthesized in the form of inactive enzymes (pro-caspases) and get stimulated by a cascade of cleavage reactions. Observation of caspase cleavage by immunoblotting is a common method to showcase the induction of apoptosis. To investigate the potential role of the lncRNA candidates *BDNF-AS*, *GMDS-AS1* and *XLOC030781* in the initiation of apoptotic mechanisms, their expression was downregulated using a CRISPRi system. In more detail, 501-mel-tetON dCas9 KRAB and WM1361A-tetON dCas9 KRAB cell lines were cultured in the presence of 2 µg/mL doxycycline, to induce the expression of dCas9, and subsequently 2.0×10^5 cell/well were seeded in 6-well cell culture plates. On the following day, cells were infected with 50 µL sgRNA lentivirus of the respective lncRNAs in separate wells. One well was infected with 50 µL lentivirus sgROSA (non-targeting sgRNA) as negative control and one well was later treated with Etoposide as positive control for apoptosis. 24 hours post infection, the appropriate growth medium for each cell line supplemented with 2 µg/mL doxycycline was renewed. 72 hours post infection, the growth medium was changed again and 150 µM of Etoposide were added in the respective well marked as positive control. For the next 48 hours there was no growth medium renewal, only 2 µg/mL doxycycline were added to keep the dCas9 expression constant. After this period of time, the supernatant for each well was collected in a 15 mL separate labeled conical tube. Cells were washed with cold PBS 1X, trypsinized and after detachment were added in the corresponding conical tube. After centrifugation at $500 \times g$ for 5 minutes, the supernatant was aspirated, and the cell pellet was washed once with PBS 1X and collected in a 1.5 mL low-protein binding tube. Thereafter, the samples were used for immunoblotting in accordance with the protocol described in section 5.2.8. As primary antibodies, anti-PARP1 antibody was used to detect the endogenous levels of full length PARP1 (116 kDa), as well as the large fragment (89 kDa) of PARP1 resulting from caspase cleavage and also anti-GAPDH antibody as reference protein.

5.2.4.8 Cell Cycle Analysis by Flow Cytometry

To investigate the cell cycle phase distribution, the cellular DNA content was stained with a fluorescent dye and its intensity was measured by employing flow cytometry. The DNA staining was performed with two different protocols.

5.2.4.8.1 Click-iT EdU Cell Proliferation Assay

This assay utilized 5-ethynyl-2'-deoxyuridine (EdU) as a nucleoside analog to thymidine, which was incorporated into the newly synthesized DNA during active DNA replication. Unlike Bromodeoxyuridine (BrdU), EdU didn't require staining with antibodies to be detected. It was easily labeled with a fluorescent dye and afterwards the proportions of cells in the different cell cycle stages were quantified by flow cytometry. 2.5×10^5 cells of 501-mel, 501-mel-tetON dCas9 KRAB, WM1361A and WM1361A-tetON dCas9 KRAB were seeded in 6-well cell culture plates. The parental melanoma cell lines 501-mel and WM1361A were used for the set up and adjustment of the flow cytometer settings, since the CRISPRi cell lines carried a fluorescent marker (mCherry/Red) for the detection of dCas9 expression and the sgRNA lentiviruses also carried a fluorescent marker (GFP/Green) for the successful confirmation of cell transduction. The CRISPRi cell lines were kept under constant treatment with 2 $\mu\text{g}/\text{mL}$ doxycycline during the experiment for induction of dCas9 expression. On the following day of seeding, 501-mel-tetON dCas9 KRAB and WM1361A-tetON dCas9 KRAB cells were infected with 50 μL of one sgRNA lentivirus for each lncRNA *BDNF-AS*, *GMDS-AS1* and *XLOC030781* in separate wells and 50 μL of sgROSA as negative control. 24 hours post infection, the growth medium was changed. 48 hours post infection, 1 $\mu\text{g}/\text{mL}$ Actinomycin D was added in the wells marked as positive control. 72 hours post infection, all cells were incubated for 2 hours with EdU by renewing the appropriate growth medium for each cell line, which was supplemented with 10 μM EdU as final concentration. Thereafter, the growth medium was aspirated, cells were washed and detached with 2 mL 1 % BSA in PBS 1X, collected in 15 mL conical tubes and centrifuged at $500 \times g$ for 4 minutes. The cell pellet was resuspended with 100 μL fixative solution (provided with the EdU Click FC-647 ROTI® Kit) and incubated for 15 minutes at room temperature protected from light. The fixative solution was carefully removed with centrifugation. Cells were washed with 2 mL 1 % BSA in PBS 1X and 100 μL 1X saponin-based permeabilization buffer in PBS 1X (provided with the Kit) was added to the cell pellet. The assay cocktail, containing fluorescent dye Eterneon-Red 645 Azide (Infrared), was prepared following strictly the manufacturer's instructions. The cells were mixed well with the assay cocktail and were incubated for 30 minutes at room temperature in the absence of light. Cells were washed with 2 mL 1X saponin-based permeabilization and wash reagent (provided in the Kit) and the cell pellet was resuspended in 500 μL of the reagent. The samples were ready for analysis through flow cytometry.

5.2.4.8.2 Staining with 7-AAD Solution

The cells were treated as previously described in section 5.2.4.8.1, up to the point where Actinomycin D was added in the wells marked as positive control. 72 hours post infection, cells were washed twice with PBS 1X, trypsinized and collected in 15 mL conical tubes. Supernatant was removed and the cell pellet was resuspended in 1 mL PBS 1X. Cells were counted so that 1.0×10^6 cells were distributed in each FACS tube. 3 mL ice cold 70 % ethanol for molecular biology were added dropwise in the cell solution while mixing. Cells were incubated for 1 hour at 4 °C. Afterwards, cells were washed twice with 1 mL PBS 1X, mixed with 200 μ L in-house staining solution buffer containing 7-AAD (Infrared) (Table 5.1.2) and incubated for 30 minutes at room temperature protected from light. Cells were washed twice with 1 mL PBS 1X, resuspended in 300 μ L in-house flow buffer (Table 5.1.2) and were ready for flow cytometry analysis.

5.2.4.9.1 Transwell Invasion Assay

To investigate the involvement of the lncRNA candidates in cell invasion phenomena, their expression was upregulated and downregulated utilizing a CRISPRa and CRISPRi system respectively. 501-mel SAM (CRISPRa) and 501-mel-tetON dCas9 KRAB (CRISPRi) cell lines were used in a transwell invasion assay. The same protocol was followed for both cell lines with two main differences. 501-mel SAM cell line didn't carry a doxycycline inducible dCas9 transgene and secondly the seeding number for each cell line was different. More analytically, FluoroBlok™ 24-well inserts with 8.0 μ m colored PET Membrane were coated with Matrigel for 2 hours at 37 °C. Prior to use, Matrigel was diluted to 1:40 at a final concentration of 300 μ g/mL in coating buffer solution (0.01 M Tris-HCl pH 8.0, 0.7 % NaCl). 100 μ L diluted Matrigel were added per insert. After incubation, residual Matrigel was removed carefully from the inserts, not to disrupt the layer that was created on the top surface of the insert's membrane, and 5×10^4 cells 501-mel SAM and 1.4×10^5 501-mel-tetON dCas9 KRAB cells were seeded per insert in 300 μ L serum-free growth medium. Cells were allowed to settle for 10 minutes. The lower chamber of the 24-well cell culture plate was filled with 700 μ L complete growth medium with 1 μ M Lysophosphatidic acid (LPA). LPA is considered an invasion stimulator¹⁸⁵. Cells were incubated for 48 hours at 37 °C. Thereafter, growth medium was aspirated from the upper chamber and the inserts were transferred to a new 24-well cell culture plate. Invading live cells were stained with 500 μ L per insert Calcein AM 2 μ g/mL in HBSS 1X and were incubated for 10 minutes at 37 °C before imaging. For each independent experiment, uncoated inserts were used as invasion controls, 3 inserts were used per condition, 501-mel-tetON dCas9 KRAB cells before harvesting were under 2 μ g/mL doxycycline treatment for 72 hours and cultured in serum-free growth medium the day before. One sgRNA was used per lncRNA candidate, sgNeg. Ctrl as CRISPRa control and sgROSA as CRISPRi control. An

inverted fluorescence microscope with an objective of 10X was used for live imaging. Images were taken from a complete diameter either vertically or horizontally from randomly selected areas.

5.2.4.9.2 Quantification of Invading Cells

Invading cells were counted using the following automated macro in ImageJ (FIJI)¹⁸⁶:

```
macro "Batch Convert to Binary" {
dir = getDirectory("Choose a Directory ");
list = getFileList(dir);
setBatchMode(true);
for (i=0; i<list.length; i++) {
path = dir+list[i];
open(path);
run("8-bit");
setAutoThreshold();
run("Threshold...");
setThreshold(30, 255);
run("Convert to Mask");
setThreshold(255, 255);
run("Watershed");
run("Analyze Particles...", "size=400-Infinity circularity=0.00-1.00 show=Outlines display clear summarize");
dotIndex = lastIndexOf(path, ".");
if (dotIndex!=-1)
path = substring(path, 0, dotIndex); // remove extension
save(path+"-bin.tif");
close();
}
}
saveAs("Text");
dir = getDirectory("Choose a Directory ");
list = getFileList(dir);
```

5.2.4.10 RNA-Fluorescence *in situ* Hybridization [FISH]

5.2.4.10.1 Preparation of fixed mammalian cells on a chambered slide

Firstly, each chamber of an Ibidi μ -Slide 8 well slide was coated by adding 300 μ L of 0.01 % poly-D-lysine, which was prepared in cell culture grade H₂O, and the slides were incubated for minimum 30 minutes at room temperature. The coating solution was carefully removed, and the slide chambers were washed thoroughly with molecular grade H₂O. Thereafter, 2.0×10^4 cells/chamber were seeded and were left to proliferate to desired confluency for 48 hours. After 2 days the growth medium was removed from each chamber, and cells were washed with 300 μ L of DPBS 1X. Fixation preparation was initiated by adding 300 μ L of 4 % formaldehyde. The cells were incubated for 10 minutes at room temperature, the fixative was removed carefully since its characterized by hazardous properties, and each chamber was washed twice with 300 μ L of DPBS 1X. After the second DPBS wash, 300 μ L of ice-cold 70 % ethanol for molecular biology were added. Cells were permeabilized overnight at -20 °C. Here upon, cells could be stored -20 °C or 4 °C until use.

5.2.4.10.2 Multiplexed *in situ* HCR v3.0

Detection Stage

Ethanol was removed from the chambers and samples air dried at room temperature. The chambers were washed twice with 300 μ L of SSC 2X. Samples were pre-hybridized in 300 μ L of 30 % probe hybridization buffer for 30 minutes at 37 °C. The buffer was aspirated, and the probe solution was added. Probe solution consists of 3 pmol of each probe mixture with 300 μ L of 30 % probe hybridization buffer at 37 °C. Samples were incubated overnight at 37 °C. Excess probes were removed by washing 4 times for 5 minutes with 300 μ L of 30 % pre-warmed probe wash buffer at 37 °C. Finally, samples were washed twice for 5 minutes with SSCT 5X at RT.

Amplification Stage

Samples were pre-amplified in 300 μ L of amplification buffer for 30 minutes at 37 °C. Hairpin solution was prepared in two steps, firstly by separately snap cooling 18 pmol of hairpin H1 and 18 pmol of hairpin H2 (6 μ L of 3 μ M stock). This was performed by heating the hairpins in separate tubes for 90 seconds at 95 °C and then cool to room temperature in a dark drawer for 30 minutes with light protection. Second step included the addition of all snap-cooled hairpins in 300 μ L of amplification buffer at room temperature. The clear amplification buffer that was used for the pre-amplification was removed from the samples and the hairpin solution was added. Samples were incubated for 60 minutes in the dark at room temperature. The following day excess of hairpins was removed by washing 5 times for 5 minutes with 300 μ L of SSCT

5X at room temperature. Lastly, samples were stained with 1 µg/mL DAPI for nuclei detection, through incubation for 1-4 minutes, while being protected from light and then were washed 3 times with PBS 1X.

Probe Sequences Design

Candidate probe sequences for our respective lncRNA targets were designed by Molecular Instruments® (MI) based on their RNA sequence. Alignment to the human transcriptome was performed to minimize off-target complementarity to random genomic regions and to maximize specificity to distinctive regions of the lncRNA candidates.

5.2.4.11 Lentivirus Titration by Flow Cytometry

Prior to performing the CRISPRi screen, the quantification of the infectious lentiviral vector titer of the sgRNAs used for the 4 positive controls (*BRAF*, *EGFR*, *MITF* and *RPA3*) and the lncRNA KRAB library, was obligatory. Therefore, 2.5×10^5 cells of 501-mel-tetON dCas9 KRAB were seeded in 6-well culture plates. Cells were under 2 µg/mL doxycycline for 3 days to ensure the robust dCas9 expression before seeding. One 6-well culture plate was used for each sgRNA lentivirus. As stated before, 501-mel-tetON dCas9 KRAB cell line carried a red fluorescent marker (mcherry), indicative of dCas9 expression, and the sgRNA lentiviruses carried a green fluorescent marker (GFP), which confirmed successful cell transduction. Because the titer determination was implemented using flow cytometry, it was essential to have one negative control (no-color) to adjust the instrument to the experiment's settings and also single-color controls to be able to separate the cells according to their state (infected/not infected, expressing dCas9/not expressing dCas9, expressing dCas9 and infected), thus 2.5×10^5 cells of 501-mel parental were seeded in two wells of a 6-well culture plate; one would serve as the no-color control and the other as the infected-control (green). Additionally, 2.5×10^5 cells of 501-mel-tetON dCas9 KRAB were seeded in two other wells; one well would serve as the only expressing dCas9 control (red) and the other would serve as the control for counting the number of cells prior to infection.

501-mel parental and 501-mel-tetON dCas9 KRAB cells were cultured in 2 mL complete DMEM medium without and with 2 µg/mL doxycycline respectively. After 24 hours, before performing the lentiviral infection, firstly the appropriate culture medium for each cell line was changed and supplemented with 8 µg/mL polybrene (except for the no-colour and red-control well where no polybrene was required). Subsequently, 10-fold serial dilutions tubes were created separately for each lentivirus in 1.5 mL sterile Eppendorf as follows: 45 µL of complete DMEM medium were added in 3 different tubes for each lentivirus and labeled 1/10X, 1/100X, and 1/1,000X. 5 µL of each concentrated lentivirus were added in the labeled 1/10X tube, then the solution was mixed properly and 5 µL diluted lentivirus were transferred to the 1/100X tube. Similarly, the solution in 1/100X tube was mixed and 5 µL diluted lentivirus were transferred to the 1/1,000X tube. Afterwards the number of cells in the well with 501-mel-tetON dCas9 KRAB was recorded.

As already stated, separate 6-well culture plates were used for each lentivirus; four wells were seeded and were labeled: 1X, 1/10X, 1/100X and 1/1,000X. During infection 5 μ L of concentrated/diluted lentivirus infected the corresponding wells so that the final lentiviral volume was 5 μ L/2 mL in the 1X well, 0.5 μ L/2 mL in the 1/10X well, 0.05 μ L/2 mL in the 1/100X well and 0.005 μ L/2 mL in the 1/1,000X well. For the infection in the green-control well, the type and volume of lentivirus was irrelevant, so 30 μ L of one randomly chosen concentrated lentivirus were used to ensure a good signal. The double positive mCherry-GFP and GFP positive single 501-mel-tetON dCas9 KRAB cells were detected using a flow cytometer 24 hours and 48 hours post infection.

For the determination of the lentivirus titer, from the acquired data, the timepoint/dilution that was selected for the calculations was based on the infection rate being strictly between 1-20 % for each lentivirus to ensure that the lentiviral replication was within the linear growth phase. Then the titer in viral particles/mL (TU/mL) was calculated using the formula^{187,188}.

$$\text{TU/mL} = (\text{no. of cells at transduction} \times \% \text{ mCherry-GFP cells} \div 100) \div (\text{virus input volume} \times \text{dilution factor})$$

5.2.4.12 CRISPRi Proliferation lncRNA Screen

For the CRISPRi lncRNA screen, the in-house 501-mel-tetON dCas9 KRAB cell line was used, that had incorporated the dCas9-KRAB gene, labeled with a red fluorescent marker (mCherry). It was crucial to ensure that upon the lentiviral infection more than 95 % of the cells were expressing the protein dCas9-KRAB. Therefore prior to performing the experiment, 501-mel-tetON dCas9 KRAB cells were cultured under constant treatment with 2 μ g/mL doxycycline to maintain continuous expression of dCas9, were frequently checked under a fluorescent inverted microscope and underwent two rounds of sorting through flow cytometry where the mCherry positive cells were collected and expanded. For the conduction of the screen the in-house lncRNA CRISPRi library 1.0 was utilized, which comprised of 2,761 sgRNAs (10 sgRNAs per lncRNA gene and 50 negative scrambled sgRNA controls) and the transduction was carried out using MOI=0.3, so that each cell only received one genetic perturbation. In addition, four sgRNAs targeting the protein-coding genes *BRAF*, *EGFR*, *MITF* and *RPA3* (one sgRNA per gene) were used as positive controls and were spiked-in during infection at an MOI_{single}=0.005 each. Our aim was to achieve a coverage of 1,000X, equivalent to infecting 1,000 cells with an individual sgRNA. To calculate the minimum number of cells required at the infection point, we used the formula:

$$(\text{sgRNA Library size} \times \text{Coverage}) \div 0.3 \text{ MOI} = \text{starting cell number}$$

The screening vessel format was 150 mm cell culture plates. We used two technical replicates, and one negative control. Cells were cultured the last three days before infection with complete DMEM medium but without doxycycline, to avoid leakiness, thus no sgRNAs would over-compete others. Based on the formula, the required number of cells at infection point was $\sim 9.2 \times 10^6$ cells, so 7.7×10^6 501-mel-tetON

dCas9 KRAB cells were seeded in each 150 mm cell culture plate the day before infection. Two 150 mm cell culture plates for the two technical replicates, one 150 mm cell culture plate for the negative control and one 150 mm cell culture plate for counting the initial cell number. On the following day, the cells were counted, and the number was recorded. Using the TU/mL for each lentivirus, the volume required for infection was calculated based on the two formulas:

$$(\text{desired MOI}) \times (\text{total number of cells at starting point}) = \text{total TU needed}$$

$$(\text{total TU needed}) / (\text{TU/mL lentiviral titer}) = \text{total mL of lentiviral particles}$$

Infection was performed and the following day the growth medium was changed supplemented with 2 µg/mL puromycin in the 150 mm cell culture plates of two technical replicates and the negative control. Puromycin was used for the sgRNA selection, and it lasted for three sequential days. Afterwards, selection ended, and the growth medium was changed with new, supplemented with 2 µg/mL doxycycline *only* in the two 150 mm plates of the technical replicates and was renewed frequently till the end of the screen. On the contrary, there was no doxycycline added in the 150 mm plate of the negative control. The screen lasted 28 days and cells were frequently passaged to keep constant the 1,000X coverage. On day 7 after infection, pellet from $\sim 2.76 \times 10^6$ cells (=1,000X coverage) was collected from all 3 plates and that served as the control set point 0. Subsequently, cell pellet (same number of cells every time as above) was collected on day 14 and it served as day 7, day 21 as day 14 and day 27 as day 21. Genomic DNA was extracted from all samples and underwent preparation for sgRNA sequencing. A timeline graph is included in the results section.

5.2.4.13 Preparation of CRISPRi sgRNA Library for Next Generation Sequencing Analysis

Genomic DNA Isolation

Genomic DNA was harvested on pre-determined timepoints (Day 7, Day 14, Day 21 and Day 28) during the CRISPRi lncRNA melanoma Screen from a sufficient number of cells to maintain a coverage of 1,000X. The lncRNA sgRNA library 1.0 consisted of 2,761 unique sgRNAs, therefore a minimum of $\sim 2,761 \times 10^6$ cells were required, so 3.5×10^6 cells were collected. The growth medium was aspirated from 150 mm cell culture dishes, cells were washed with PBS 1X, subsequently redissolved in 1 mL resuspension buffer (Tris 1 M pH 8.0, EDTA 0.5 M pH 8.0, NaCl 5 M, Triton X-100 (10 %, w/v)) and centrifuged at $500 \times g$ for 5 minutes at 4 °C. Supernatant was removed and the cell pellet was resuspended thoroughly in 500 µL SDS extraction buffer (Tris-HCl 1 M pH 7.5, EDTA 0.5 M pH 8.0, SDS (10 %, w/v)) to initiate cell lysis. 50 µL Proteinase K 100 µg/mL were added and the mixture was incubated for 15 minutes at 65 °C. After incubation, 60 µL NaOAc 0.3 M were added with smooth blending. 600 µL phenol:chloroform:isoamyl alcohol were added and the cell solution was centrifuged at $1,000 \times g$ for 5 minutes. The aqueous phase was carefully removed and 1 µL Glycoblue and 2.5 volumes equivalent to the aqueous phase volume, ice-cold absolute ethanol were

added. The mixture was kept for 1 hour at $-80\text{ }^{\circ}\text{C}$ and later was centrifuged at $12,000 \times g$ for 30 minutes at $4\text{ }^{\circ}\text{C}$. The supernatant was aspirated, the pellet was resuspended with $500\text{ }\mu\text{L}$ 70% ethanol and again centrifuged at $12,000 \times g$ for 30 minutes at $4\text{ }^{\circ}\text{C}$. The supernatant was removed, the cell pellet got air dried, was resuspended in $100\text{ }\mu\text{L}$ PCR-grade water and quantified on Nanodrop™ 2000c.

Genomic DNA Purification

Since the DNA samples were intended for NGS analysis, it was essential for the isolated DNA to be purified from any contaminants and especially melanin which melanoma cells contain in high concentration. For this purpose, the DNA samples were purified using OneStep™ PCR Inhibitor Removal Kit following the manufacturer's instructions. Briefly, the Zymo-Spin™ III-HRC Columns were prepared for use. Each column was inserted in a collection tube, $600\text{ }\mu\text{L}$ Prep-Solution (provided with the Kit) were added and the columns were centrifuged at $8,000 \times g$ for 3 minutes. After centrifugation the columns were ready for use and were transferred into a clean 1.5 mL DNA LoBind® tube. $100\text{ }\mu\text{L}$ DNA were added in the columns and subsequently were centrifuged at $16,000 \times g$ for 3 minutes. The filtered DNA was suitable for amplification.

Amplification of sgRNA Library

PCR reactions for each purified genomic DNA sample were performed using Next Generation Sequencing primers that amplify the sgRNA target region with the illumina adaptor sequences. The PCR product size was $270\text{-}280\text{ bp}$ and could be identified by 1.5% agarose gel electrophoresis. For each $50\text{ }\mu\text{L}$ PCR reaction, $2.5\text{ }\mu\text{g}$ of DNA were used and mixed with $0.5\text{ }\mu\text{L}$ Phusion Hot Start II DNA polymerase, $10\text{ }\mu\text{L}$ Phusion HF buffer 5X , $1\text{ }\mu\text{L}$ dNTPs 10 mM and $1\text{ }\mu\text{L}$ of each Primer (Forward and Reverse) specific for the DNA sample. Before the PCR reaction started, the primers were denatured for 5 minutes at $98\text{ }^{\circ}\text{C}$ and then directly on ice. The PCR reaction was performed using the following cycling conditions: initial denaturation for 30 seconds at $98\text{ }^{\circ}\text{C}$, denaturation for 10 seconds at $98\text{ }^{\circ}\text{C}$, annealing for 15 seconds at $60\text{ }^{\circ}\text{C}$, extension for 90 seconds at $72\text{ }^{\circ}\text{C}$, final extension for 5 minutes at $72\text{ }^{\circ}\text{C}$ and then the reaction was cooled down to $4\text{ }^{\circ}\text{C}$ for infinite time. The steps from denaturation to extension were performed for 25 cycles.

Purification of sgRNA Library

For each DNA sample, $4 \times 50\text{ }\mu\text{L}$ PCR reactions were performed according to the instructions in the section above. The PCR reactions per sample were pooled, and subsequently were purified using Agencourt® AMPure® XP beads following protocol instructions included in KAPA Hyper Prep Kit. Briefly, the purification was performed in a two-step protocol, in which the volume of magnetic beads added each time, was strictly determined (Adapter-ligated or amplified DNA ($0.6\text{X}\text{-}0.8\text{X}$)). During the first phase, all the unwanted DNA fragments or library molecules were bound on the magnetic beads after a 15 minutes incubation at room temperature. The supernatant was carefully removed, it was very critical that no beads were transferred. Thereafter, during the second phase, appropriate amount of magnetic beads were mixed and incubated with the supernatant for 15 minutes at room temperature. The supernatant was discarded, the tubes remained on the magnet and two washes with $200\text{ }\mu\text{L}$ of 80% ethanol were performed. The magnetic

beads were air dried for 5 minutes at room temperature and were resuspended in 25 μ L PCR-grade water. The tubes were incubated for 3 minutes at room temperature to elute the DNA off the magnetic beads. The clear supernatant containing the size-selected DNA was transferred to a new 1.5 mL DNA LoBind® tube and was stored at -20 °C till further use.

5.2.4.14 Transcriptome profiling of *XLOC030781* Knock-Down

2.5×10^5 cells of 501-mel parental and 501-mel-tetON dCas9 KRAB cell lines were seeded in 6-well cell culture plates. Prior to seeding the 501-mel-tetON dCas9 KRAB cell line had been kept in culture for 4-5 days under 2 μ g/mL doxycycline to establish the constitutive expression of dCas9 protein. For the screen the top 2 sgRNAs that depicted the most efficient knock-down of lncRNA *XLOC030781* were used. On the following day, the 501-mel-tetON dCas9 KRAB cells were infected with 50 or 100 μ L sgRNA lentivirus, separately for each sgRNA. 24 hours post infection the growth medium was changed with new, supplemented with 2 μ g/mL doxycycline and cells were kept under constant treatment till the end of the screen. For each condition, three technical replicates were created, two replicates to isolate RNA for NGS analysis and one replicate to isolate RNA for RT-qPCR for knock-down confirmation. The 501-mel parental cell line was used as control during the NGS analysis. 72 hours and 120 hours post infection, cells from all triplicates of each condition were harvested after being washed with ice-cold PBS 1X and trypsinized. Minimum of 1×10^6 cells were collected from each well up on centrifugation at $500 \times g$ for 5 minutes. Subsequently, RNA isolation was performed using TRIzol reagent. For the samples intended for qPCR the standard protocol was followed as described in section 5.2.6, but for the samples intended for NGS analysis two washings with chloroform and two washings with 70 % ethanol were performed during the protocol.

5.2.4.15 Preparation of RNA Samples for Next Generation Sequencing Analysis

5.2.4.15.1 Total RNA Isolation

Cells were harvested by trypsinization on pre-arranged timepoints (Day 3 and Day 5) during the CRISPRi *XLOC030781* Screen. The cell pellet was washed twice with PSB 1X and thereafter total RNA was isolated using TRIzol Reagent, following the protocol described at section 5.2.5, with two variations to acquire total RNA of higher quality and greater purity. These variations included two washes with chloroform and two washes with 70 % ethanol instead of one respectively. The RNA concentration was measured on Nanodrop™ 2000c, where also the quality was checked based on the 260:280 and 260:230 ratios.

5.2.4.15.2 mRNA Purification and Fragmentation

The predominant component of RNA within cells is the ribosomal RNA (rRNA). mRNA corresponds to only 1-5 % of the total cellular RNA. In whole transcriptome next-generation sequencing analysis, it is essential to maximize the amount of information generated from a single sequencing run, therefore removal of rRNA is a necessary step. For this reason, 1 µg total RNA of each sample was utilized by following the manufacturer's protocol instructions of QIAseq FastSelect RNA Removal Kit. Briefly, in 1 µg total RNA, 1 µL of rRNA removal was added and the final volume of the reaction was adjusted to 29 µL by adding Nuclease-free water. Thereafter, 8 µL of RT Buffer 5X from the QIAseq Stranded Total RNA Library Kit were added with good mixing, the mixture (37 µL) was spun down and was incubated in a thermal cycler with a heated lid under the following cycling conditions: 15 minutes at 95 °C, 2 minutes at 75 °C, 2 minutes at 70 °C, 2 minutes at 65 °C, 2 minutes at 60 °C, 2 minutes at 55 °C, 5 minutes at 37 °C, 5 minutes at 25 °C and then the reaction was cooled down to 4 °C.

5.2.4.15.3 Preparation of strand-specific Next Generation Sequencing Library

First-strand Synthesis

The final reaction from the previous step was used as the starting material for first-strand synthesis following manufacturer's instructions included in the QIAseq Stranded Total RNA Library Kit. In more detail, the 37 µL reaction was mixed with 1 µL DTT 0.4 M, 1 µL RT enzyme and 1 µL RNase Inhibitor. The reaction was incubated for 10 minutes at 25 °C, 15 minutes at 42 °C, 15 minutes at 70 °C and was cooled down to 4 °C. 56 µL of resuspended QIAseq beads were added, mixed thoroughly and the mixture was incubated for 5 minutes at room temperature. The tubes were put on a magnet and after the solution was clear, the supernatant was carefully removed. Thereafter, the magnetic beads containing the DNA of interest, were

washed twice with 200 μ L 80 % ethanol. After removing the ethanol, the magnetic beads air dried for 7 minutes at room temperature, while the tubes remained on the magnet stand. The DNA was eluted from the beads by adding 40 μ L Nuclease-free water.

Second-strand Synthesis, End-repair and A-addition

Like at the previous step, the entire end-product (38.5 μ L- there was always a small loss after elution) was used for the second-strand synthesis reaction. Therefore, the product was mixed with 5 μ L Second Strand Buffer, 10X, 6.5 μ L Second Strand Enzyme Mix and was incubated for 30 minutes at 25 $^{\circ}$ C, 15 minutes at 65 $^{\circ}$ C and cooled down to 4 $^{\circ}$ C. 70 μ L of resuspended QIAseq beads were mixed thoroughly with the reaction. The mixture was incubated for 5 minutes at room temperature. The tubes were placed on the magnetic stand and after the solution was clear, the supernatant was removed carefully. The magnetic beads were washed twice with 200 μ L 80 % ethanol and were allowed to air dry for 7 minutes at room temperature. DNA was eluted from the beads by adding 52 μ L Nuclease-free water.

Strand-specific Ligation

The entire product from the previous step (50 μ L) was used for the Strand-specific ligation. The Kit included a 96-well plate on which the adapters were distributed. Based on the total RNA input amount, the adapters were diluted. For our experiment 1 μ g of total RNA was initially used, so according to the protocol instructions the adapters were diluted 1:12.5 with RNase-free water (10 μ L QIAseq Adapter and 115 μ L RNase-free water). The Strand-specific ligation reaction was set up as follows: the product from Second-strand Synthesis reaction was mixed with 2 μ L diluted adapter (different for each sample), 25 μ L Ultralow Input Ligation Buffer 4X, 5 μ L Ultralow Input Ligase, 6.5 μ L Ligation Initiator and 11.5 μ L Nuclease-free water. The mixture was incubated for 10 minutes at 25 $^{\circ}$ C. Subsequently, 80 μ L resuspended QIAseq beads were added to the reaction, were mixed thoroughly and were incubated for 5 minutes at room temperature. The tubes were placed on a magnet stand and the clear supernatant was discarded. The beads were washed twice with 200 μ L 80 % ethanol and air dried for 7 minutes at room temperature. 92 μ L Nuclease-free water were added to the magnetic beads to elute the DNA. 90 μ L clear supernatant were transferred to a new tube per sample and mixed with 108 μ L resuspended QIAseq beads. The mixture was incubated for 5 minutes at room temperature. The tubes were placed on the magnet stand and the clear supernatant was discarded. The DNA of interest is bound on the magnetic beads. Two washings with 200 μ L 80 % ethanol followed and the beads air dried for 7 minutes at room temperature. The DNA was eluted from the beads by adding 25 μ L Nuclease-free water.

CleanStart Library Amplification

The library amplification reaction was prepared on ice. The product (23.5 μ L) from the previous step was mixed with 25 μ L CleanStart PCR Mix 2X and 1.5 μ L CleanStart PCR Primer Mix. The PCR reaction was performed with the following cycling conditions: CleanStart decontamination for 15 minutes at 37 $^{\circ}$ C, initial denaturation for 2 minutes at 98 $^{\circ}$ C, denaturation for 20 seconds at 98 $^{\circ}$ C, annealing for 30 seconds at 60

°C, extension for 30 seconds at 72 °C, final extension for 1 minute at 72 °C and then cooled down to 4 °C. The PCR reaction was performed for 11 cycles. After the PCR, 60 µL resuspended QIAseq beads were mixed with the reaction and were incubated for 5 minutes at room temperature. The tubes were placed on the magnet stand and the clear supernatant was discarded. Two washings with 200 µL 80 % ethanol were performed. The residual ethanol was removed and the magnetic beads air dried for 7 minutes at room temperature. The DNA from the beads was eluted by adding 22 µL Nuclease-free water. 20 µL was transferred to new tubes. This is the QIAseq Stranded Sequencing Library ready for NGS analysis.

5.2.5 RNA Isolation using TRIzol Reagent

To acquire total RNA from human melanoma cells, growth media was aspirated from the cell culture vessels and cells were washed once with cold PBS 1X. 0.3-0.4 mL of TRIzol were added to 1×10^5 - 10^7 cells directly, to initiate lysis by applying mechanical pressure through pipetting the cell lysate up and down to achieve homogenization. The cell lysate was transferred to a sterile Eppendorf tube and was incubated for 5 minutes at room temperature. 0.2 mL of chloroform per 1 mL of TRIzol was added, followed by incubation for 2-3 minutes. Samples were centrifuged for 15 minutes at $12,000 \times g$ at 4 °C and the upper aqueous phase containing the RNA was transferred to a new tube. 5-10 µg of RNase-free glycogen were added to increase the RNA yield. 0.5 mL of isopropanol per 1 mL of TRIzol were added. The samples were incubated for 10 minutes at room temperature and centrifuged for 10 minutes at $12,000 \times g$ at 4 °C. The supernatant was removed, the pellet was resuspended in 1 mL of 75 % ethanol per 1 mL of TRIzol and centrifuged for 5 minutes at $7,500 \times g$ at 4 °C. The supernatant was removed, the RNA pellet was left to air dry for 5-10 minutes, was resuspended in 20-50 µL RNase-free water and its concentration was measured using Nanodrop™2000c.

5.2.6 Reverse Transcription-Quantitative PCR (RT-qPCR)

cDNA was synthesized from 1 µg total RNA of each sample using High-Capacity cDNA Reverse Transcription Kit following the manufacturer's instructions. 50 ng of the cDNA obtained, were utilized for quantitative real-time PCR. The reaction was performed with the GoTaq® qPCR Master Mix by following the manufacturer's protocol recommendations. Summarily, the cDNA was diluted 1:3 with PCR grade water and 4 µL were mixed with 6 µL SYBR® Green master mix containing the corresponding primers. Quantitative real-time PCR was carried out in 96-well culture plates, and each sample was represented in triplicates to acquire reliable statistical analysis. For each target lncRNA expression cDNA threshold (Ct) values were normalized in relation to the Ct values of the housekeeping gene *GAPDH*. The cDNA Ct values

were analyzed through the comparative Ct method ($\Delta\Delta Ct$). Data were plotted as linear fold change ($2^{\Delta\Delta Ct}$) with standard deviation.

5.2.7 Agarose Gel Electrophoresis

Traditional agarose gel electrophoresis was performed to separate and analyze DNA fragments as part of the process of various experiments in the project. The separation was activated in the presence of an electric field and the fragments were mobilized mainly based on the molecular weight, and less on the DNA conformation. The agarose concentration, the electrophoresis TBE buffer, and the applied voltage were secondary factors. The gels were prepared by adding 1.2-1.5 g agarose powder in 100 mL TBE buffer 1X. The mixture was heated up in a microwave oven. When the agarose was fully dissolved and the solution became clear, it was cooled down and 5 μ L ethidium bromide were added. The solution underwent polymerization inside a casting chamber with a 15 well-comb. DNA samples were diluted with 6X DNA Gel Loading Dye and then loaded carefully into the wells, along with 7 μ L 1 kb or 100 bp DNA Ladder. The gel electrophoresis was performed at 110 V for 60-80 minutes in a chamber filled with TBE buffer 1X. An image was acquired using Bio-Rad ChemiDoc™ MP Imaging System.

5.2.8 Immunoblotting

5.2.8.1 Cell Lysate Preparation

Growth medium was removed from the cell culture dish (i.e. 6-well culture plate), cells were trypsinized, centrifuged at $300 \times g$ for 4 minutes, washed with PBS 1X and collected in a 1.5 mL sterile low-protein binding tube. Cell pellet was resuspended with in-house RIPA buffer (Table 5.1.2) supplemented with 1X cOmplete™ ULTRA Tablet protease inhibitor cocktail (100-150 μ L/well of a 6-well culture plate), was left on ice for 15 minutes and thereafter centrifuged for 15 minutes at maximum speed at 4 °C. Supernatant containing the whole cell lysate was collected in a new tube, and stored at -20 °C for further use. For long-term preservation, whole cell lysates were snap frozen and kept in a -80 °C freezer.

5.2.8.2 Protein Concentration Quantification (DC Protein Assay)

To determine the total protein concentration in the cell lysate, the Bio-Rad DC Protein Assay was used following the manufacturer's protocol instructions. In principle, the DC Protein Assay is a colorimetric assay relying on detergent solubilization for acquiring absolute quantification of protein concentration. Briefly, 8 dilutions of a BSA (Bovine Serum Albumin) standard solution, in a concentration range from 0.25 mg/mL to 2 mg/mL, were used to produce a reference calibration curve. 5 μ L of the BSA standard dilutions or the whole cell lysates were added in duplicates in a well of a transparent 96-well culture plate. Subsequently were mixed with 25 μ L of an alkaline copper tartrate solution in and then 200 μ L of the Folin Reagent were added. The plate was incubated for 15 minutes at room temperature under light deprivation. The absorbance was measured at 750 nm and the protein concentration of the samples was calculated based on the standard curve that was produced. The absorbance was directly proportional to the protein content of each sample and should have been within the range of the BSA standard dilutions absorbance, otherwise the samples were prediluted with ddH₂O before the assay.

5.2.8.3 SDS-PAGE Electrophoresis

Protein separation was attained through SDS-polyacrylamide gel electrophoresis, according to differences in their molecular weight. 20 μ g of each protein sample were diluted 3:1 with NuPAGE™ LDS Sample Buffer 4X and were incubated on a heat block for 10 minutes at 70 °C for denaturation. Subsequently, the protein samples and 6 μ L of PageRuler™ Prestained Protein Ladder as a standard control, were loaded carefully on a 10 % in-house 1.5 mm thickness Bis-Tris polyacrylamide gel. The electrophoresis was performed at 110 V for ~1.5 hours in SDS-Running buffer 1X.

5.2.8.4 Blotting

After protein separation was completed with SDS-PAGE gel electrophoresis, detection and semi-quantification of the proteins of interest was obtained with immunoblotting. In more detail, the separated proteins were transferred from the gel to an Immobilon®-P polyvinylidene difluoride (PVDF) membrane 0.45 μ m pore by electroblotting. Prior to use, the transfer membrane was saturated in 100 % methanol for 2 minutes for activation and afterwards in transfer buffer 1X for equilibration. The transfer was performed in a Mini Trans-Blot® Cell tank filled with transfer buffer 1X at 4 °C in a coldroom, either at 120 V for 1.5 hours or at 25 V overnight. The first indication of a successful transfer of the protein complexes on the membrane is the protein marker's bands imprint on it. Thereafter, the transfer membrane was washed with ddH₂O, stained in Ponceau S solution to check the transfer quality, and then rinsed off carefully with ddH₂O.

The membrane was blocked in 3 % non-fat milk powder in TBST (blocking buffer) for 1 hour at 4 °C and was incubated with the primary antibody solution under constant shaking overnight at 4 °C. The primary antibodies were diluted in blocking buffer according to manufacturer's recommendations. On the following day, the primary antibody solution was collected in a 15 mL falcon tube and stored for future use at -20 °C. The blot was rinsed 3 times with TBS-T for 5 minutes with agitation and then was incubated in the secondary antibody solution (anti-goat or anti-mouse depending on the primary antibody) for 1 hour at room temperature. Horseradish-Peroxidase conjugated secondary antibodies were used for detection and were diluted up on manufacturer's instructions. The secondary antibody solution was removed, and the blot was washed twice with TBS-T and the last time with TBS for 5 minutes. The chemo luminescence was detected using Clarity™ Western ECL Substrate and Bio-Rad ChemiDoc™ MP Imaging System was used for protein visualization.

5.2.9 Bioinformatic Analysis

sgRNA sequencing Analysis

The analysis of sgRNA raw sequencing data was conducted using an in-house developed custom script. The script utilized "seqtk," a toolkit specifically designed for processing, trimming, and combining raw sgRNA reads. Subsequently, it employed "cutadapt" to remove the adapter sequences. The resulting trimmed sgRNA reads were then aligned to the sgRNA library sequences using an R script. For each time point, a count was generated for each sgRNA, representing the number of reads that aligned with the respective sgRNA target sequence from the CRISPRi lncRNA library 1.0. To assess the differential abundance of all sgRNAs between Day 21, 14, 7 and Day 0, the average fold change (Day X/Day 0) and p-value was calculated using Student's t test. (Protocol provided by Dr. Sama Shamloo who performed the analysis.)

RNA sequencing Analysis

The raw fastq files were processed using the zarp pipeline which implemented FastQC, zpc and MultiQC for quality control and the adapters were trimmed using Cutadapt¹⁸⁹⁻¹⁹². The reads were mapped to the human genome (hg38, Genome Reference Consortium GRCh38) using STAR and quantized Salmon^{193,194}. The final output was a counts matrix which was used as input for the R package DESeq2 to identify differentially expressed genes¹⁹⁵. Genes with a log2 Fold Change >1 and adjusted p-value <0.05 were used for further analysis. The gene sets were obtained using the msigdb R-package and clusterProfiler and enrichplot were used for generating the GeneOntology and Gene-Set Enrichment plots¹⁹⁶⁻¹⁹⁸. (Protocol provided by Shashank Tiwari, M.Sc. who performed the analysis and the dot plots.)

6. Results

6.1 Preliminary Experimental Research

During this PhD journey involvement in multiple projects (Dual CRISPR Activation System, Drug Compound Screen Assay) occurred, but the emphasis will be on a particular project for the purpose of this PhD dissertation. This project constitutes a continuation of previous extensive experimental research performed by Dr. Imig and his collaborators at Dr. Aifantis laboratory located at the New York University Medical Centre (NYUMC). Dr. Imig employed a comprehensive bioinformatics methodology to identify both previously annotated and novel lncRNAs that demonstrate high expression levels in melanoma cells. The in-house lncRNA identification pipeline tool was developed by Aifantis lab. In more detail, *bona fine* lncRNA transcripts are typically distinguished by their association with active histone marks, like H3K4me3 and/or H3K27ac, at their transcription initiation region. Consequently, a differential gene expression (DGE) analysis was performed using datasets obtained from RNA sequencing (RNA-Seq) and H3K4me3/H3K27ac chromatin immunoprecipitation sequencing (ChIP-Seq) results, thereby enabling a comparison between melanocytes and the 501-mel cell line, as well as melanoma cells originating from different metastatic locations (brain and lymph nodes). Regarding the latter, biopsy samples were directly obtained from patients and employed in generating short-term cell cultures (STCs).

By adopting a combinatorial approach, the in-depth analysis resulted in the identification of 1176 potentially *novel* and 321 already annotated lncRNAs, that were expressed across all tested cell types thus far. Among these, 469 lncRNAs exhibited differential expression between melanocytes and 501-mel cells, as indicated in Figure 5A. Additionally, there were 382 and 444 lncRNAs with distinct expression patterns in brain metastatic (BM) and lymph node metastatic (LN) samples, respectively, demonstrating a significant overlap of deregulated lncRNAs in concordant directions as depicted on the Venn diagram in Figure 5B. Consequently, the differentially expressed lncRNAs specifically deregulated in brain or lymph node metastatic samples were given priority, owing to their presumed involvement as drivers in the process of metastatic formation (Figure 5C-D).

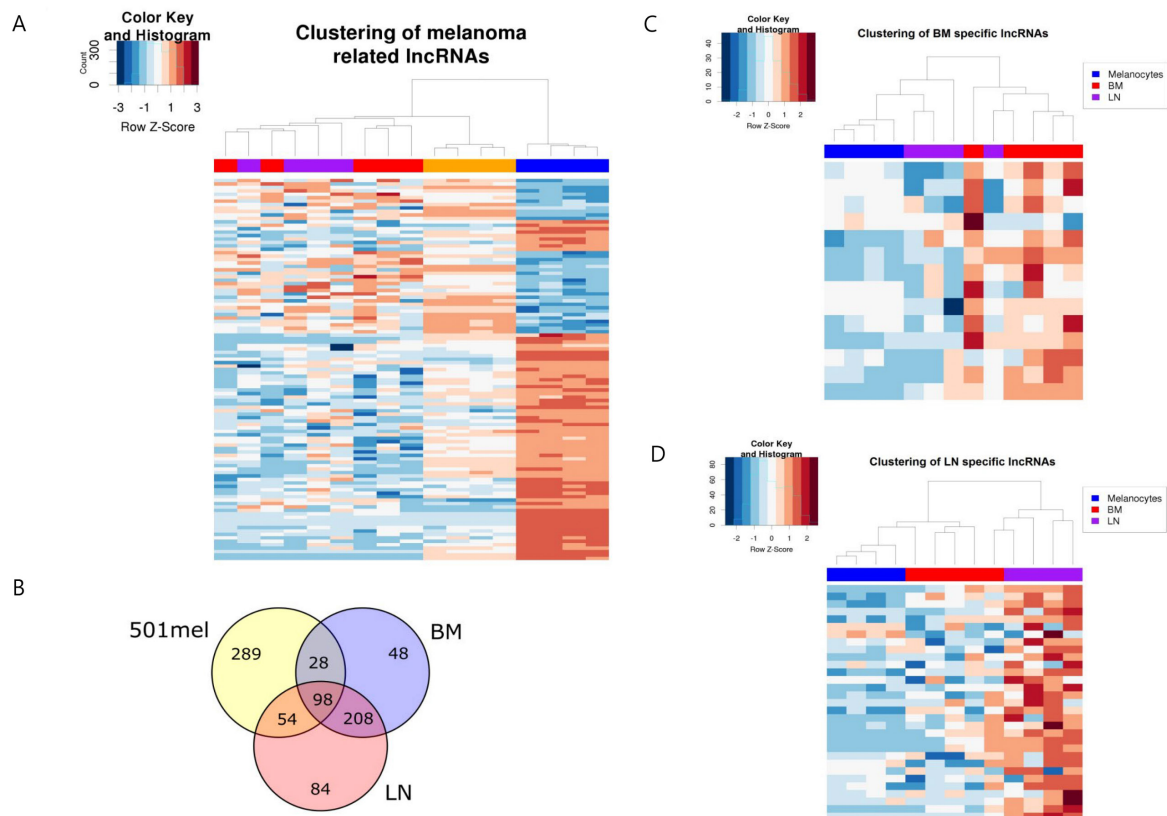


Figure 5.A. Heatmap illustrating expression patterns of 464 lncRNAs, both novel and annotated, that exhibit significant differential expression between 501-mel (orange) and melanocytes (blue). Additionally, the supervised clustered heatmap includes expression data of these lncRNAs in metastatic samples from bone marrow (BM) (red) and lymph nodes (LN) (purple). **B.** Venn diagram depicting substantial differential expression of lncRNAs in pairwise comparisons between melanocytes and 501-mel (yellow) as well as BM and LN metastatic samples. **C.** and **D.** supervised clustered heatmaps showcasing upregulated lncRNAs in BM samples compared to melanocytes and LN samples or upregulated lncRNAs in LN samples compared to melanocytes and BM samples respectively. (The data provided is under the exclusive copyright ownership of Dr. Jochen Imig and Aifantis Lab.)

The objective was to meticulously select a limited set of the upregulated lncRNAs reasoning a likely oncogenic gain-of-function and for the purpose of constructing a sgRNA library in order to subsequently conduct a CRISPR-dCas9 proliferation screen (CRISPRi proliferation screen 1.0), aiming to comprehensively dissect their involvement in the cellular processes associated with proliferation. To ensure the relevancy of the selected lncRNAs within the experimental context, specific filters and thresholds were cautiously implemented. These analytical filters encompassed: a. maintaining a false discovery rate of less than or equal to 0.05 ($FDR \leq 0.05$) in order to effectively regulate the occurrence of falsely identified significant results, b. adhering to a log₂-fold change threshold of 0.75 or higher ($\log_2FC > 0.75$) to ascertain that the lncRNAs were significantly overexpressed, c. requiring a RNA-Seq read counts per million of at least 1 ($CPM \geq 1$) in the higher expressed cellular type, effectively excluding genes with low expression levels, d. mandating that the lncRNA gene bodies carried an active histone mark, specifically H3K4me3 or H3K27ac,

in the higher expressed cell type, and e. excluding any lncRNAs that consisted solely of mono-exonic transcripts as they may exhibit alternative function such as enhancer RNAs.

The application of these filters yielded a collection of 268 upregulated lncRNAs. For each lncRNA, a maximum of 10 sgRNAs were designed aiming to the window -50 bp to +300 bp in relation to the TSS, and 50 non-targeting sgRNAs were incorporated as negative controls. The necessity of utilizing both negative and positive controls when performing an experiment was a basic principle to ensure scientific correctness. In this way, erroneous conclusions due to false positive or false negative results could be easily eliminated. As such, the CRISPRi lncRNA library 1.0 incorporated approximately 10 sgRNAs for each of 8 designated positive controls, specifically 5 lncRNAs *BANCR*, *CDKN2B-AS1*, *HOTAIR*, *MALAT1*, *SAMMSON* and 3 protein coding genes *CDKN1A*, *FBXW7* (E-Box And WD Repeat Domain Containing ζ), and *HSF1* (Heat Shock Factor 1). Ultimately, the sgRNA KRAB library comprised an estimated total of 2761 sgRNAs.

The CRISPRi proliferation screen 1.0 was carried out employing the 501-mel-tetON dCas9 KRAB cell line and spanned a duration of 21 days. At specific intervals, every 7 days, genomic DNA was isolated, incorporated sgRNA sequences PCR amplified and subsequently subjected to NGS analysis. Herein, precise details regarding the experimental parameters will not be provided. Nonetheless, it is vital to underscore that the identification of prominent lncRNA candidates from this study laid the groundwork for the current doctoral project.

The sgRNA sequencing analysis yielded a compilation of lncRNAs that exhibited the highest depletion during the screen; the parameters of inclusion were a. log₂FC of top 3 depleted sgRNAs mean > 1 and b. p-value > 0.05 (Figure 6A). To ascertain the selection of the most promising candidates for subsequent functional characterization research, it was imperative to validate the screening observations. The results attained from the differential expression analysis were utilized to generate boxplots, enabling a direct comparison of the expression levels of the top lncRNA candidates across the investigated cell lines (melanocytes, primary melanoma cells, BM and LN samples from STCs) (Figure 6B). The primary objective of developing this data visualization was to appraise the clinical significance of the leading candidates within a small patient cohort, but subsequently it allowed a first level evaluation.

In more detail it was shown that: a. *RP11-267N12.3* demonstrated significantly elevated expression levels in both primary melanoma and metastatic samples in comparison to melanocytes. The median of the values for these samples was higher compared to that of the melanocytes even if the overall values were widely spread, b. *RP11-1205.1* displayed strong upregulation only in lymph node metastatic samples and suppression in both primary melanoma and brain metastatic samples compared to melanocytes, c. *BDNF-AS* revealed higher expression levels in primary melanoma cells, and for the both metastatic samples (BM and LN) the distribution of the values were skewed positively showcasing an overexpression but the median value was lower than that of the melanocytes, d. *XLOC030781* showed a significant upregulation in both lymph node and brain metastatic samples, regarding primary melanoma cells and brain metastatic samples

interestingly a downregulation was observed which was also shown in melanocytes, and e. *GMDS-AS1* demonstrated a notable overexpression in all primary and metastatic samples in relation to melanocytes. Consequently, a competition assay was carried out for a duration of 24 days, wherein the expression of the previously stated lncRNAs was suppressed (Figure 6C). The expression levels were quantified by measuring the % GFP every 4 days and the results showed that *RP11-267N12.3* exhibited the highest depletion over time, followed by *BDNF-AS*, *GMDS-AS1* and *XLOC030781*, but *RP11-1205.1* didn't perform well so it was decided to be excluded from any further analysis. The genomic analysis of *RP11-267N12.3* revealed its dependence on a bidirectional promoter shared with the *NUF2* gene, which posed a potential challenge when attempting to modulate the expression of this lncRNA in research studies. Due to this concern, it was deemed appropriate to exclude *RP11-267N12.3* as a candidate in order to avoid potential false results. Finally, *BDNF-AS*, *GMDS-AS1* and *XLOC030781* were the selected lncRNA candidates to be investigated.

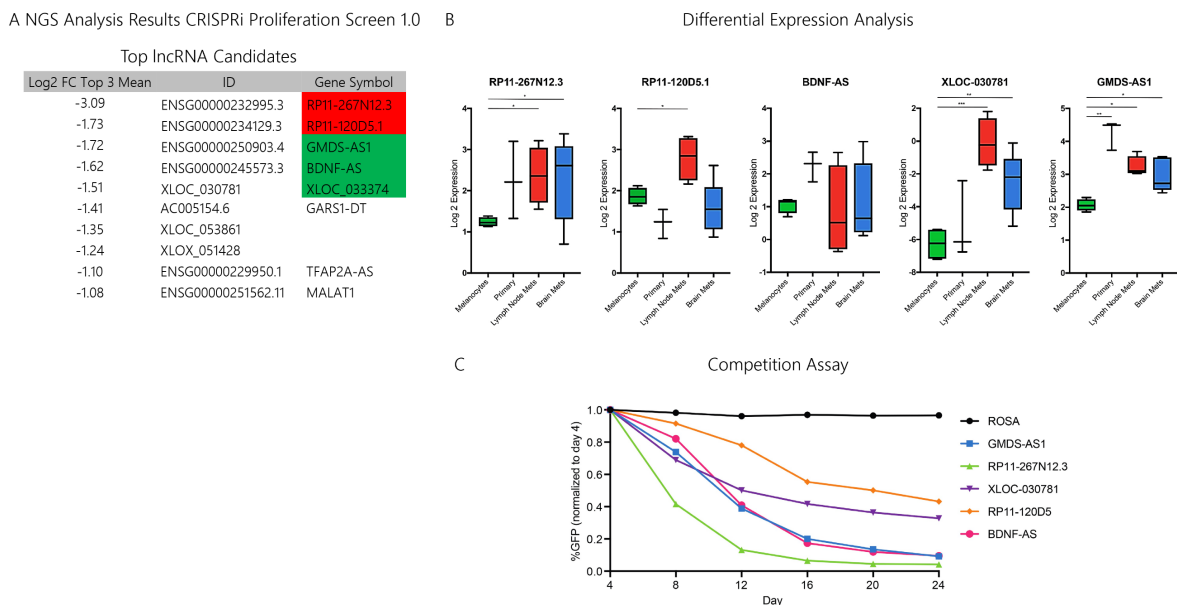


Figure 6. A. Table showing the top 10 depleted lncRNAs at the final timepoint of CRISPRi proliferation screen 1.0 (day 21). The ranking was established by calculating the average log₂ fold change (FC) for the top 3 sgRNAs depleted, associated with each lncRNA. Top lncRNAs *RP11-267N12.3* and *RP11-120D5.1* (red) were omitted from subsequent analysis due to *RP11-267N12.3* being regulated by and sharing a bidirectional promoter with cell cycle associated *NUF2* gene, and unsatisfactory results observed upon depletion of *RP11-120D5.1* during the competition assay. Therefore, *BDNF-AS*, *GMDS-AS1* and *XLOC030781* were selected for functional characterization studies. **B.** Boxplots showing differential expression of top lncRNA candidates across primary melanoma and metastatic BM and LN samples in comparison to melanocytes. **C.** Verification of prominent hits from initial lncRNA screening. Quantification of depletion levels (% GFP) normalized to day 4. (The data provided is under the exclusive copyright ownership of Dr. Jochen Imig and Aifantis Lab.)

6.2 CRISPRi Proliferation Screen 2.0

6.2.1 Design and Evaluation of sgRNA Positive Controls

One major aim of the doctoral study was to replicate the CRISPRi proliferation screen 1.0 conducted by Dr. Imig, as mentioned in the preceding section. By precisely targeting specific lncRNA genes and closely analyzing their impact on cellular phenotypes, the exploration of novel gene functions and potential therapeutic targets was attainable. Repeating the CRISPRi loss of function screen permitted an assessment of its robustness and reproducibility, thereby validating the credibility and dependability of the already acquired results. This repetition underscored the significance of consistent experimental techniques, encompassing the selection of target genes, cell lines, and screening assays.

The CRISPRi proliferation screen 2.0 was performed under slightly different conditions, which will be further analyzed. As already discussed, the in-house CRISPRi lncRNA library 1.0 consisted of sgRNAs designed for 264 upregulated lncRNAs in melanoma cells versus melanocytes, 50 non-targeting sgRNAs as negative controls and sgRNAs engineered specifically for 8 positive controls based on latest literature. In addition to these 8 positive controls, the CRISPRi proliferation screen 2.0 was augmented by the introduction of sgRNAs engineered to target 4 protein coding growth-related genes. This decision stemmed from three primary factors: a. in the initial CRISPRi proliferation screen 1.0, apart from *MALAT1*, none of the other positive controls were included among the top 20 depleted lncRNA genes. b. the considerably higher expression levels observed for protein coding genes compared to lncRNAs would lead to a more noticeable knock-down effect¹⁹⁹, and c. their pivotal roles in essential proliferation related molecular pathways linked to the advancement of melanoma which will be analytically described in the discussion.

In-depth research into the genomic profiling of melanoma patients unveiled the inclusion of *BRAF*, *EGFR*, *MITF*, and *RPA3* genes in the study. To precisely target these genes of interest, three distinct sgRNA sequences were designed for each of *BRAF*, *EGFR*, and *MITF* genes, utilizing the web design tool provided by the Broad Institute. Following the established protocol details presented in sections 5.2.1-5.2.3, the sgRNA sequences were initially inserted into the pLVx U6se EF1a sfPac vector. Subsequently, these constructs were introduced into the bacterial genome through chemical transformation and ultimately isolated in significant quantities from liquid LB bacterial cultures. Regarding *RPA3*, the Imig lab already possessed a plasmid with a very potent sgRNA for its downregulation. Lentiviruses were produced according to the protocol in 5.2.4.5. Their knock-down efficiency was investigated in 501-mel-tetON dCas9 KRAB cells, which was the designated cell line for both CRISPRi proliferation screens 1.0 and 2.0. The aforementioned cells were subjected to transduction, following the procedure outlined in section 5.2.4.6, and cell pellets were collected on day 3 and day 5 after the lentivirus transduction. This dual-timepoint approach was employed to simultaneously evaluate the efficacy and stability of the knock-down impact.

The most effective sgRNA for downregulation of each gene was selected to be spiked-in the CRISPRi screen library 1.0 and is depicted in red color in Figure 7.

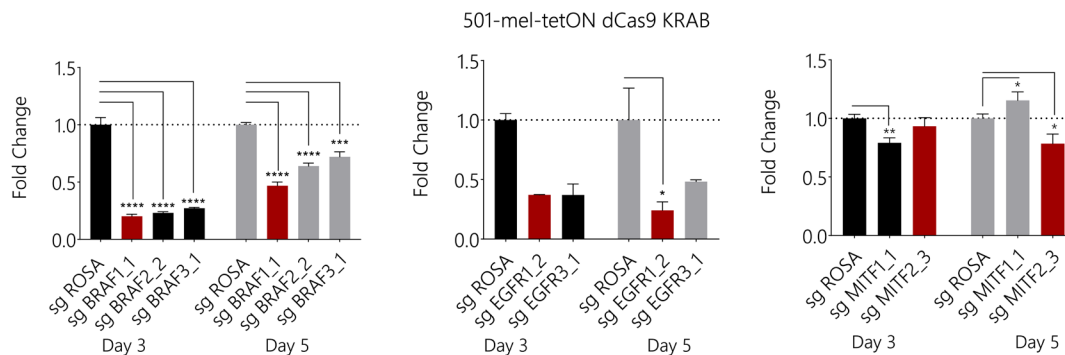
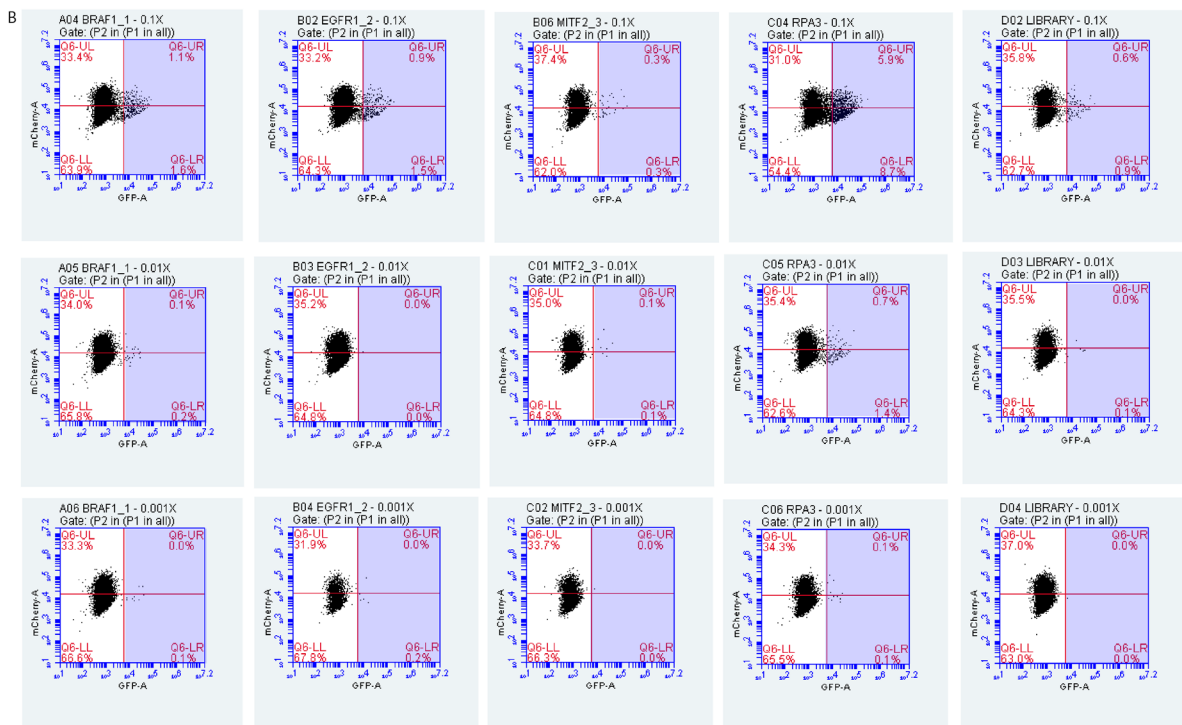
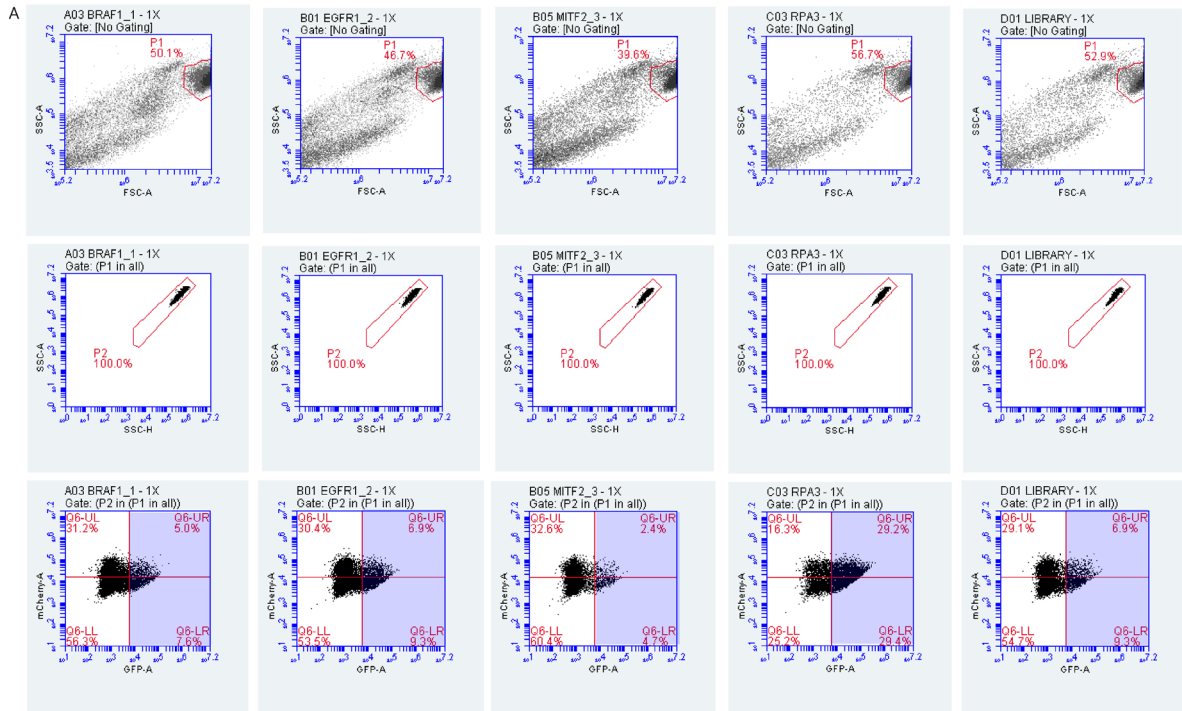


Figure 7. Quantitative real-time PCR validation of sgRNA efficiency targeting *BRAF*, *EGFR* and *MITF* positive control genes in 501-mel-tetON dCas9 KRAB cells on day 3 and day 5 post lentiviral transduction. For each gene, three sgRNAs were designed and their knock-down efficiency was compared to the non-targeting control sgROSA. Highlighted (light grey) are the top sgRNAs selected to be spiked-in the CRISPRi proliferation screen 2.0. Relative gene expression was calculated using *GAPDH* as the housekeeping gene. Data are represented as the mean \pm standard error (SE). Student's t test was used to determine statistical significance: $p < 0.05$ (*), $p < 0.01$ (**), $p < 0.001$ (***), $p < 0.0001$ (****). (sgRNA_X_Y: X indicates the sgRNA sequence (1-3) and Y indicates the bacterial colony from which it was isolated.)

6.2.2 Preparation for CRISPRi Proliferation Screen 2.0

6.2.2.1 Lentivirus Titration

Performing a titration of the lentiviruses produced for the in-house CRISPRi lncRNA library 1.0 and the sgRNAs for the positive controls *BRAF*, *EGFR*, *MITF*, and *RPA3*, before the CRISPRi proliferation screen 2.0, was essential to optimize transduction efficiency, and obtain consistent knock-down levels, thereby improving the reliability and reproducibility of the screen results. The protocol as described in section 5.2.4.11 was followed. The number of 501-mel-tetON dCas9 KRAB cells prior to infection was recorded to be 3.05×10^5 per well of a 6-well-culture plate. Thereafter, the cells were infected with 10-fold serial dilutions from 1X to 1/1000X of the lentiviruses in separate 6-well culture plates and the double positive mCherry-GFP and GFP positive single 501-mel-tetON dCas9 KRAB cells were detected using flow cytometry after 24 hours and 48 hours. Both of the groups mCherry-GFP+ and GFP+ are included in the calculations for the titration, even if the GFP+ cells seemingly don't express dCas9 because herein the virus infectivity is measured, and it is directly proportional to the total sum of cells expressing GFP. On the scatter plots are highlighted in blue the groups mCherry-GFP+ and GFP+ for the two timepoints and in green are highlighted which percentages and dilution of each sample were selected for calculating TU/mL (Figure 8A-C).



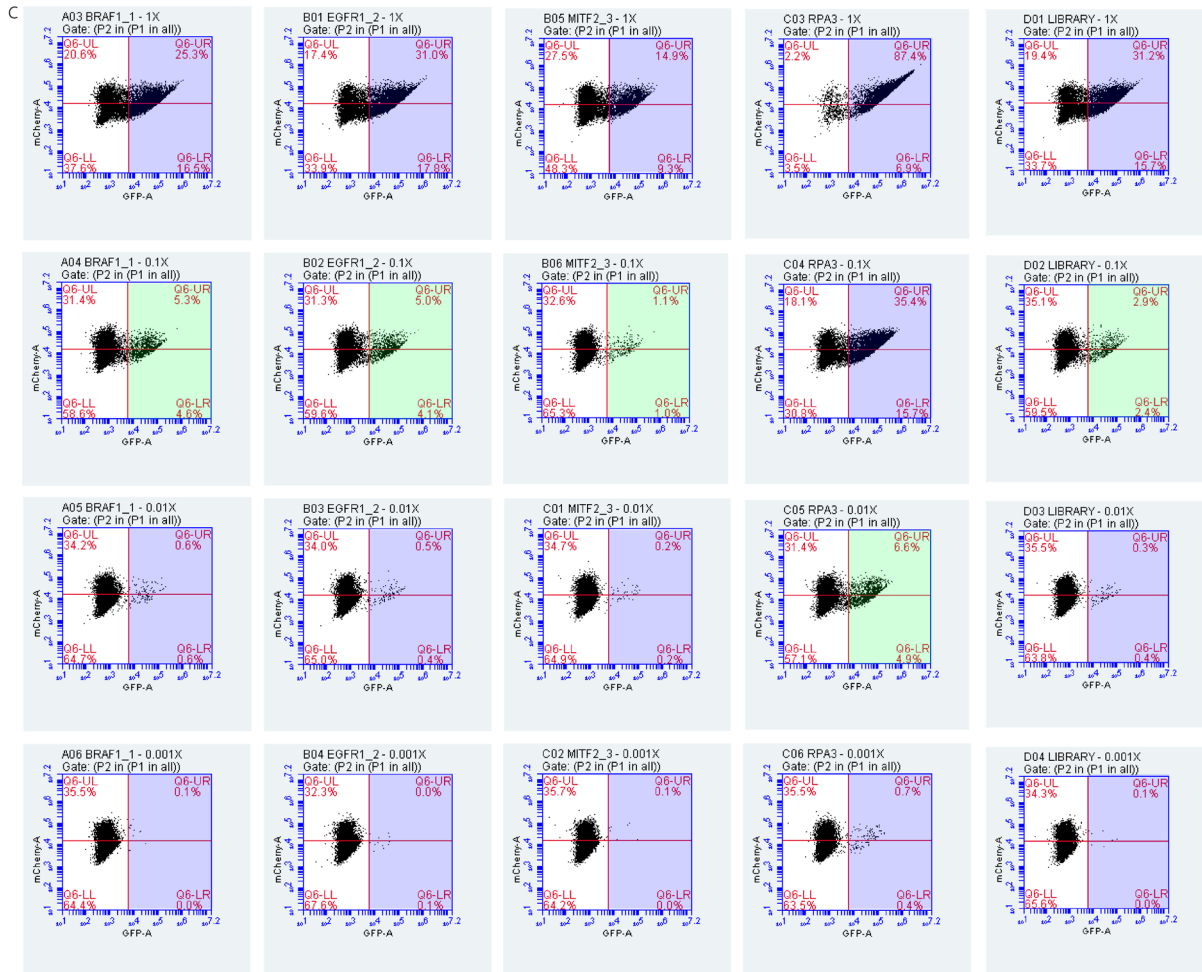


Figure 8. Panels A and B of FACS plots showcasing the distribution in % percentages of single 501-mel-tetON dCas9 KRAB cells for all samples *BRAF*, *EGFR*, *MITF*, *RPA3* and the CRISPRi lncRNA library 1.0 in all dilutions after 24 hours post lentiviral transduction. First two rows of each column outline the gating strategy used for flow cytometry analysis. Highlighted in blue are the double positive mCherry-GFP and single positive GFP 501-mel-tetON dCas9 KRAB cells. **Panel C** of FACS plots depict the results for 48 hours post transduction; highlighted in green is the dilution of each sample that was selected for the calculation of TU/mL for all the lentiviruses. (To avoid repetition, the gating strategy is not shown for the second timepoint.)

		Timepoint		
		24 Hours	48 Hours	TU/mL (N*P% ÷ 100) ÷ (V*D)
sgRNA	Dilution	% GFP	% GFP	
BRAF1_1	1X	12.57	41.76	
BRAF1_1	0.1X	2.70	9.93	6.06 x 10 ⁷
BRAF1_1	0.01X	0.25	1.14	
BRAF1_1	0.001X	0.07	0.12	
EGFR1_2	1X	16.13	48.76	
EGFR1_2	0.1X	2.47	9.11	5.56 x 10 ⁷
EGFR1_2	0.01X	0.02	0.96	
EGFR1_2	0.001X	0.28	0.14	
MITF2_3	1X	7.01	24.23	
MITF2_3	0.1X	0.60	2.08	1.27 x 10 ⁷
MITF2_3	0.01X	0.17	0.40	
MITF2_3	0.001X	0.03	0.08	
RPA3	1X	58.58	92.24	
RPA3	0.1X	14.62	51.13	
RPA3	0.01X	2.03	11.45	6.98 x 10 ⁸
RPA3	0.001X	0.22	1.08	
LIBRARY	1X	16.23	46.9	
LIBRARY	0.1X	1.50	5.38	3.28 x 10 ⁷
LIBRARY	0.01X	0.12	0.74	
LIBRARY	0.001X	0.02	0.08	

Table 6.1.All data acquired by flow cytometry and the calculations analytically performed for the lentiviral titration are depicted.

6.2.2.2 Confirmation of dCas9 Expression

Additionally, to the lentiviral titration, the second influencing factor ahead of conducting the CRISPRi proliferation screen 2.0 was the validation of the expression of dCas9 KRAB in the 501-mel-tetON dCas9 KRAB cell line. There was always a reasonable risk of performing a CRISPRi screen where the targeted gene repression was either not achieved or suboptimal. Confirming dCas9 expression allowed the evaluation of transduction efficiency. Low transfection efficiency might have led to a significant proportion of cells lacking the dCas9 construct, resulting in unreliable or inconclusive screening results. Therefore, the expression of dCas9 was investigated on mRNA level by RT-qPCR, and on protein level by western blot, after the cells were cultured in complete DMEM medium supplemented with 2 $\mu\text{g}/\text{mL}$ doxycycline. Since the dCas9 KRAB construct was carrying an mCherry fluorescent marker, the cells were checked under a fluorescent inverted microscope (Figure 9D). Both western blot and the RT-qPCR analyses verified the robust expression of dCas9, so it was safe to proceed with the conduction of CRISPRi proliferation screen 2.0 (Figure 9A-C).

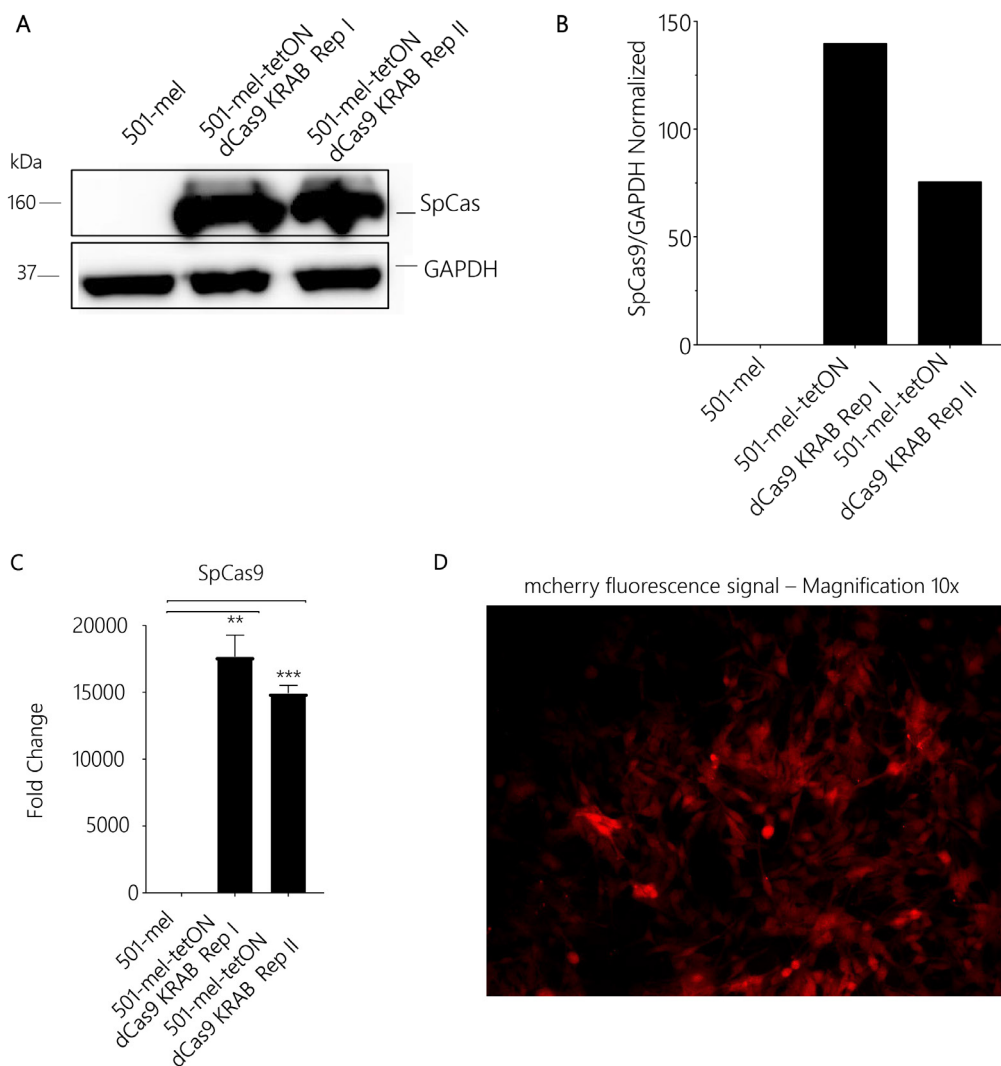


Figure 9. A. and B. Western blot analysis and relative quantification by densitometry of whole cell lysates from 501-mel cell line as negative control and from both technical replicates of 501-mel-tetON dCas9 KRAB cell line intended for the CRISPRi proliferation screen 2.0. High expression levels of dCas9 protein are recorded for both technical replicates. GAPDH was utilized as reference protein. **C.** RT-qPCR results depicting relative levels of dCas9 expression (n=2). Normalized to *GAPDH* as the reference gene. Statistical analysis was performed using unpaired Student's t test by Prism GraphPad 8: $p < 0.01$ (**), $p < 0.001$ (***). **D.** Representative image of strong mCherry signal detected in using 501-mel-tetON dCas9 KRAB cell line under fluorescence inverted microscope with objective lens 10X.

6.2.3 Conduction of CRISPRi Proliferation Screen 2.0

After completing the lentiviral titration and confirming the robust dCas9 expression in the 501-mel-tetON dCas9 KRAB cell line, the CRISPRi proliferation screen 2.0 was implemented following the protocol guidelines described in section 5.2.4.12. To ensure optimal experimental conditions, the screen design parameters were set to 1000X coverage with an MOI of 0.3 for the CRISPRi IncRNA library 1.0, along with MOI values of 0.005 for each of positive controls *BRAF*, *EGFR*, *MITF*, and *RPA3*. Calculating the required cell count for infection using the formula [(sgRNA Library size x Coverage) ÷ 0.3 MOI = starting cell number], it was determined that approximately 9.2×10^6 cells in total were necessary. As a result, 7.7×10^6 501-mel-tetON dCas9 KRAB cells were seeded in each 150 mm cell culture plate the day before infection. On the day of infection, the number of cells in the control 150 mm cell culture plate was recorded to be 8.21×10^6 . Unfortunately, the cell growth rate overnight wasn't as expected, so that reduced the screen coverage to ~900X. Thereafter, utilizing the lentivirus titration results, the volume required of each lentivirus for the infection was calculated (Table 6.2). The visual representation and comprehensive elucidation of the step-by-step timeline implemented for the screening process can be found in Figure 10.

sgRNA	TU/mL	V= (MOI*N÷TU)*1000 (μL)
BRAF1_1	6.06×10^7	0.68
EGFR1_2	5.56×10^7	0.74
MITF2_3	1.27×10^7	3.23
RPA3	6.98×10^8	0.059
LncRNA LIBRARY 1.0	3.28×10^7	75.05

Table 6.2. Approximate lentivirus volume employed in the CRISPRi proliferation screen 2.0. Calculations were performed utilizing the formula provided in the third column, based on the TU/mL measurement of each lentivirus, as determined in section 6.2.2.1, in conjunction with the appropriate MOI and the recorded number of cells recorded at the time of infection.

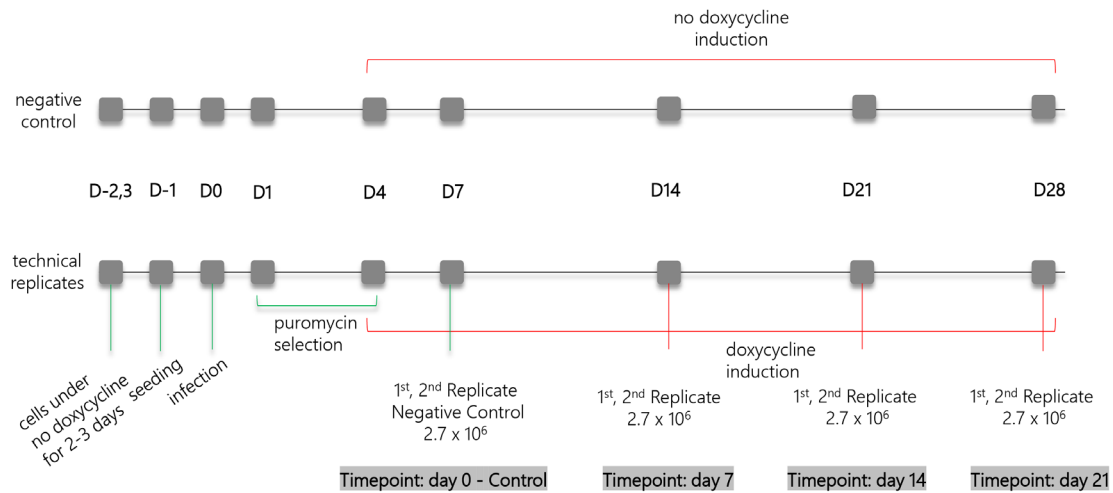
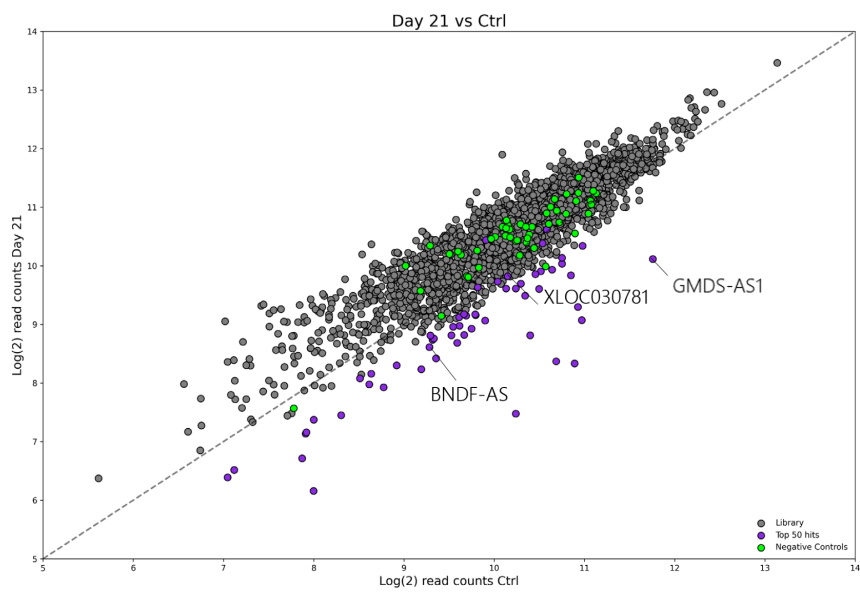
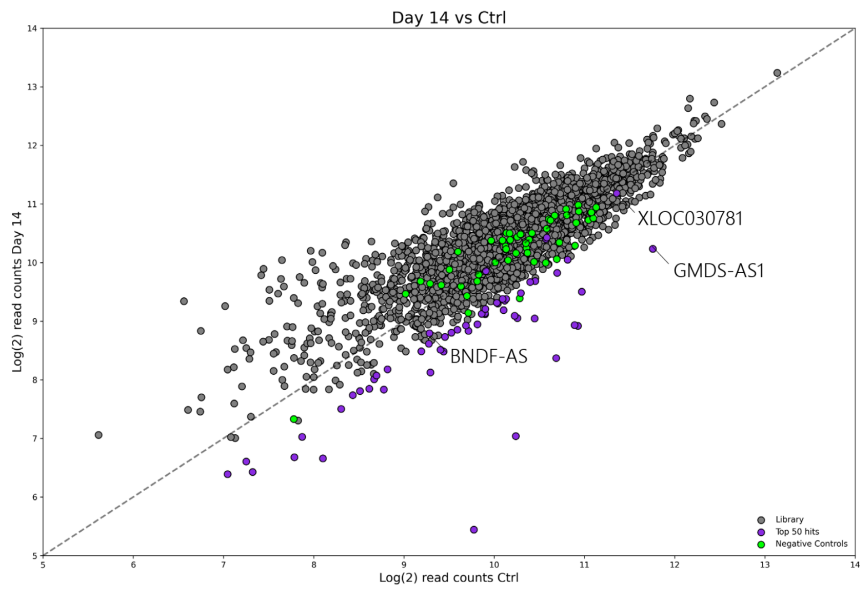
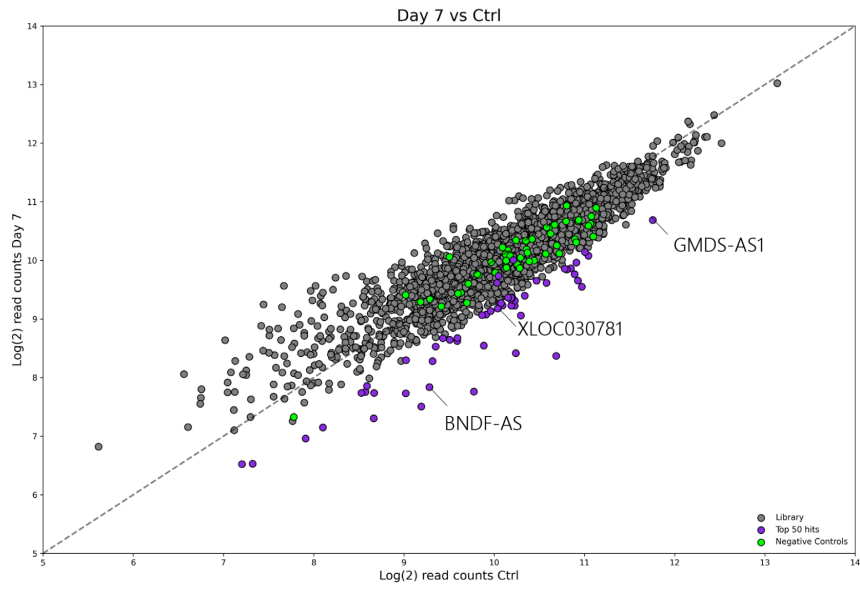


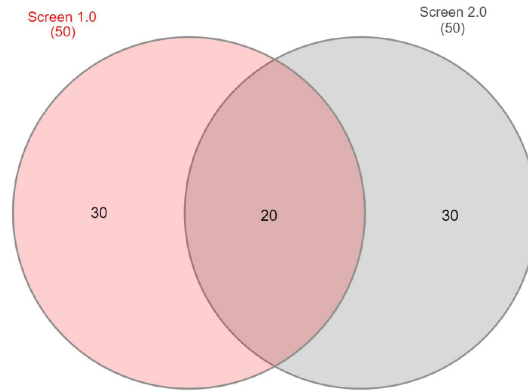
Figure 10. Timeline visualization depicting the specifications of CRISPRi proliferation screen 2.0 regarding the treatment of the negative control and two technical replicates. 501-mel-tetON dCas9 KRAB cells were expanded under continuous induction of dCas9-KRAB expression with 2 $\mu\text{g}/\text{mL}$ doxycycline. Induction was halted around 2-3 days before seeding. On day 0 lentiviral infection was performed. On day 1 up on growth medium change, selection started with 2 $\mu\text{g}/\text{mL}$ puromycin for 3 days, till this point both the negative control and the two technical replicates were treated identically. On day 4 and till the end of the screen growth media supplemented with 2 $\mu\text{g}/\text{mL}$ doxycycline was utilized for the culture/expansion of the cells representing the two technical replicates; on the contrary the negative control was cultured in growth media with no doxycycline. Pellets of minimum 2.7×10^6 cells were collected on day 7 post infection from all the samples and afterwards every 7 days till day 28 only from the two technical replicates and subsequently subjected to gDNA extraction for NGS analysis.

Upon completion of the CRISPRi proliferation screen 2.0, next-generation sequencing was performed on the samples to determine the sgRNA sequences present in the library and their relative abundances. The number of reads associated with each sgRNA was utilized as an indicator of the strength of its gene-suppressing capability, and a comparison was made against control conditions. The average sgRNA reads were calculated for each timepoint by combining data from two technical replicates, and then compared to the control. Subsequently, the \log_2 fold change (FC) was calculated. The resulting observations are presented in the dot plots in Figure 11, where emphasis was placed on both the negative controls and selected lncRNA candidates that surfaced from the CRISPRi proliferation screen 1.0.

Figure 11. Dot plots illustrating the sgRNA abundance at all 3 timepoints (day 7, 14 and 21) compared to control. (As already stated, the control was collected on day 7; for simplicity reasons and for the experiment to be in alignment with the previous CRISPRi proliferation screen 1.0 (not shown), day 7 was characterized as day 0 and therefore all timepoints were reduced by 7 to day 7, 14, 21 instead of day 7, 14, 21 and 28). On all dot plots, on the y axis are the \log_2 read counts of the average of the two technical replicates and the x axis are the \log_2 read counts of the negative control. All the sgRNAs consisting of the CRISPRi lncRNA library 1.0 are shown; highlighted in green are the non-targeting sgRNAs and purple the top 50 sgRNAs. The depletion rate throughout the screen is depicted for the top hits in the CRISPRi proliferation screen 1.0.



A Comparison of CRISPRi Proliferation Screens 1.0 and 2.0



B NGS Analysis Results - log₂FC Day 21 top3 mean

Rank	gRNA_ID Screen 1.0	logFC_D21_top3_mean	Top Candidates	gRNA_ID Screen 2.0	logFC_D21_top3_mean	Top Candidates
1	ENSG00000232995.3	-3.089	RP11-267N12.3	ENSG00000232995.3	-2.315	RP11-267N12.3
2	ENSG00000249859.3	-1.758		ENSG00000235726.1	-2.003	
3	ENSG00000234129.3	-1.735	RP11-120D5.1	ENSG00000196295.7	-1.163	
4	ENSG00000250903.4	-1.619	GMDS-AS1	ENSG00000250903.4	-0.864	GMDS-AS1
5	ENSG00000245573.3	-1.581	BDNF-AS	ENSG00000238113.2	-0.707	
6	XLOC_030781	-1.511	XLOC_030781	ENSG00000248049.2	-0.535	
7	ENSG00000196295.7	-1.411		XLOC_030781	-0.528	XLOC_030781
8	XLOC_153861	-1.346		ENSG00000261824.2	-0.525	
9	XLOC_051428	-1.238		ENSG00000245573.3	-0.513	BDNF-AS
10	ENSG00000229950.1	-1.102		ENSG00000233184.2	-0.460	
11	ENSG00000251562.3	-1.085		ENSG00000234129.3	-0.422	RP11-120D5.1
12	ENSG00000223745.3	-1.028		XLOC_072031	-0.417	
13	ENSG00000238113.2	-0.978		XLOC_093606	-0.409	
14	XLOC_072031	-0.966		XLOC_009062	-0.405	
15	ENSG00000227195.4	-0.962		ENSG00000229950.1	-0.402	
16	ENSG00000226869.2	-0.877		XLOC_021144	-0.402	
17	ENSG00000265688.1	-0.875		ENSG00000261373.1	-0.396	
18	ENSG00000254837.1	-0.867		CTRL0026	-0.395	
19	XLOC_099636	-0.867		ENSG00000223745.3	-0.393	
20	XLOC_018352	-0.863		XLOC_068603	-0.373	
21	ENSG00000257261.1	-0.856		ENSG00000254813.1	-0.362	
22	XLOC_135337	-0.841		ENSG00000234377.3	-0.359	
23	ENSG00000230590.3	-0.817		ENSG00000243069.3	-0.358	
24	ENSG00000224897.2	-0.816		XLOC_046592	-0.353	
25	XLOC_071208	-0.795		XLOC_019913	-0.336	
26	ENSG00000248049.2	-0.788		XLOC_065392	-0.321	
27	XLOC_016079	-0.787		XLOC_018810	-0.314	
28	XLOC_018810	-0.786		ENSG00000253379.1	-0.313	
29	XLOC_000806	-0.760		XLOC_064785	-0.309	
30	ENSG00000229852.2	-0.743		ENSG00000272142.1	-0.307	
31	XLOC_160748	-0.725		ENSG00000224897.2	-0.298	
32	XLOC_008652	-0.711		XLOC_026035	-0.292	
33	XLOC_102857	-0.701		XLOC_105526	-0.292	
34	XLOC_091603	-0.689		ENSG00000244342.1	-0.270	
35	XLOC_068603	-0.676		XLOC_067196	-0.257	
36	ENSG00000226419.2	-0.672		ENSG00000177640.11	-0.252	
37	ENSG00000259380.1	-0.665		XLOC_051428	-0.243	
38	XLOC_065392	-0.652		XLOC_019678	-0.237	
39	ENSG00000233008.1	-0.642		XLOC_083847	-0.224	
40	XLOC_042148	-0.642		ENSG00000264278.1	-0.224	
41	XLOC_067196	-0.629		XLOC_102231	-0.220	
42	XLOC_041345	-0.628		XLOC_152345	-0.215	
43	XLOC_032515	-0.619		ENSG00000230590.3	-0.213	
44	ENSG00000203865.5	-0.616		ENSG00000235703.1	-0.209	
45	ENSG00000272142.1	-0.615		XLOC_004731	-0.207	
46	XLOC_050877	-0.607		ENSG00000261761.2	-0.204	
47	ENSG00000245067.2	-0.605		ENSG00000265688.1	-0.202	
48	XLOC_023788	-0.605		ENSG00000223797.1	-0.201	
49	ENSG00000247828.3	-0.602		ENSG00000248690.2	-0.197	
50	XLOC_037362	-0.601		ENSG00000229140.4	-0.195	

Figure 12. Comparison of CRISPRi proliferation screens 1.0 and 2.0. **A.** Venn diagram illustrating the common top 50 hits between CRISPRi screen 1.0 and 2.0, when comparing the log₂FC top 3 sgRNAs/lncRNA depleted (40% similarity)²³². **B.** The lists consisting of the 50 first hits of the log₂FC top 3 sgRNAs/lncRNA depleted.

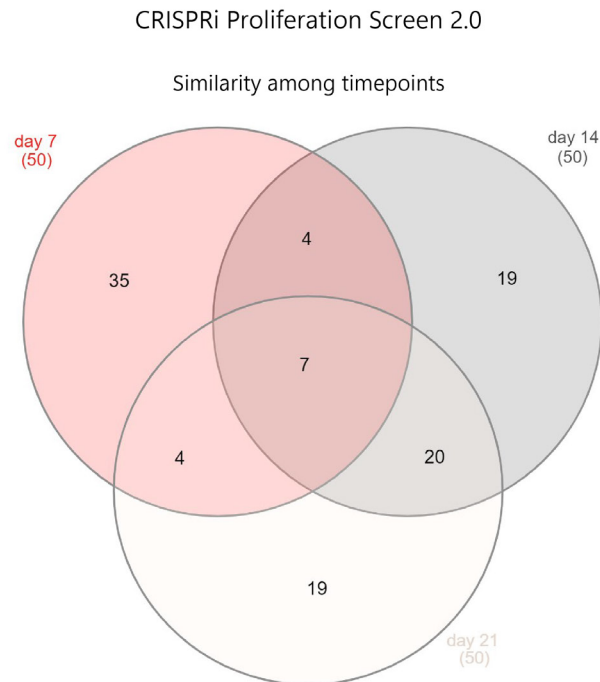


Figure 13. Venn diagrams showcasing the common hits in CRISPRi proliferation screen between the three different timepoints (day 7, 14 and 21) in absolute numbers²³²

Utilizing the same processing analysis implemented in the CRISPRi proliferation screen 1.0, the log₂ FC was ascertained for the top 3 sgRNAs exhibiting significant depletion with respect to each lncRNA in screen 2.0. Given our interest in validating CRISPRi screen 1.0 and confirming the reproducibility of the results, it was indispensable to compare the lists of the top 50 depleted lncRNAs derived from both screening analyses. The observed similarity was remarkable, accounting for 40 % (20/50) of the overall results as depicted in Figure 12A. The most promising lncRNA candidates (*BDNF-AS* #5, *GMDS-AS1* #4, *XLOC030781* #6) that were selected from screen 1.0 for subsequent functionalization studies maintained comparable rankings in screen 2.0 (*BDNF-AS* #9, *GMDS-AS1* #4, *XLOC030781* #7), thereby reinforcing the robustness, legitimacy, and significance of their inclusion in further investigations (Figure 12B).

Examination of the top 50 candidates at three different timepoints during the CRISPRi proliferation screen 2.0 uncovered that day 7 displayed 11 hits in common with day 14 (22 %) and 11 hits in common with day 21 (22 %). Interestingly, day 14 and day 21 demonstrated 27 shared hits, accounting for 54 % of the total hits, thereby suggesting that the depletion of these top-ranked sgRNAs had plateaued by day 14 (Figure 13). The CRISPRi screen 2.0 experiment culminated with the identification of enrichment solely in the positive control *FBXW7* (#15), as anticipated due to its tumour suppressor characteristics and influence in restraining cellular proliferation. None of the remaining positive controls displayed significant associations. It is important to mention the non-appearance of the four positive controls that were spiked into the lncRNA library, likely due to the implementation of a low MOI.

6.3 Functional Characterization of Top Depleted lncRNA Candidates

The second objective of this doctoral research was the in-depth investigation of some of the top depleted lncRNA genes that emerged from both CRISPRi proliferation screen 1.0 and 2.0. For these functional characterization studies lncRNAs *BDNF-AS*, *GMDS-AS1* and novel *XLOC030781* were selected. In essence, CRISPRi proliferation screen 1.0 was a drop out screen, therefore lncRNA genes that were essential for the survival or/and growth in 501-mel-tetON dCas9 KRAB cells were identified. The top depleted sgRNAs represented the sgRNAs that had the most significant impact on the cell survival or proliferation. Depletion referred to a decreased abundance or loss of the sgRNAs, indicating that the targeted genes were critical for the cell viability and growth. The selected lncRNA candidates were then subjected to a series of in vitro experiments to unravel their functional significance. Functional assays, such as downregulation or overexpression of the lncRNAs, were conducted to assess their impact on key cellular processes, such as proliferation, invasion, and apoptosis. Additionally, RNA sequencing was employed to identify the regulatory networks and signaling pathways influenced by these lncRNAs. Finally, fluorescence *in situ* hybridization technique was implemented to collect information on their subcellular localization and expression.

6.3.1 Investigation of Apoptosis Induction in a CRISPRi Environment

Apoptosis is a natural process of programmed cell death that serves as a protective mechanism in maintaining homeostasis and eradicating damaged cells, thus prohibiting the development of various diseases, including cancer. However, cancer cells can exploit certain pathways to evade apoptosis, leading to uncontrolled cell proliferation. Dysregulation of apoptosis is a hallmark of cancer development and progression²⁰⁰. To substantiate the importance of the *BDNF-AS*, *GMDS-AS1*, and *XLOC030781* expression in cell viability in melanoma context, an examination was performed to determine whether their downregulation would trigger apoptotic events. Two different melanoma cell lines were utilized for this experiment: a. 501-mel cell line that has derived from a metastatic site, carries deletions in *CDKN2A* and *PTEN* genes and also two mutations in *BRAF*, and b. WM1361A cell line that has derived from a tumorigenic primary melanoma, carries deletions in *CDKN2A*, *CDKN2B* and *PTEN* and one mutation in *BRAF* and one mutation in *NRAS* (data acquired from Cellosaurus). Due to the pronounced mutational burden typically observed in melanoma tumours, it was advantageous to include two cell lines that each exhibit a unique genomic profile, thereby facilitating a more comprehensive and informative study. For both of the aforementioned cell lines, their CRISPRi cell line derivative was utilized in order to investigate the occurrence of apoptosis in conditions where gene expression was curtailed. As stated, the 501-mel-tetON dCas9 KRAB had been produced in previous time in the Imig lab but the WM136A-tetON dCas9 KRAB had

to be generated. For this reason, the lentivirus production protocol in section 5.2.4.5 was followed and the Lenti_tetOn-dCas9-KRAB plasmid was used to generate concentrated lentivirus. Thereafter, 2×10^6 WM1361A cells were seeded in 2 wells of a 6-well cell culture plate, one would serve as negative control. Upon infection with 50 μ L lentivirus, cells were subjected to blasticidine selection using a concentration of 10 μ g/mL. The selection process continued until complete cell death was observed in the negative control well. Subsequently, the transduced cells were expanded for the purpose of accomplishing generation of the new cell line. A confirmation was achieved through western blot analysis utilizing an anti-SpCas9 antibody (Figure 14). Worth noting is that although the expression of dCas9 didn't appear strong on the blot, the RT-qPCR results demonstrated a high downregulation of the respective lncRNAs (Figure 15).

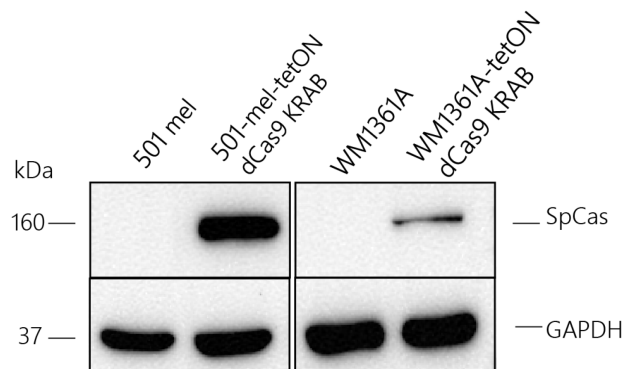


Figure 14. Western blot analysis of whole cell lysates from 501-mel, WM1361A parental cell lines (negative controls) and from their CRISPRi derivative 501-mel-tetON dCas9 KRAB, WM1361A-tetON dCas9 KRAB respectively. Successful confirmation of the dCas9 expression on day 5 post lentiviral transduction but with different intensity for the in-house cell line 501-mel-tetON dCas9 KRAB and the newly generated WM1361A-tetON dCas9 KRAB prior to the apoptosis assay. GAPDH was utilized as the reference protein.

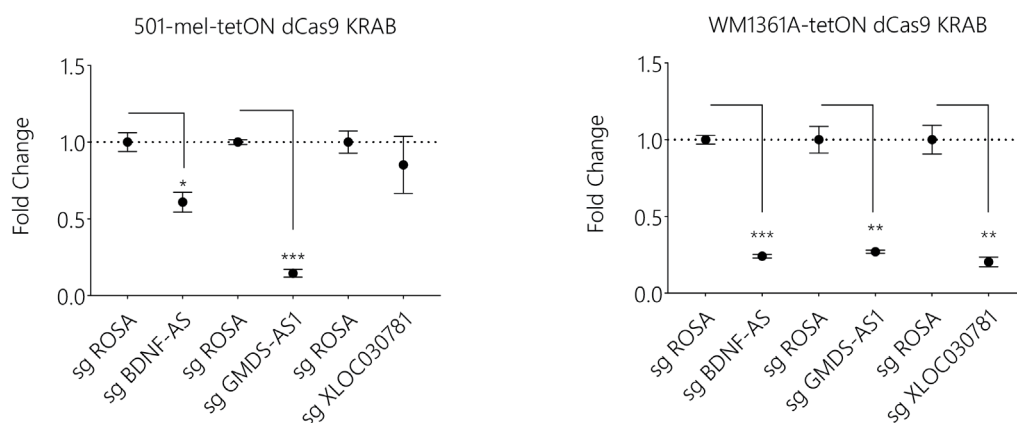


Figure 15. Quantitative real-time PCR validation of robust downregulation of lncRNAs *BDNF-AS*, *GMDS-AS1* and *XLOC030781* in both 501-mel-tetON dCas9 KRAB and WM1361A-tetON dCas9 KRAB cell lines on day 5 post lentiviral transduction in comparison to the non-targeting control sgROSA. Relative gene expression was calculated using *GAPDH* as the housekeeping gene. Data are represented as the mean \pm standard error (SE). Student's t test was used to determine statistical significance: $p < 0.05$ (*), $p < 0.01$ (**), $p < 0.001$ (***).

To ensure adherence to the protocol outlined in section 5.2.4.7, the expression of dCas9 was verified at mRNA and protein levels for both cell lines, as visually presented in Figure 15. The functionality of the CRISPR dCas9 KRAB system holds great importance; thus, the observed results arise from an effective knock-down. Cells were subjected to doxycycline treatment for a total duration of 5 days. To investigate apoptosis, the detection focused on the cleavage of PARP1 fragments measuring 89 and 24 kDa. PARP1 exhibits responsiveness towards DNA damage repair, and its cleavage by Caspase-3 serves as a prominent indicator of apoptosis. Herein, the quantitative results acquired through densitometry of two independent experiments and one blot image are shown for each cell line (Figure 16). Interestingly, it was observed that downregulation of all three lncRNAs *BDNF-AS*, *GMDS-AS1*, and *XLOC030781* initiated apoptosis on different levels for each lncRNA but in both cell lines, illustrating the importance of their expression in cell viability. Of greater statistical significance the initiation of apoptosis was depicted upon suppression of lncRNAs *GMDS-AS1* and *XLOC030781*.

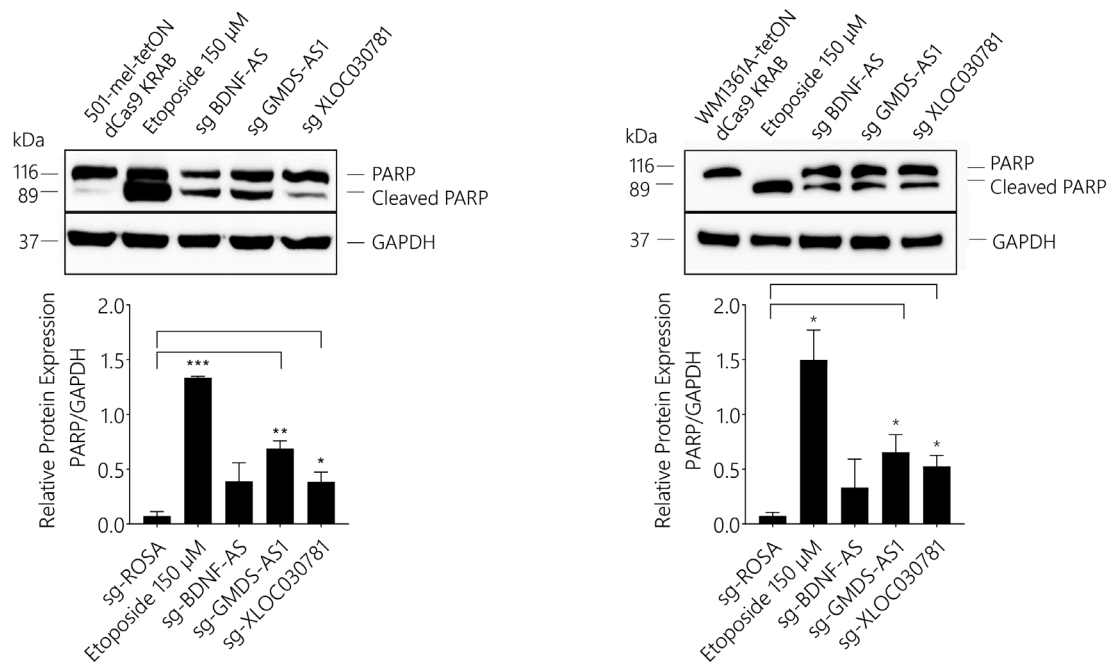
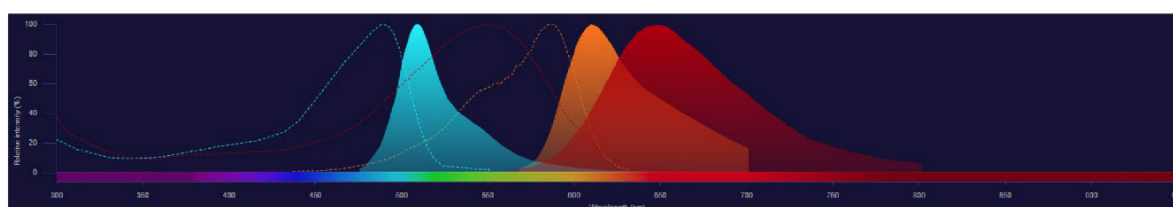


Figure 16. Western blot analysis and relative quantification by densitometry of whole cell lysates (20 μg) from 501-mel-tetON dCas9 KRAB and WM1361A-tetON dCas9 KRAB infected with 50 μL of lentiviruses suppressing lncRNAs *BDNF-AS*, *GMDS-AS1* and *XLOC030781*. Non-infected cells of both cell lines were used as negative controls and cells treated with 150 μM Etosposide as positive control. Anti-PARP1 antibody was utilized for detection of apoptosis on day 5 post lentiviral transduction and *GAPDH* as the reference protein. The statistical analysis was performed on two independent experiments. Student's t test was used to determine statistical significance: $p < 0.05$ (*), $p < 0.01$ (**), $p < 0.001$ (***).

6.3.2 Role of lncRNA Candidates in Cell Cycle Regulation

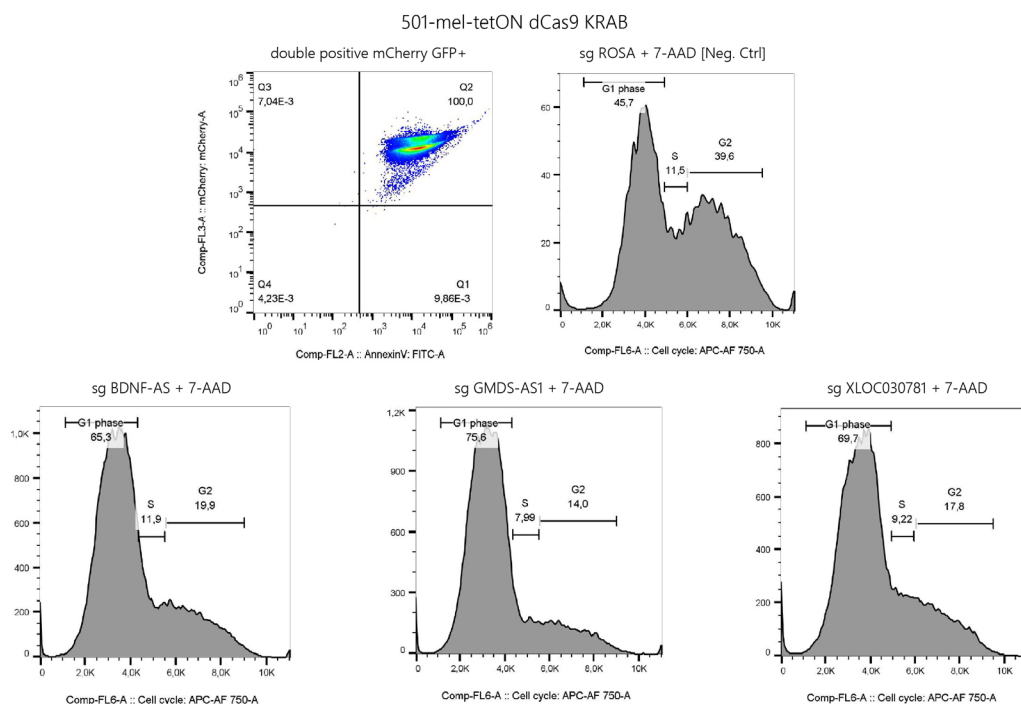
Having already established that the suppression of all three lncRNAs elicits apoptotic events, the examination of the repercussions of CRISPR knock-down on the intricate machinery of the cell cycle, was subsequently pursued. Cell cycle is divided into four stages; named as G1, S, G2, and M phases. G1 and G2 phases serve as intervals referred to as “gaps” between DNA synthesis and mitosis. During the preliminary G1 phase, the cell undergoes preparations for DNA synthesis. Active DNA synthesis in the S phase results in a DNA content that ranges between 2N and 4N. Subsequently, the G2 phase designates the second gap in the cell cycle, enabling the cell to make necessary preparations for the M phase. The most common approach to study the cell cycle and determine the cell distribution in the four phases is by measuring the cellular DNA content²⁰¹. Fluorescent dyes are employed for nuclei labeling of cells in suspension and the fluorescence properties of each cell in the population are analyzed. For this experiment, 501-mel-tetON dCas9 KRAB and WM1361A-tetON dCas9 KRAB were utilized as described in the protocol in section 5.2.4.8. As previously mentioned, the cell lines carried two fluorescent markers, an mCherry marker for the Cas9 expression and a GFP marker for the transduction validation. To visualize the amount of DNA content, we employed an infrared-emitting 7-AAD dye. Given that our experiment involved the utilization of three fluorochromes, it became imperative to implement compensation techniques during analysis, since there was significant spillover mainly between mCherry and 7-AAD fluorescent channels (Figure 17).



fluorophore	excitation wavelength (nm)	emission wavelength (nm)
GFP	488	507
mCherry	587	610
7-AAD	546	647

Figure 17. Fluorophore spectra viewer depicting the absorption and emission spectra of GFP, mCherry and 7-AAD, the overlap regions are also shown between mCherry and 7-AAD. (Image obtained by Thermofisher Scientific fluorophore spectra viewer tool.) Table showing the excitation and emission wavelengths of the three fluorophores.

Two individual experiments incorporating two technical replicates per condition were conducted to examine the impact of downregulating the three lncRNAs in both cell lines, as compared to the negative control sgROSA. Herein, the depiction of the FACS plot together with the investigation of an individual experiment are showcased in Figure 18-19. Our findings demonstrate that repression led to a G1 phase arrest in both cell lines, which was indicated by the predominant distribution of cells in this particular state. The highest percentages occurred in 501-mel-tetON dCas9 KRAB cells where *BDNF-AS* (76 %) and *GMDS-AS1* (74.1 %) were downregulated, slightly lower levels observed under *XLOC030781* suppression (72.7 %) (sgROSA 49.25 %). Furthermore, it was shown that during phase S, the stage where DNA synthesis happens, a minor decline in cell population was evident for both cell lines compared to the negative control. The most noteworthy reduction was identified in 501-mel-tetON dCas9 KRAB cells (sgROSA 7.26 %), where knock-down of *BDNF-AS* (6.69 %) and *GMDS-AS1* (6.1 %) was observed. Regarding the WM1361A-tetON dCas9 KRAB cell line (sgROSA 17.35 %), the highest decrease was where *XLOC030781* (13 %) was suppressed. At last, prior to mitosis, phase G2 witnessed a higher cell occupancy rate for both cell lines when compared to phase S. Nevertheless, a substantial decrease in relation to the negative control was detected, where knock-down of all three lncRNAs (*BDNF-AS* 16.65 %, *GMDS-AS1* 19.10 % and *XLOC030781* 18.10 %) occurred in 501-mel-tetON dCas9 KRAB cell line (sgROSA 42.15 %). A decrease in G2 phase was likewise observed in all three lncRNAs (*BDNF-AS* 19.90 %, *GMDS-AS1* 16.10 % and *XLOC030781* 20.80 %) within the WM1361A-tetON dCas9 KRAB cell line (sgROSA 27.20 %), although statistical significance was not reached due to elevated standard deviation values. Nonetheless, the phenomenon remained evident. The cell cycle distribution assay was conducted concurrently with the apoptosis assay, thus the RT-qPCR results hold validity for both experiments.



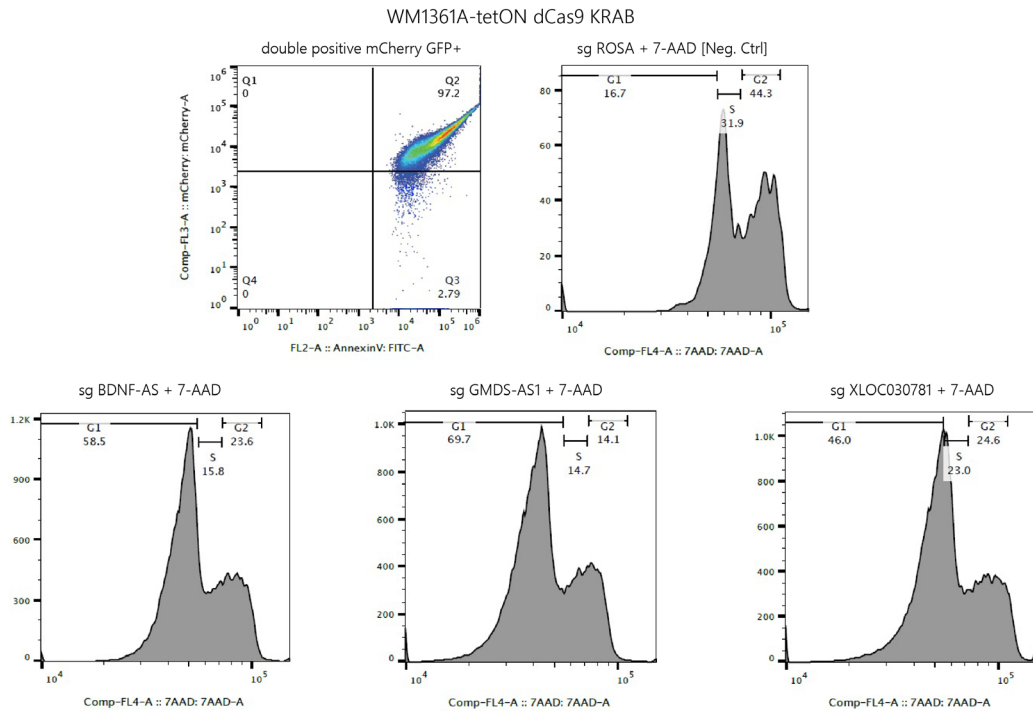


Figure 18. Cell Cycle analysis using flow cytometry. Visualization of the mCherry-GFP double-positive single cells is demonstrated on both FACS set plots. To quantify the DNA content, these cells were subjected to staining using 7-AAD. The recorded percentages reflect the distribution of the single cells across the G1, S, and G2 phases. Upper FACS set visually depicts the consequences associated with downregulating *BDNF-AS*, *GMDS-AS1*, and *XLOC030781* in the cellular cycle in 501-mel-tetON dCas9 KRAB cell line compared to the negative control sgROSA. Similarly, the lower FACS set of plots highlights the findings specific to the WM1361A-tetON dCas9 KRAB cell line.

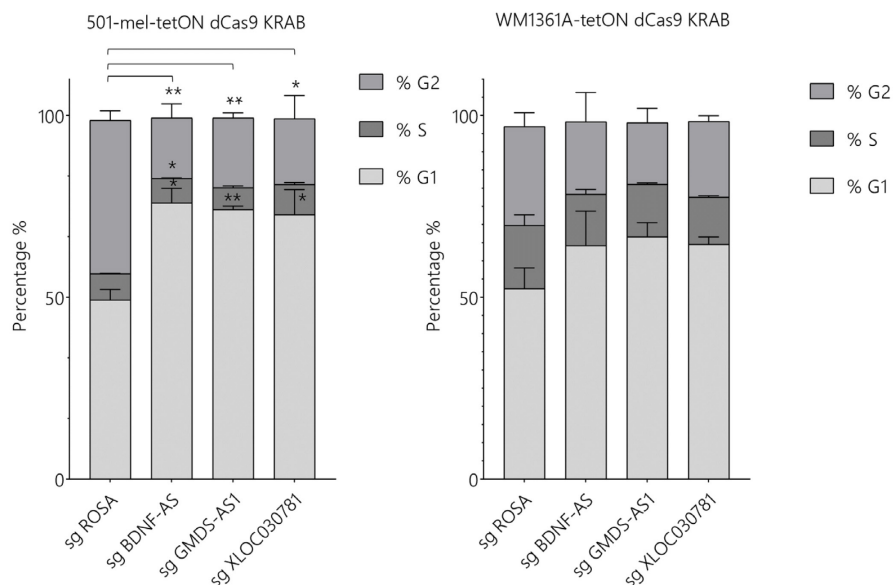


Figure 19. Quantitative analysis of cell cycle distribution assay in both 501-mel-tetON dCas9 KRAB and WM1361A-tetON dCas9 KRAB cell lines, by utilizing data obtained from flow cytometry. To enhance comparability, a consolidated bar graph incorporating all three stages (G1, S, and G2) was generated for each sample. The results were derived from two distinct experiments, and the necessary compensation analysis was conducted using Flowjo software. The data are presented as the mean \pm standard error (SE), with statistical significance determined through Student's t test: $p < 0.05$ (*), $p < 0.01$ (**).

6.3.3 Exploring the Invasive Aptitude of Top lncRNA Candidates

6.3.3.1 Invasion Assay in CRISPRi Environment

Cancer lethality predominantly arises from the occurrence of metastasis, wherein the extensive dissemination of cancer cells to distant locations accounts for up to 90 % of fatalities caused by solid tumours. The process involves various movement tactics employed by cancer cells to spread from the primary tumour through the circulatory and lymphatic systems, eventually colonizing peripheral organs²⁰². Within the objective of achieving a comprehensive functional profiling of *BDNF-AS*, *GMDS-AS1* and *XLOC030781*, an evaluation of their invasive abilities was conducted. To accomplish this, we employed only 501-mel-tetON dCas9 KRAB cells, leveraging the fact that its parental cell line, 501-mel, originated from a metastatic melanoma site; and utilized the well-established transwell migration and invasion assays (Boyden Chamber Assay) wherein two chambers containing growth medium are separated by a porous membrane following the protocol guidelines described in sections 5.2.4.9.1-5.2.4.9.2²⁰³.

The systematic repetition of the assay was performed due to the intricate cellular requirements crucial for the invasion process, encompassing factors such as seeding density, assay duration, and the chemotactic agent employed to stimulate cell invasion. Moreover, the inconsistent results obtained upon silencing two lncRNAs (*BDNF-AS* and *GMDS-AS1*) emphasized the significance of obtaining reproducible experimental outcomes. Hereby, two separate representative experiments involving the whole set of three lncRNAs, as well as three experiments focusing on *XLOC030781* are presented along with their quantitative analysis (Figure 20-21). All experiments were performed with two technical replicates per condition. After establishing the optimal experimental conditions (seeding density of 1.4×10^5 cells/well and a 48-hour incubation in the transwell insert) it was demonstrated that downregulation of *XLOC030781* consistently hindered invasion. On the other hand, the suppression of *BDNF-AS* in relation to *GMDS-AS1* consistently exerted a greater inhibitory effect on invasion. However, the overall reduction in invasion levels resulting from their suppression lacked consistency and displayed an arbitrary pattern, thus prompting a redirection of our research emphasis towards *XLOC030781*. Figure 22 elucidates the results acquired from the employment of RT-qPCR to validate the suppression of all three lncRNAs on days 3 and 5, as part of the experimental process.

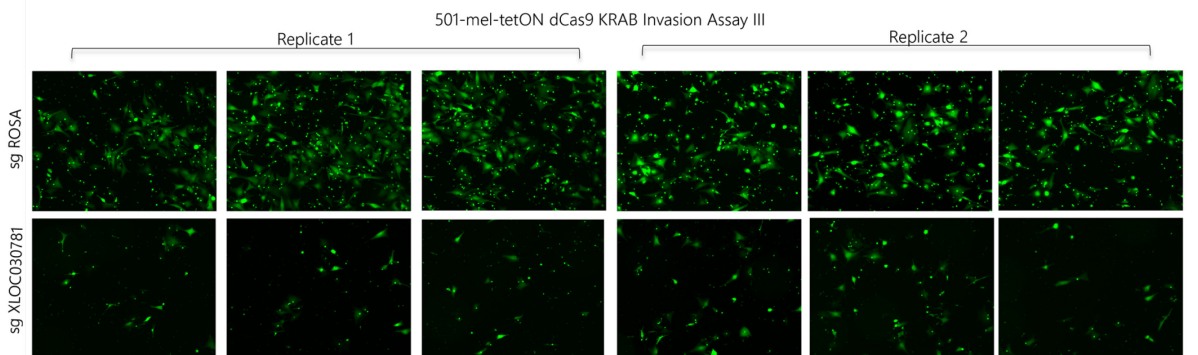
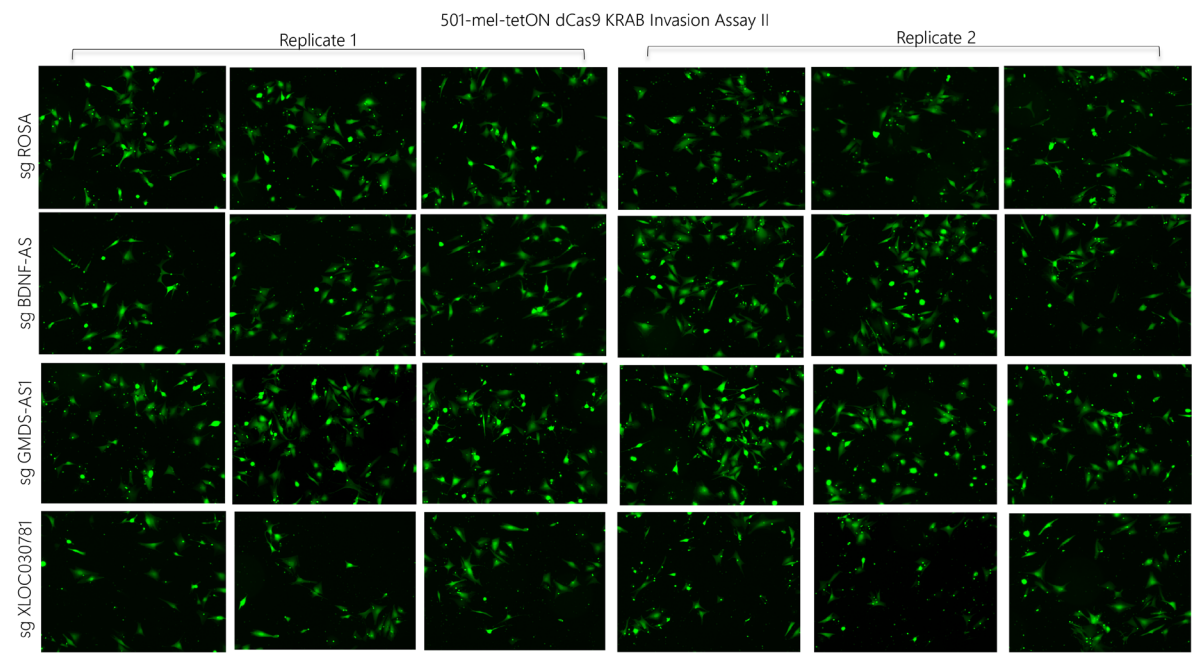
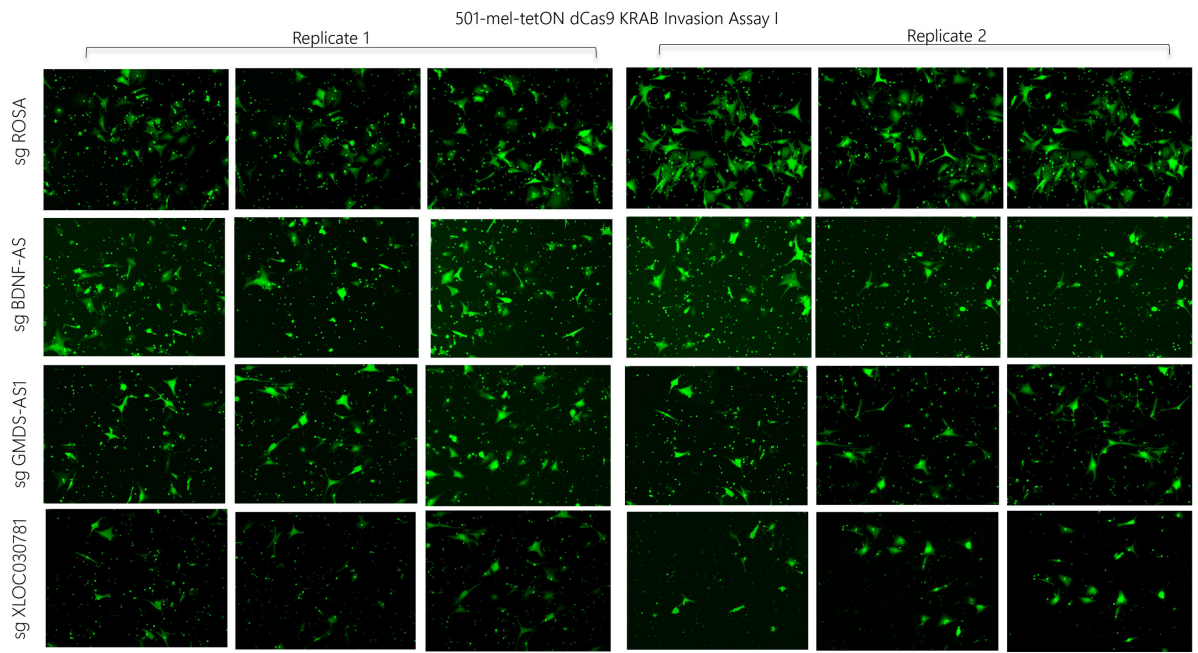


Figure 20. Qualitative analysis of cell migration assessed by an *in vitro* transwell assay. Representative fluorescent images from three independent experiments in 501-mel-tetON dCas KRAB cell line, employing two replicates per condition and acquiring a minimum of 10 images of each sample (herein, 3/10 images are shown for each replicate) using an objective lens 10X. Images were captured on day 5 post lentivirus transduction and after 48 hours of incubation at 37 °C with treatment of a combination of chemo-attractants 10 % FBS and 1 μM LPA and subsequent staining with Calcein AM 2 μg/mL. First and second image series illustrate from two independent experiments the alterations in invasion patterns resulting from the suppression of *BDNF-AS*, *GMDS-AS1*, and *XLOC030781* in 501-mel-tetON dCas KRAB compared to non-targeting control sgROSA. The third image series (third individual experiment) is focused specifically on knock-down of *XLOC030781* showcasing statistically significant reduced invasive potential. Student's t test was used to determine statistical significance: $p < 0.05$ (*), $p < 0.01$ (**), $p < 0.001$ (***)

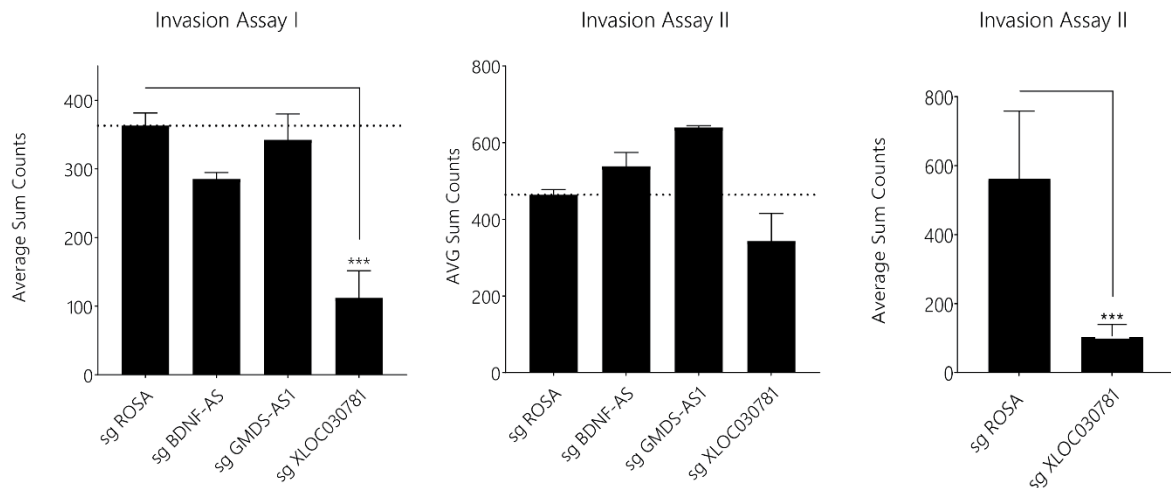


Figure 21. Quantitative analysis of cell migration assessed by an *in vitro* transwell assay. Results originate from the above shown three individual experiments. Cells were counted using the automated macro in ImageJ as mentioned in section 5.2.4.9.2. Bar graphs were created on Prism Graph 8.0 and statistical analysis was performed using Student's t test to determine statistical significance: $p < 0.05$ (*), $p < 0.01$ (**), $p < 0.001$ (***)

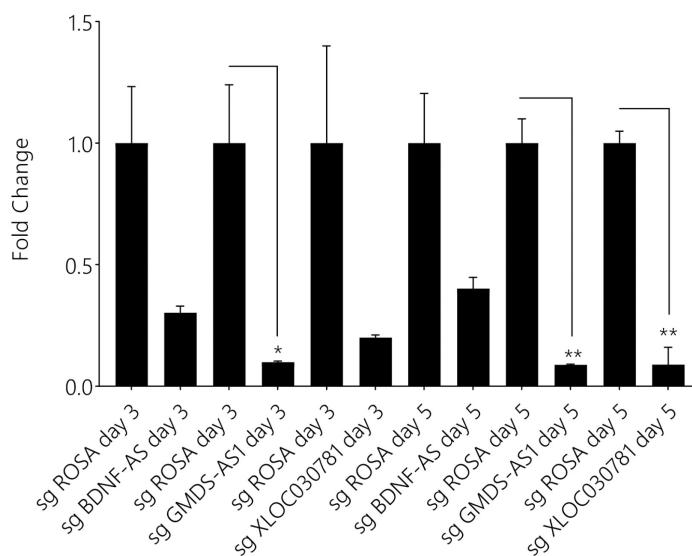


Figure 22. Quantitative real-time PCR validation of strong downregulation of lncRNAs *BDNF-AS*, *GMDS-AS1* and *XLOC030781* in both 501-mel-tetON dCas9 KRAB cell line on day 3 and 5 post lentiviral transduction in comparison to the non-targeting control sgROSA. Relative gene expression was calculated using *GAPDH* as the housekeeping gene. Data are represented as the mean \pm standard error (SE). Student's t test was used to determine statistical significance: $p < 0.05$ (*), $p < 0.01$ (**).

6.3.3.2 Invasion Assay in CRISPRa Environment

After evaluating the invasive potential modulated by the lncRNA downregulation, the analysis progressed to explore the impact of their overexpression on cell invasiveness. For this purpose, Benchling was utilized to design three sgRNA sequences, with the objective of targeting the -200 bp window upstream of the transcription start site for *BDNF-AS*, *GMDS-AS1*, *XLOC030781*, and *PVT1*. The inclusion of *PVT1* as an additional target lncRNA, was justified based on existing scientific evidence indicating its upregulation in melanoma cases²⁰⁴. Following the established protocols presented in sections 5.2.1-5.2.3, the sgRNA sequences were cloned into Lenti-sgRNA-(MS2)-puro-backbone vector and subsequently lentiviruses were produced using protocol 5.2.4.5. In order to identify the most effective sgRNA for each lncRNA, the in-house 501-mel SAM cell line was utilized. Following cell infection (100 μ L of each lentivirus), the efficacy of all sgRNAs in promoting lncRNA overexpression was quantified on day 6 post-transduction through RT-qPCR analysis. The most potent sgRNA is depicted in green in Figure 23.

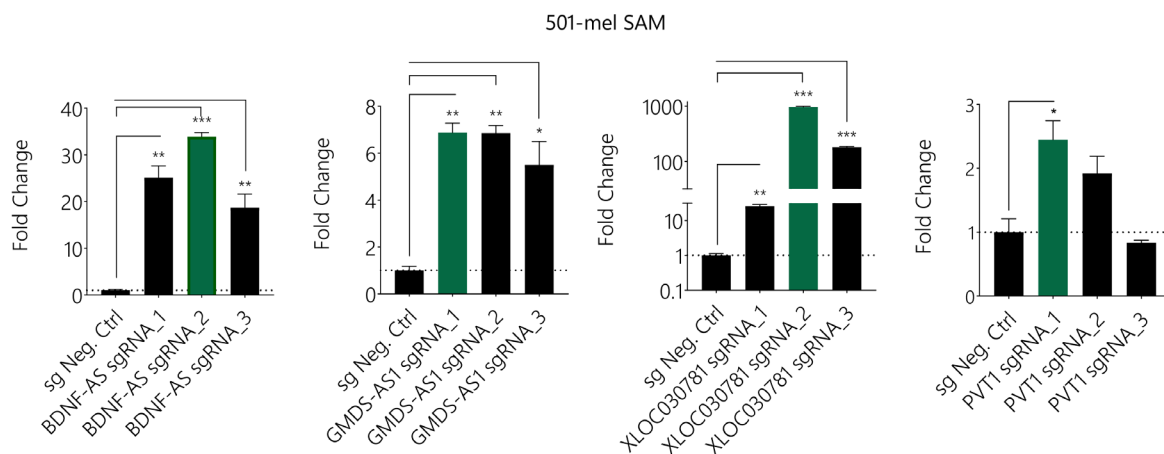
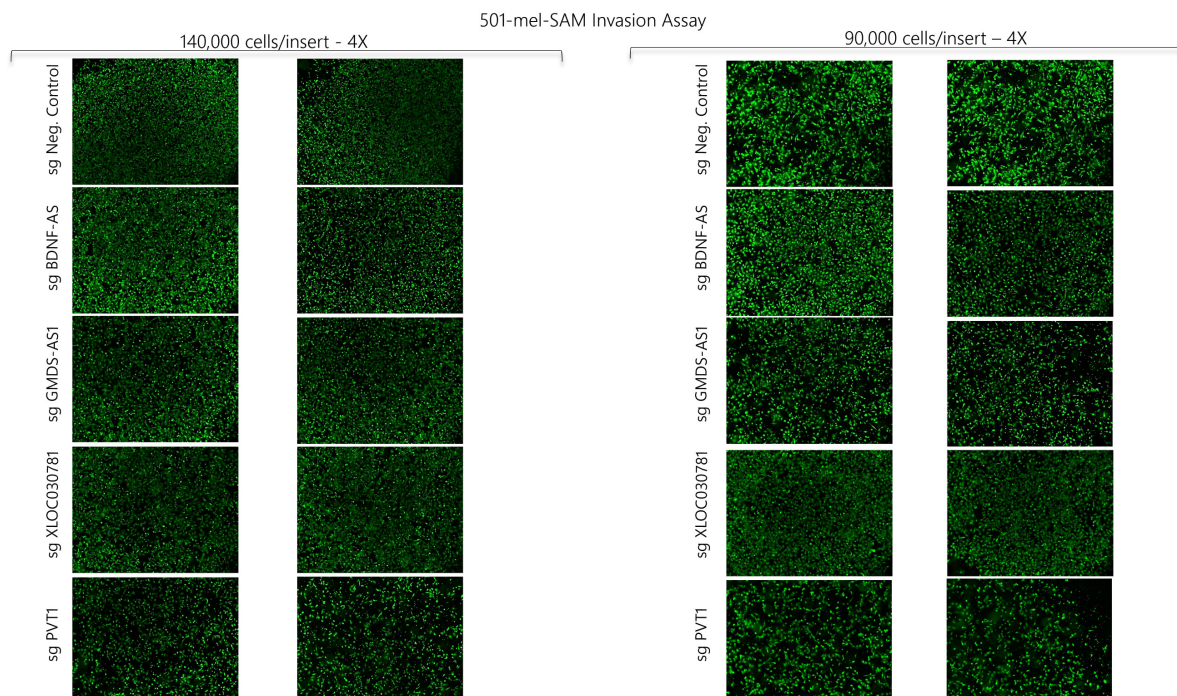


Figure 23. Quantitative real-time PCR validation of sgRNA efficiency targeting lncRNAs *BDNF-AS*, *GMDS-AS1*, *XLOC030781* and *PVT1* in 501-mel SAM cells on day 3 and day 5 post lentiviral transduction. For each gene, three sgRNAs were designed and their upregulation efficiency was compared to the non-targeting control sgNeg Ctrl. Highlighted (light grey) are the top sgRNAs selected to be utilized in the in vitro transwell invasion assay. Relative gene expression was calculated using *GAPDH* as the housekeeping gene. Data are represented as the mean \pm standard error (SE). Student's t test was used to determine statistical significance: $p < 0.05$ (*), $p < 0.01$ (**), $p < 0.001$ (***).

Consequently, an analysis was implemented to identify the optimal conditions required for the assay's implementation (Figure 24-25). As reiterated earlier, the process of in vitro invasion is highly complex and sensitive, influenced by numerous variables that intricately shape its manifestation. Hence, our initial approach focused on applying the protocol used for the CRISPRi system, which entailed seeding 140,000 cells per insert, as seeding density emerged as the paramount factor. However, this attempt was proven unsuccessful because the pore membrane was completely saturated, prompting a subsequent reduction in seeding density by 35.71 % to 90,000 cells per insert. Nevertheless, this adjustment similarly failed to

yield the expected outcomes. Thereafter, a more drastic reduction of 60 % was implemented, seeding 55,000

cells per insert. To ascertain the effects of this altered seeding density, both 501-mel parental and 501-mel-tetON dCas9 KRAB cell lines were also utilized but for 501-mel SAM only the negative control and *XLOC030781* were examined. It was clearly shown that 501-mel parental cell line was highly invasive even under the low seeding density, verifying its metastatic origin. Furthermore, quite interestingly, it was demonstrated that the type of CRISPR system transduced in the parental cell line altered its invasive potential. Consistent with our findings regarding 501-mel-tetON dCas9 KRAB, such low density was prohibitive for the cells to penetrate the chamber's pore membrane. On the contrary for 501-mel SAM, it appeared to be optimal. An additional experiment was performed using 50,000 cells per insert for *BDNF-AS* and *XLOC030781*, where it was shown that the invasiveness levels remained nearly equivalent among the negative control and the two lncRNAs, signifying that the overexpression of these genes did not significantly amplify the cell line's invasiveness. Worth noting is that the cell line already exhibited substantial invasiveness post integration of the SAM system and that there is significant morphological difference of the invading cells compared to 501-mel-tetON dCas9 KRAB. Concerning *GMD5-AS1* and *PVT1*, repetition of the assay is required with seeding density of 50,000 cells per insert, since in this doctoral study we mostly focused on the establishment of the protocol and on *BDNF-AS* and *XLOC030781*.



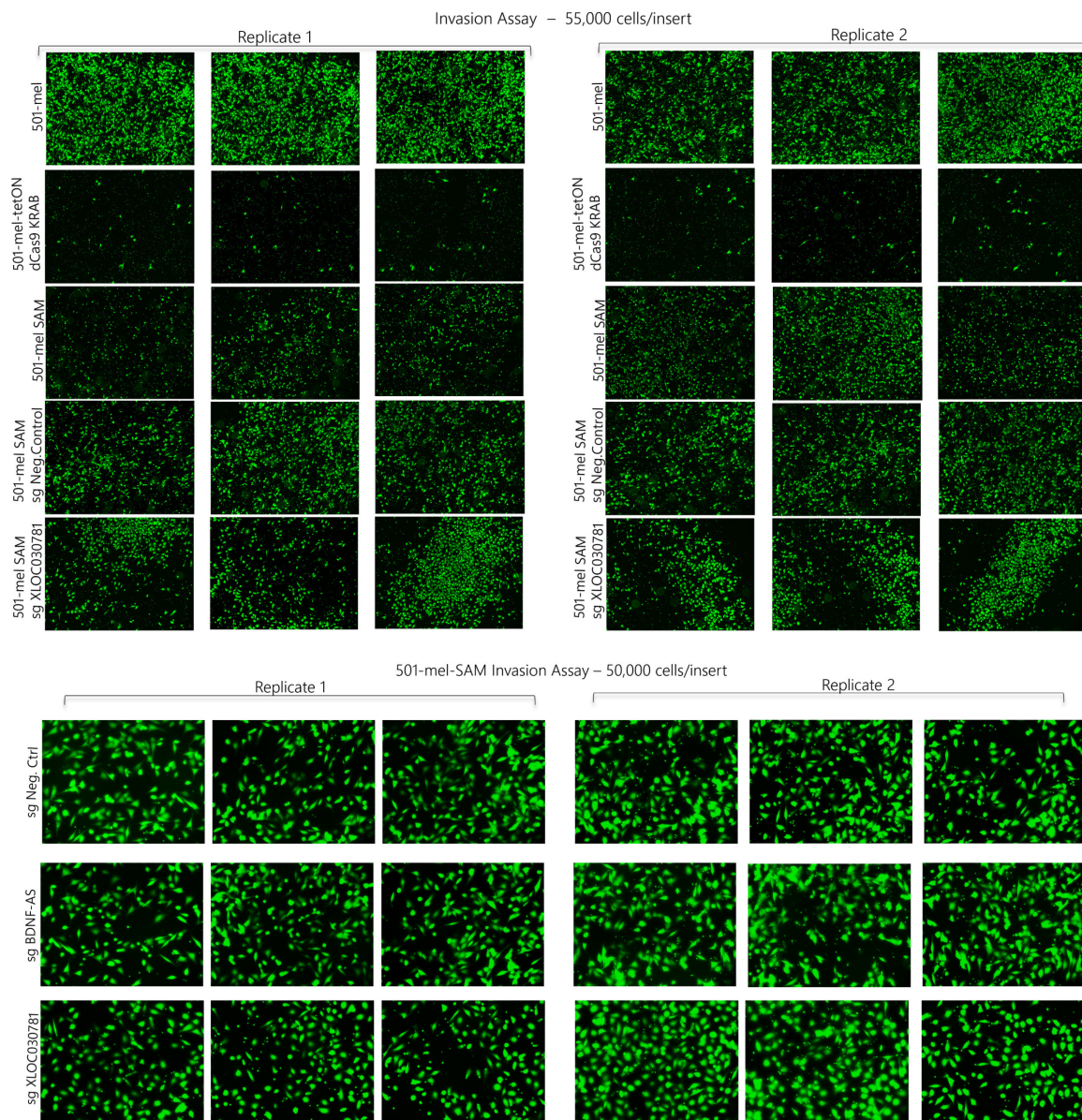


Figure 24. Qualitative analysis of cell migration assessed by an *in vitro* transwell assay. Representative fluorescent images from three independent experiments utilizing different cell lines deriving from 501-mel parental, employing two replicates per condition and acquiring a minimum of 5 images of each sample (herein, 2-3/5 images are shown for each replicate) using an objective lens 4X. Images were captured on day 5 post lentivirus transduction (regarding CRISPRi and CRISPRa cell lines) and after 48 hours of incubation at 37 °C with treatment of a combination of chemo-attractants 10 % FBS and 1 μ M LPA and subsequent staining with Calcein AM 2 μ g/mL. First image series illustrate results in invasion potential in exclusively 501-mel SAM cell line where *BDNF-AS*, *GMDS-AS1*, *XLOC030781* and *PVT1* were upregulated when 140,000 cells/insert where seeding for the assay. No significant difference was shown among the samples comparing to the sgNeg. Control. The second image series focused on investigating the invasion patterns among 501-mel cell line, 501-mel-tetON dCas9 KRAB (CRISPRi derivative system) and 501-mel SAM (CRISPRa derivative system). For 501-mel SAM cells also infected with sg Neg. Control and sgXLOC030781 were used. The seeding density was reduced to 55,000/insert. Significant differences were revealed amongst the different cell lines. Finally, the third image series showcase the results of invasion assay in 501-mel SAM cells where *BDNF-AS* and *XLOC030781* were overexpressed in comparison to sgNeg. Ctrl using the most optimal seeding density of 50,000 cells/insert. Student's t test was used to determine statistical significance: $p < 0.05$ (*), $p < 0.01$ (**), $p < 0.001$ (***)

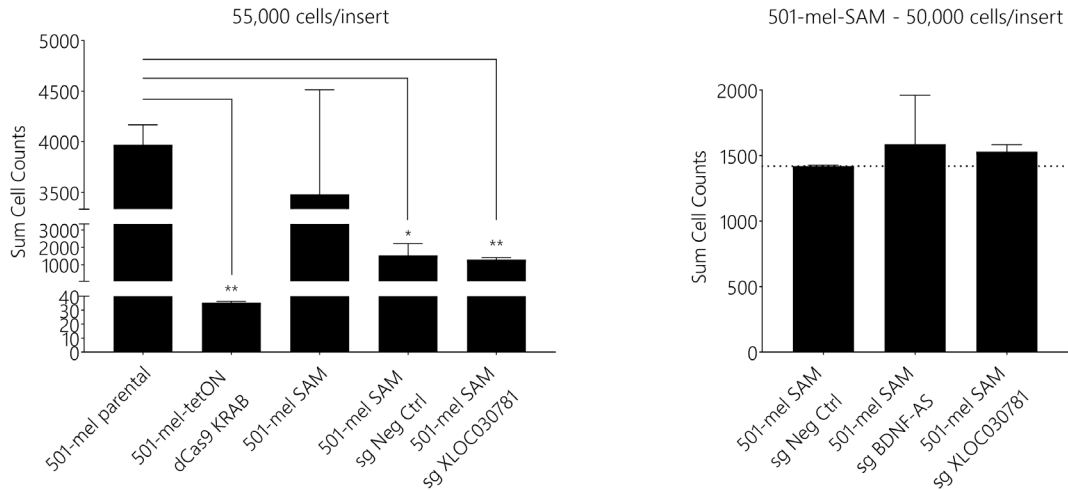


Figure 25. Quantitative analysis of cell migration assessed by an *in vitro* transwell assay. Results originate from the above shown two last individual experiments. Cells were counted using the automated macro in ImageJ as mentioned in section 5.2.4.9.2. Bar graphs were created on Prism Graph 8.0 and statistical analysis was performed using Student's t test to determine statistical significance: $p < 0.05$ (*), $p < 0.01$ (**).

6.3.4 Subcellular Localization utilizing Fluorescence *in situ* Hybridization

Initially, the prevailing notion was that lncRNAs were predominantly found within the nucleus and chromatin, engaging in an epigenetic modulation of gene expression. However, increasing evidence has emerged in support of the considerable abundance of lncRNAs in the cytoplasmic compartment. The determination of the intracellular localization of lncRNA molecules holds substantial implications for understanding their functional role thus necessitating its inclusion as a critical aspect in their comprehensive analysis. Therefore, the subcellular localization of *BDNF-AS*, *GMDS-AS1*, and *XLOC030781* was examined employing the multiplexed *in-situ* fluorescence hybridization technique. The DNA probe set designed to target lncRNAs *BDNF-AS* and *XLOC030781* were both marked with the identical fluorochrome, namely, Alexa Fluor 647 (AF-647). However, the DNA probe set used for *GMDS-AS1* was marked with a distinct fluorochrome, labelled as Alexa Fluor 546 (AF-546). By following this probe labelling strategy, it became feasible to simultaneously detect two lncRNAs (*BDNF-AS*, *GMDS-AS1*) in a single sample, considering the high cost of reagents associated with this technique. The CRISPRi stable cell lines 501-mel-tetON dCas9 KRAB and WM316A-tetON dCas9 KRAB were compared with their respective controls, the parental cell lines 501-mel and WM1361A. In order to evaluate the accuracy of the protocol outlined in section 5.2.4.10, the detection of *PPIB* (Peptidylprolyl Isomerase B) served as a positive control labeled with fluorochrome Alexa Fluor 546 (AF-546), and its selection was based on its consistent expression and ubiquitous presence at relatively high levels in most cells, thus providing a reliable reference gene to assess validation of FISH technique.

501-mel parental & 501-mel-tetON dCas9 KRAB

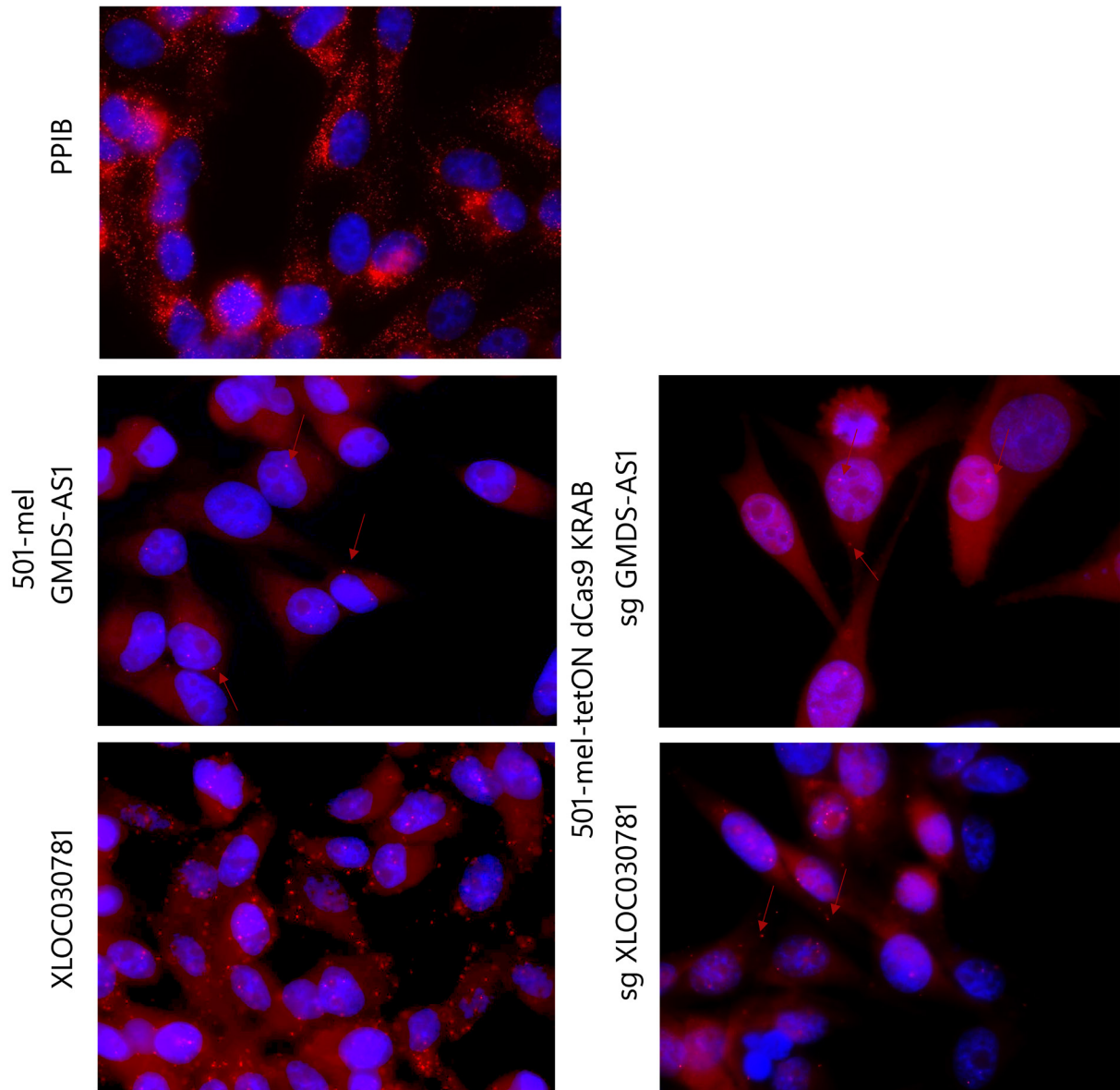


Figure 26. Subcellular detection of lncRNA transcripts *GMDS-AS1* and *XLOC030781* in 501-mel (control) and 501-mel-tetON dCas9 KRAB (knock-down) cell lines. FISH using DNA probes against *GMDS-AS1* (AF-546), *XLOC030781* (AF-647) and *PPIB* (AF-546), and nucleus was stained with DAPI. Robust signal against *PPIB* which was utilized as positive control. Signal is significantly stronger for *XLOC030781* in relation to *GMDS-AS1*. Arrows depict signal where it is of low intensity. Representative Images were processed and merged using software Image J.

WM1361A parental & WM1361A-tetON dCas9 KRAB

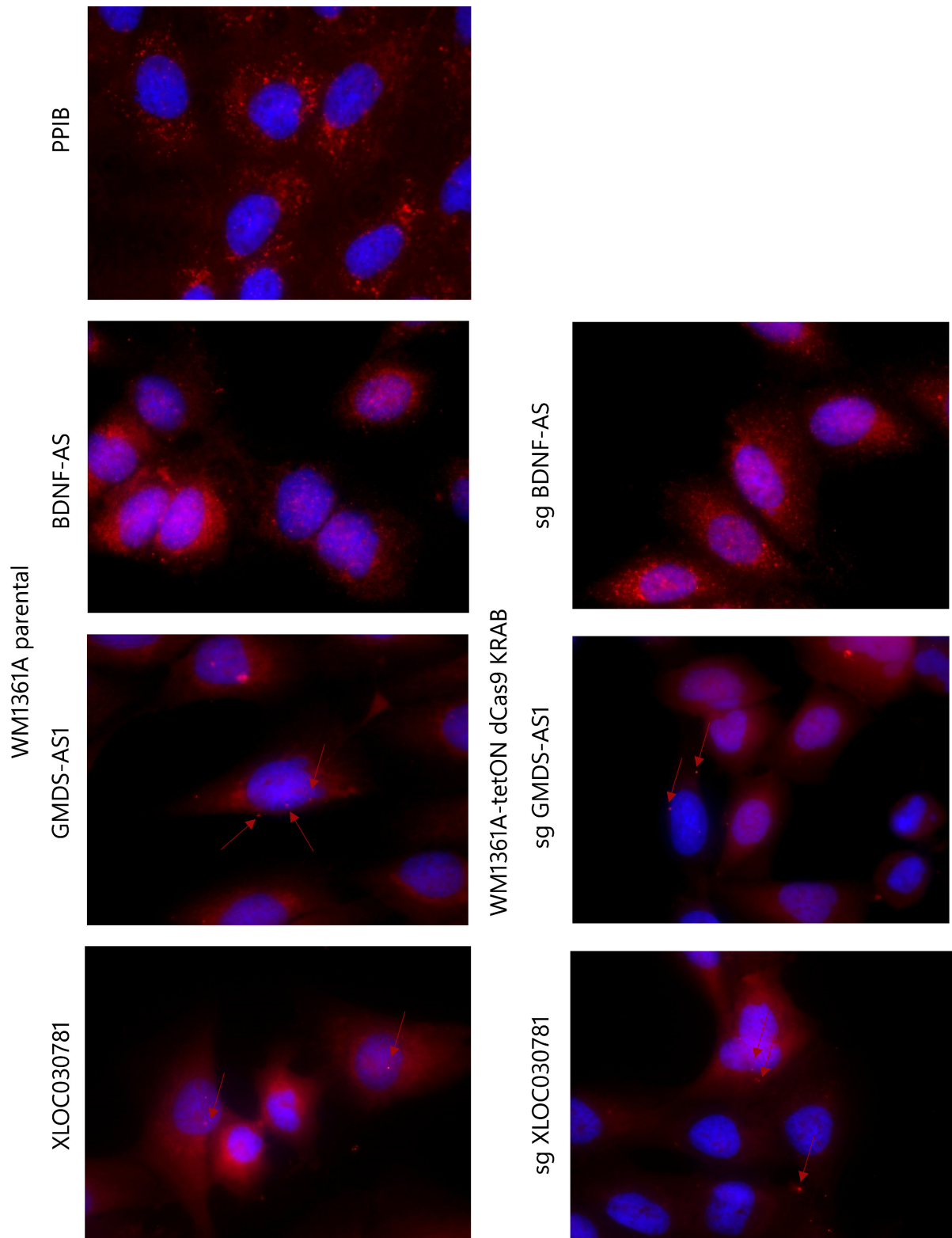


Figure 27. Subcellular detection of lncRNA transcripts *BDNF-AS*, *GMDS-AS1* and *XLOC030781* in WM1361A (control) and WM1361A-tetON dCas9 KRAB (knock-down) cell lines. FISH using DNA probes against *GMDS-AS1* (AF-546), *BDNF-AS* and *XLOC030781* (AF-647), *PPIB* (AF-546), and nucleus was stained with DAPI. Robust signal against *PPIB* which was utilized as positive control. Signal is significantly stronger for *BDNF-AS* in relation to *GMDS-AS1* and *XLOC030781*. Arrows depict signal where it is of low intensity. Representative images were processed and merged using software Image J.

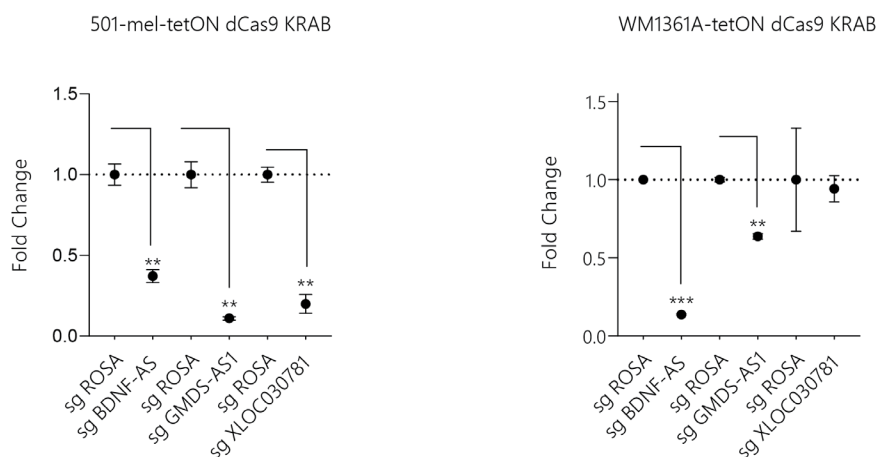


Figure 28. Quantitative real-time PCR validation of robust downregulation of lncRNAs *BDNF-AS*, *GMDS-AS1* and *XLOC030781* in both 501-mel-tetON dCas9 KRAB and WM1361A-tetON dCas9 KRAB cell lines on day 5 post lentiviral transduction in comparison to the non-targeting control sgROSA. Relative gene expression was calculated using GAPDH as the housekeeping gene. Data are represented as the mean \pm standard error (SE). Student's t test was used to determine statistical significance: $p < 0.05$ (*), $p < 0.01$ (**), $p < 0.001$ (***).

Consistent with our standard practice in all experimental setups, verification of the decreased expression levels of the target lncRNAs was explored through RT-qPCR on day 5 subsequent to lentiviral transduction, which coincides with the day of cellular fixation inside the designated chambers. Our findings show that the positive control *PP1B* was highly expressed in both parental cell lines 501-mel and WM1361A. Regarding the subcellular localization of the three lncRNAs in 501-mel parental cell line which serves as a positive control (endogenous expression) and in 501-mel-tetON dCas9 KRAB which serves as the knock-down cell line, it was observed that *GMDS-AS1* exhibited low expression levels in 501-mel; based on the acquired images a few lncRNA molecules were detected within the nucleus and the perinuclear region. Consistently, the weak signal also displayed in the 501-mel-tetON dCas9 KRAB cell line reinforced the findings obtained from the control cell line. In comparison to *GMDS-AS1*, the expression of *XLOC030781* manifests a robust signal in 501-mel and a relatively weaker signal under knock-down conditions, being prominently localized in both the nucleus and cytoplasm. Regrettably, the localization of *BDNF-AS* could not be ascertained in either 501-mel or 501-mel-tetON dCas9 KRAB, potentially linked to technical issues.

The distinctive outcomes in WM1361A (control for endogenous expression) and WM1361A-tetON dCas9 KRAB demonstrate notable differences, highlighting the cell-specific nature of lncRNA expression. *BDNF-AS* exhibited substantially elevated expression levels in the control cell line, which were slightly lower in WM1361A-tetON dCas9 KRAB, contradicting the qPCR results that indicated clear downregulation. *BDNF-AS* was primarily localized in both the nucleus and the cytoplasm. Additionally, both *GMDS-AS1* and *XLOC030781* showed significantly reduced expression levels in WM1361A compared to *BDNF-AS*. Although

both lncRNAs appeared to be situated in the nucleus, the low signal intensity made it difficult to ascertain whether they were also present in the cytoplasm or if the observed signal was merely an artifact or cell debris resulting from nonspecific probe binding.

lncRNA Name	Melanoma Cell Line	Cytosol	Nucleus/Perinuclear Region
BDNF-AS	501-mel	Not Determined	Not Determined
GMDS-AS1	501-mel	Not Determined	+
XLOC030781	501-mel	+++	+++
BDNF-AS	WM1361A	++	++
GMDS-AS1	WM1361A	Not Determined	+
XLOC030781	WM1361A	Not Determined	+

Table 6.3 Summary of subcellular localization data for *BDNF-AS*, *GMDS-AS1* and *XLOC030781* as acquired from fluorescence *in situ* hybridization.

6.3.5 Transcriptome Profiling of *XLOC030781* Knock-Down

Upon obtaining intriguing data from the aforementioned experiments concerning the functionality and subcellular localization of *XLOC030781*, our focus shifted towards elucidating the consequences of the downregulation of this lncRNA in particular on the transcriptome. This subsequent analysis aimed to determine the specific pathways and genes that exhibited significant alterations, either beneficial or detrimental. The experiment was conducted in accordance with the protocols outlined in sections 5.2.4.14-5.2.4.15. The most effective sgRNAs (sgRNA6 and sgRNA7) for downregulating *XLOC030781* were employed in triplicate samples of 501-mel-tetON dCas9 KRAB cells at two different timepoints. Prior to RNA sequencing, the efficacy of the knock-down was validated in all samples through RT-qPCR (Figure 29).

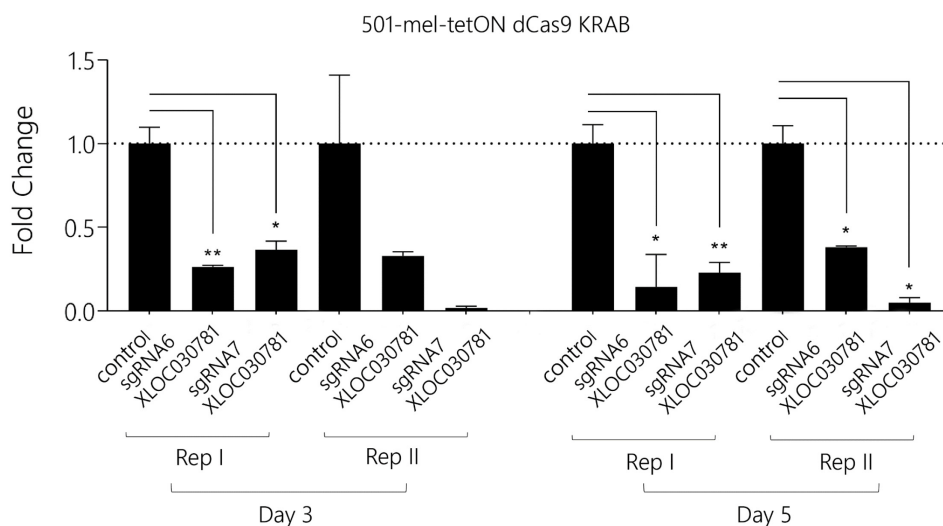
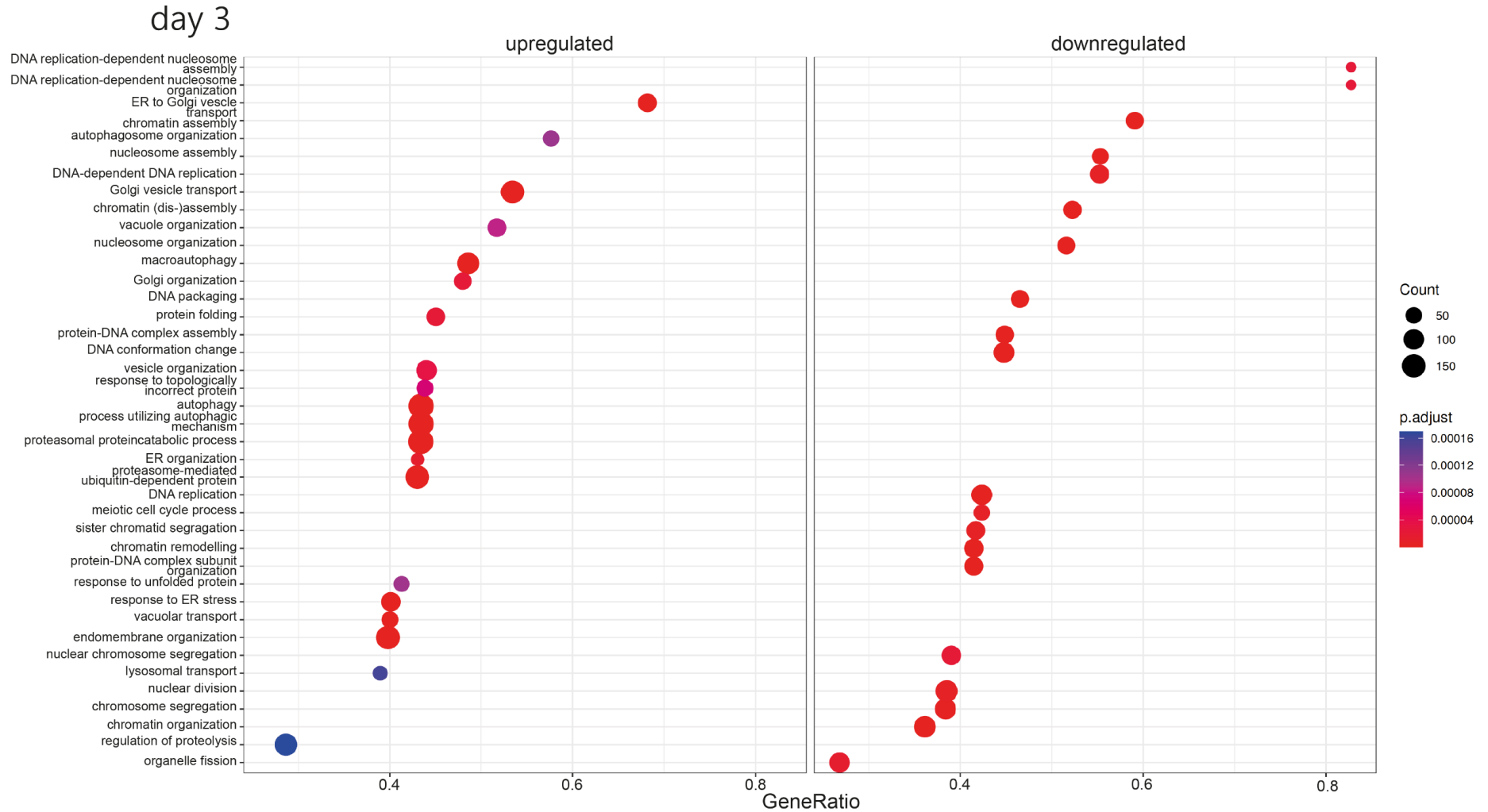


Figure 29. Quantitative real-time PCR validation of sgRNA efficiency (sgRNA6 and sgRNA7) targeting *XLOC030781* in 501-mel-tetON dCas9 KRAB cells in two technical replicates and at two timepoints day 3 and day 5 post lentiviral transduction. Relative gene expression was calculated using β -Actin as the housekeeping gene. Data are represented as the mean \pm standard error (SE). Student's t test was used to determine statistical significance: $p < 0.05$ (*), $p < 0.01$ (**).

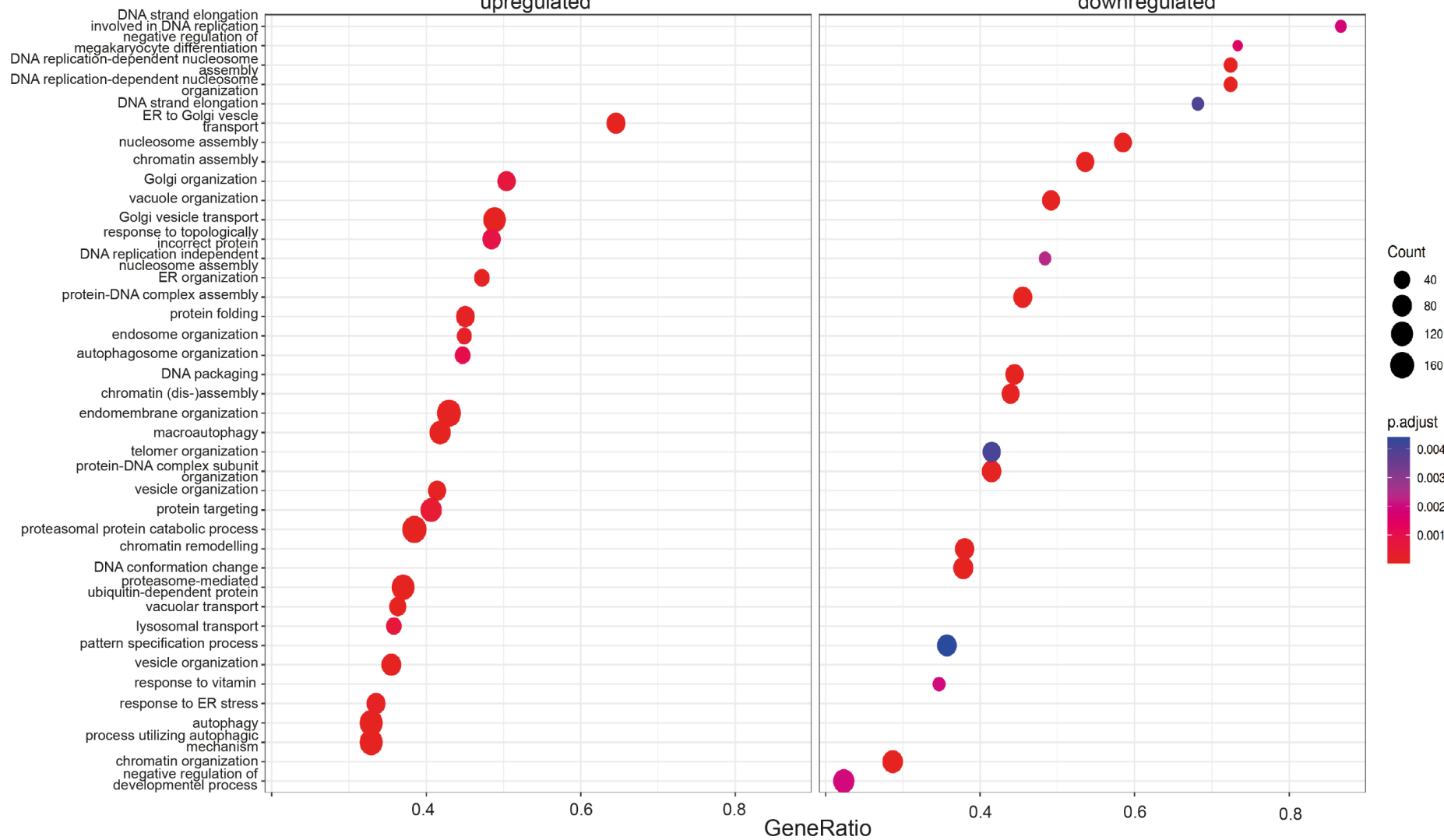
Figure 30. Results of the GSEA analysis. **A.** and **B.** Dot plots of GSEA results illustrating GO biological processes upregulated and downregulated in 501-mel-tetON dCas9 KRAB cells upon downregulation of *XLOC030781*, respectively. The figures show the significant top 20 positively and the top 20 negatively enriched GO terms, based on co-expressed genes. Gene count refers to the number of genes associated with each GO biological process. Gene ratio is the percentage of genes that significantly correlated with *XLOC030781* suppression from the total number of genes associated to that process. Ranking is performed by decreasing gene ratio.



day 5

upregulated

downregulated



Utilizing the data acquired through RNA sequencing, a gene set enrichment analysis (GSEA) was employed to evaluate the functional importance of genes that showed notable differential expression. This analysis involved examining the enrichment of these genes within predefined gene sets, thereby facilitating the identification of biological pathways and processes that exhibited significant alterations in the dataset. Moreover, the results of this analysis were compared and correlated with prior experiments to confirm existing conclusions regarding the *XLOC030781* downregulation.

Figure A and B provide an overview of the top 20 upregulated and downregulated biological processes at both day 3 and day 5 when compared to the control. The three most highly upregulated biological processes on day 3 were endoplasmic reticulum to Golgi vesicle-mediated transport, autophagosome organization, and Golgi vesicle transport. These processes exhibited the greatest enrichment of differentially expressed genes. Additionally, seven separate molecular pathways involved in cell death were observed to cluster closely together. Despite showing a lower gene ratio, these pathways exhibited comparable statistical significance, suggesting that the suppression of *XLOC030781* triggers apoptotic mechanisms. DNA-replication-dependent nucleosome assembly, DNA-replication-dependent nucleosome organization, and chromatin assembly were the three biological processes that experienced significant downregulation on day 3. Moreover, additional molecular pathways associated with DNA replication and meiotic cell cycle process, albeit with a lower gene ratio, were also evident in the identified list. Collectively, these findings indicate a suspension of the cell cycle.

The highest upregulated biological processes at the second timepoint mirrored the pattern observed previously, with endoplasmic reticulum to Golgi vesicle transport and Golgi organization maintaining their prominent positions. Furthermore, molecular pathways associated with the proteasome once again exhibited notable enrichment. This observation suggests that even on day 5, the cells remained in an apoptotic state. Conversely, at the opposite end of the expression spectrum, the most significantly downregulated biological processes were found to be associated with DNA replication and nucleosome assembly.

7. Discussion – Conclusions

7.1 Evaluation of CRISPRi Proliferation Screen 2.0

This research endeavour sought to assess the efficacy of CRISPR technology in modulating cell viability, with the aim of enhancing our comprehension of cellular vitality and proliferation and identifying both established and novel lncRNA targets for therapeutic interventions in melanoma treatment. The vigilant design of the screening process, which encompassed a diverse range of genetic perturbations, generated data that will be analysed herein at two distinct levels: firstly, evaluating the results of the CRISPRi proliferation screen 2.0 as an independent experiment, and subsequently carrying out a comparison between the two CRISPRi screens.

CRISPR screens represent a highly robust and formidable methodology, yet their utilization demands navigating through intricate complexities and challenges. The precision, execution, and reliability of the experimental parameters played a significant role in the CRISPRi proliferation screen 2.0. With this in mind, the experiment utilized the same modified melanoma cell line (501-mel tetON dCas9 KRAB), in which the expression of dCas9-KRAB was constitutively induced through doxycycline treatment. Prior to conducting the experiment, the potent expression of dCas9-KRAB was thoroughly validated. Additionally, lentivirus titration was executed to ensure optimal volume transduction of the lncRNA KRAB library at MOI 0.3, thereby mitigating the delivery of multiple sgRNAs to individual cells, potential off-target effects, and cellular stress arising from toxicity.

An accurate evaluation of screen 2.0 compared to screen 1.0 requires an explicit specification of the distinctions in their implementation. Initially, in screen 1.0, the internal lncRNA positive controls (except for *MALAT1*) did not yield any discernible results, prompting the introduction of an optimization step in screen 2.0. This involved disrupting the expression of dCas9 KRAB 3 days prior to lentiviral transduction, followed by induction, 4 days after transduction, once puromycin selection was completed. By employing this scheme, all cells that failed to be infected by the lentivirus were eliminated, and all sgRNAs integrated into the cellular genome commenced competition from a consistent baseline. Disruption of continuous dCas9 induction could have led to the advantageous depletion of highly efficacious sgRNA from the lncRNA library at an early stage. Moreover, an additional step was taken to integrate four external additional positive controls (*BRAF*, *EGFR*, *MITF*, and *RPA3*). These controls were intentionally introduced separately from the library. The rationale behind this decision will be examined subsequent to the investigation into the potential causes of the inadequate performance of the internal positive controls.

While this study doesn't encompass the justification of the experimental design of the lncRNA KRAB library, as its design wasn't developed but rather utilized within the framework of the already showcased experimental procedures, some information should be provided regarding the initially selected positive

controls. The library included a total of eight positive controls, comprising of five lncRNAs (*BANCR*, *CDKN2B-AS1*, *HOTAIR*, *MALAT1*, and *SAMMSON*) and three protein coding genes (*CDKN1A*, *FBXW7*, and *HSF1*).

The selection of lncRNA as positive controls was not without potential risks, although it was justified by the objectives of the CRISPRi proliferation screen 1.0, which primarily aimed to examine the ramifications of lncRNA gene depletion on cell growth and fitness. Unfortunately, similar to miRNAs, several lncRNAs cannot be efficiently identified in genetic screens²⁰⁵. The reason for this lies in certain characteristic traits associated with lncRNAs. The lncRNA transcriptome exhibits distinct patterns of tissue and cell type specificity. Skin tissue, alongside brain, lung, and testis, is particularly known for its abundance of tissue-specific lncRNAs, likely due to the presence of diverse cell types within these tissues. This specificity is further evident at the cellular level, as a significant differential expression of lncRNAs is observed among different cell lines of the same tissue²⁰⁶. Therefore, it is plausible that the selected lncRNAs used as positive controls, even if they have been reported to be upregulated in melanoma, in our cell model might have different expression levels, which consequently led to the inability to detect their depletion in the CRISPRi screen. Furthermore, unlike perturbations occurring in protein coding regions, which typically have pronounced impacts and are easily detectable, lncRNAs serve as regulatory elements with subtle effects on quantitative traits, making them difficult to identify as the resulting phenotype remains unobservable even in vitro conditions²⁰⁵. Within this context, a striking case in point is presented by *MALAT1*, a gene that is widely recognized for its upregulated expression in cancer and its clear contribution to the advancement of the disease. Nonetheless, investigations conducted on mice have not been able to identify this gene, as it is not associated with prominent phenotypic features^{205,207,208}. The considerable dissimilarity in expression levels between protein coding genes and lncRNA, often amounting to ratios reaching tens of thousands, presents a significant impediment to the potential use of lncRNAs as effective experimental controls¹⁹⁹. Lastly but equally important, in the introductory section the role of these lncRNAs in melanoma has been extensively elucidated, indicating that, apart from *SAMMSON*, the majority of these transcripts are correlated with cell migration and invasion. Consequently, owing to their association with an invasive phenotype, it is possible that their downregulation may not necessarily affect cell viability.

Among the three protein coding genes discussed, *CDKN1A*, also referred to as *p21*, prominently stands out as a well-recognized tumour suppressor gene. Its primary function revolves around the regulation of the cell cycle by inhibiting cyclin-dependent kinase (CDK)-cyclin complexes, enzymes responsible for propelling cell division. *CDKN1A* effectively hinders the activity of both CDK1 and CDK2, leading to a consequential interruption in cell cycle progression during the G1/S and G2/M checkpoints. Such cell cycle arrest enables cells to diligently repair DNA damage and resolve cellular stress before resuming the cell division process. By performing such a function, *CDKN1A* effectively prevents the accumulation of mutations and the occurrence of genomic instability, which are fundamental factors for carcinogenesis²⁰⁹. Likewise, *FBXW7*

serves as a tumour suppressor gene, exerting its impact through the modulation of the degradation of oncoproteins like c-Myc, mTOR, and Notch. These oncoproteins are directly involved in promoting cell proliferation and survival. As a member of the F-box protein family, *FBXW7* plays an essential role within the Skp1-Cdc53/Cullin-F-box-protein complex (SCF/ β -TrCP). The SCF complex is an E3-ubiquitin ligase, responsible for the ubiquitination of proteins and subsequent activation of their proteasome degradation^{210,211}. Instead of experiencing depletion, the aforementioned genes *CDKN1A* and *FBXW7* should exhibit an enrichment in their expression levels during a CRISPRi proliferation screen, thus potentially serving as inverse positive controls. Lastly, *HSF1* represents the primary transcriptional regulator responsible for eliciting the heat shock response, an adaptive mechanism that enables cells to overcome diverse stressors, including high temperature and infections. In the realm of cancer biology, *HSF1* has often been found to be overexpressed and hyperactivated in tumour cells, augmenting their capacity to withstand stressful conditions in tumour microenvironment²¹².

Considering that both screens were conducted to directly affect cell survival, the selection of new protein-coding genes as external positive controls was based on two criteria: a. their considerably higher expression comparing to lncRNA genes, b. their direct involvement in cell proliferation and growth, and c. their established significance in melanoma development and progression. It has been mentioned in other parts of the dissertation, that *BRAF* is a widely acknowledged proto-oncogene that plays a significant role in the MAPK-ERK signalling pathway, a crucial regulatory pathway involved in various vital biological processes such as cell growth, proliferation, migration, and apoptosis. The occurrence of *BRAF* mutations in human melanomas is a prevalent phenomenon, which results in the continuous activation of *BRAF*, subsequently causing abnormal activation of the MAP-ERK pathway²¹³. As a consequence, all the mentioned cellular processes are significantly affected, hence validating its selection as a positive control. Moreover, *EGFR* (Epidermal Growth Factor Receptor) functions as a transmembrane type I receptor tyrosine kinase that can initiate cellular differentiation and proliferation by specifically binding to its ligands. The expression of *EGFR* has been reported to be elevated in numerous cases of melanoma, particularly those characterized by *BRAF* mutations, thereby conferring resistance to melanoma treatment with BRAF inhibitors. The activation of *EGFR* corresponds to the initiation of three distinct signalling pathways: a. PI3K-AKT-mTOR, b. MAPK-ERK, and c. STAT, thereby highlighting its integral role in the advancement and infiltration of melanoma²¹⁴. Consequently, *EGFR* was considered an appropriate candidate for a positive control.

In addition, *MITF* functions as a fundamental transcriptional factor and essential regulator of melanocyte development and differentiation, with the amplification of its genomic locus occurring in 5-20 % of melanomas. The expression and function of *MITF* in melanoma show significant complexity and diversity. Melanoma cells with upregulated *MITF* levels exhibit a highly proliferative profile while demonstrating low invasive capabilities. Conversely, decreased *MITF* expression indicates high invasiveness with limited proliferation. Thus, *MITF* plays a role in regulating the phenotypic plasticity of melanoma cells, orchestrating

a shift between a proliferative phenotype ($MITF^{high} AXL^{low}$) and an invasive phenotype ($MITF^{low} AXL^{high}$) with *AXL* (AXL Receptor Tyrosine Kinase) in inversely proportional manner²¹⁵. According to many studies, 501-mell cell line demonstrates increased *MITF* expression levels and given to its fascinating functionality in the context of melanoma, *MITF* was designated as our third positive control^{216,217}. Lastly, *RPA3* (Replication Protein A3) as indicated by its name, encodes a protein that functions as part of the heterotrimeric replication protein A complex (RPA/RP-A). The high abundance of RPA proteins including RPA3 within the cell allows them to bind to exposed single-stranded DNA due quickly and effectively to its subnanomolar affinity. Consequently, any depletion or insufficiency of RPA proteins can lead to DNA replication abnormalities, deficiencies in DNA repair, and instability within the genome, this conclusion justifies its role as a positive control for evaluating the quality of our CRISPRi proliferation screen 2.0²¹⁸.

Despite the scientific justification for selecting the aforementioned genes, the experimental setup utilizing an MOI of 0.005 for each external positive control for separate transduction from the library, and a single sgRNA per control, was not conducive to validating their representation in the CRISPRi proliferation screen 2.0. It is firmly believed that by increasing carefully and with moderation the MOI, and using more than three sgRNAs for each external positive control, their presence would have higher possibilities to be detected. Unquestionably, the integration of these proposed alterations would yield a substantive metamorphosis in the experimental design, consequently unveiling potential risks. Notably, the alteration in the number of transduced cells would have a marked impact, which would not be a problem per se, but concerns could arise due to the possibility of uneven distribution of positive control sgRNAs relative to those of the library, owing to their separate integration. Regarding the internal positive controls, no depletion was detected in any of the lncRNAs, while only *FBXW7* (# 15) exhibited enrichment among the protein coding genes. Each positive lncRNA control was subjected to targeting by a set of 10 distinct sgRNAs. It is improbable that the majority of these guide RNAs were unable to induce substantial depletion and especially for this number of genes (5). The absence of lncRNAs in the results can be attributed to two factors: their downregulation does not affect cell survival, and compensatory mechanisms involving alternative genes ensure cellular viability.

Upon cross-referencing, an overlap of 20 long non-coding RNAs (lncRNAs) (40 %) was ascertained among the top 50 lncRNAs obtained from both CRISPRi screens, indicating their significance in cell integrity. Figure 12 visually elucidates the remarkable similarity between the two screens, particularly within the first 10 lncRNAs, even in sequential order. Examination of CRISPRi proliferation screen 2.0 as a standalone experiment shows that day 7 (timepoint I) shares 11 common hits (22 %) with both day 14 (timepoint II) and day 21 (timepoint III). The two last timepoints share 27 common hits (54 %) which is indicative that the screen has almost reached plateau by day 14.

Even though the positive controls, both internal and external, were proven problematic for different reasons, the significant similarity in the results between the two experiments cannot be attributed to

coincidence, to random chance or experimental variability. Additionally, as depicted in Figure 6 the top hits arising from the screen 1.0 were successfully validated. The results obtained utilizing the specific lncRNA library are reproducible and consistent. These findings definitely strengthen the evidence for the involvement of the top lncRNAs in the vital molecular pathways.

7.2 Evaluation of Functional Characterization Studies on *BDNF-AS*, *GMDS-AS1* and *XLOC030781*

Our functional characterization studies prioritized three lncRNAs (*BDNF-AS*, *GMDS-AS1*, *XLOC030781*) that ranked highly (among top 10) in both CRISPRi proliferation screen 1.0 and 2.0. *BDNF-AS* (Brain-Derived Neurotrophic Factor Antisense Strand RNA) is a lncRNA located on chromosome 11 (genomic coordinates from GRCh38.p14 assembly: chromosome 11: 27,506,830-27,698,231 forward strand) and has been implicated in a multitude of cancer types. Extensive research has consistently demonstrated a downregulated expression of *BDNF-AS* across various cancer types, including colorectal cancer, oesophageal cancer, cervical cancer, glioblastoma, and osteosarcoma, indicating a tumour suppressor role in these malignancies²¹⁹. Remarkably, the influence of *BDNF-AS* in melanoma remains unexplored. *GMDS-AS1* (GDP-mannose 4,6-dehydratase Antisense 1) is a novel lncRNA transcribed from a genomic locus on chromosome 6 (genomic coordinates from GRCh38.p14 assembly: chromosome 6: 2,245,718-2,525,976 forward strand). Compared to *BDNF-AS*, the degree of scientific evidence regarding its involvement in cancer is notably inadequate. To date, studies have demonstrated its antitumorigenic properties in lung adenocarcinoma and hepatocellular carcinoma while simultaneously promoting tumorigenesis in colorectal cancer²²⁰⁻²²². Similarly to *BDNF-AS*, there is no data regarding its association with melanoma. Lastly, *XLOC030781* represented a non-annotated lncRNA located on chromosome 18 (genomic coordinates from GRCh38.p14 assembly: chromosome 18: 15,164,633-15,164,933). Designated as *ENSG00000287723* since September 2023, this lncRNA remains relatively unexplored, with existing information limited to its expression (cortical plate, ventricular zone, ganglionic eminence and 68 other cell types or tissues) and an absence of published research²²³.

Our experimental studies aimed to dissect the role of these lncRNAs in fundamental biological processes such as proliferation, apoptosis, invasion, cell cycle dynamics and finally their subcellular localization. It was sufficiently established in two different melanoma cell lines (501-mel-tetON dCas9 KRAB and WM1361A-tetON dCas9 KRAB) that upon downregulation of all three lncRNAs using CRISPRi technology, initiation of apoptosis occurred. The strongest effect was when *GMDS-AS1* and *ENSG00000287723* were suppressed in both cell lines. After having effectively validated the activation of apoptotic pathways due to lncRNA knock-down, it became apparent that the cells were enduring considerable stress. Apoptosis and cell cycle are two fundamental cellular processes, tightly linked, thus governed by shared regulators. In instances where cellular damage exceeds repair capabilities, the cell activates the intrinsic apoptotic pathway, resulting in a

permanent inhibition of cell cycle progression. p53 serves as a prime example of a crucial protein in this interconnection, as it plays a role in arresting the cell cycle at the G1/S regulation point upon recognizing DNA damage and can induce apoptosis if the damage is found to be irreparable^{224,225}. Thus, our research was directed towards analyzing the resulting implications of the lncRNAs suppression on the cell cycle process. Utilizing the same CRISPRi cell lines, it was ascertained that the cell cycle was negatively hampered, resulting in a prominent G1 arrest subsequent to the downregulation of all three lncRNAs. Despite observing variations in cell distribution during other phases of the cell cycle among the lncRNAs, the inhibition of the cell cycle was conclusively confirmed. Having successfully documented the fundamental significance of our selected lncRNA candidates in maintaining cellular viability and growth, our focus shifted towards unraveling their potential involvement in driving invasiveness, as the fatal nature of melanoma predominantly stems from metastatic spread.

Metastasis, a major contributor to cancer mortality, is a highly complex process characterized by a finely orchestrated cascade of events, comprising the local infiltration of tumour cells into adjacent tissue, the trans endothelial migration of tumour cells into vessels (known as intravasation), survival within the circulatory system, extravasation, and subsequent proliferation in distant organs, resulting in colonization²²⁶. 501-mel-tetON dCas9 KRAB cell line was used for the investigation of the invasive properties of the three lncRNAs. Concerning *BDNF-AS* and *GMDS-AS1*, our findings did not establish a conclusive link to invasion-related pathways as their downregulation did not consistently demonstrate any impact. Their invasiveness mirrored, to a great extent, that of the negative control. Conversely, the consistent and significant reduction in cell invasion observed upon suppression of *ENSG00000287723* underscores its direct association with invasion mechanisms. It was anticipated that *ENSG00000287723* would have a substantial influence on invasion, given it derived from metastatic STCs. Subsequently, a fascinating angle through which to investigate the invasion phenomenon was to analyze it within the context of upregulated expression levels of our lncRNAs. The results did not showcase any notable elevation in invasiveness, possibility due to the fact that 501-mel cell line, being of metastatic origin, already displays a high metastatic potential. The system might be already saturated, thus a further increase in the lncRNA expression could not yield a stronger invasive phenotype. However, it was intriguing to observe that the integration of the CRISPR system into the 501-mel parental cell line consistently and significantly impacted the invasive capability across its CRISPRi and CRISPRa derivatives.

The interesting results obtained from the majority of the assays performed for *ENSG00000287723*, prompted an exploration of the transcriptome profiling in response to its reduced expression. RNA sequencing data was used to conduct gene set enrichment analysis to assess the functional value of differentially expressed genes. The analysis identified considerable shifts in biological pathways and processes, confirming previous findings regarding *ENSG00000287723* downregulation. The top upregulated processes included vesicle transport and autophagosome organization, while downregulated

processes were related to DNA replication and chromatin assembly, indicating a suspension of the cell cycle. These results suggest that the cells remained in an apoptotic state and reinforce the conclusions from the fluorescence *in situ* hybridization experiment that *ENSG00000287723* localizes in both the cytosol and the nucleus displaying significant synergistic and not opposing role.

The subcellular localization of three lncRNAs was studied in two melanoma cell lines: 501-mel and WM1361A, as well as their respective knock-down cell lines. In 501-mel, *GMDS-AS1* showed low expression levels and was detected in the nucleus and perinuclear region. *ENSG00000287723* exhibited robust expression and localized in both the nucleus and cytoplasm. *BDNF-AS* localization could not be determined. In WM1361A, *BDNF-AS* showed elevated expression levels in the control cell line, slightly lower in the knock-down cell line, contradicting RT-qPCR results. *BDNF-AS* was primarily localized in both the nucleus and the cytoplasm. *GMDS-AS1* and *ENSG00000287723* displayed reduced expression levels in WM1361A compared to *BDNF-AS*, and their subcellular localization was challenging to determine due to low signal intensity; their nuclear localization was more evident, but no conclusion could be made about the cytoplasm. These findings highlight the cell-specific nature of lncRNA expression and the challenges in accurately determining subcellular localization.

In summary, the CRISPRi proliferation screen 2.0 confirmed several of the most depleted targets from the previous CRISPRi screen and identified new targets for further verification. The functional analysis conducted as part of this doctoral study represents an initial validation of the three lncRNA candidates identified in the first screen in terms of fundamental biological functions but did not yield mechanistic insights.

In future research endeavours RNA pull-down assays in conjunction with mass spectrometry could be implemented to discern the proteins that engage in interactions with these lncRNAs, and subsequently explore the nature of these interactions and the networks they are part of.

Concurrent utilization of CLIP-seq serves as a captivating approach for comparative investigation, owing to its capability to deliver high-resolution mapping of RNA-protein interactions. By doing so, it facilitates the precise identification of binding sites/motifs, and permits investigation into the specific RNA sequences involved in interactions with RBPs (RNA Binding Proteins)²²⁷.

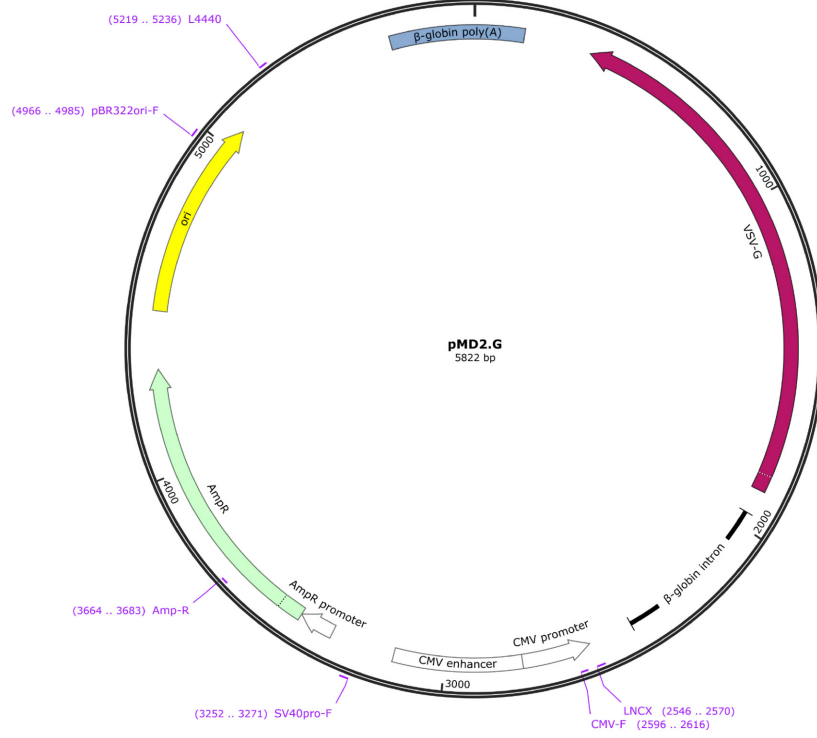
Additionally, it is worth considering transcriptome profiling experiments for *BDNF-AS* and *GMDS-AS1* while they are subjected to either suppression or overexpression (also for *ENSG00000287723*). RNA sequencing can yield informative data not only concerning the differential expression of genes in specific molecular pathways but also the expression of neighbouring genes.

Building upon the encouraging data yielded by the invasion assay highlighting the involvement of *ENSG00000287723* in cell invasiveness, it would be advantageous to incorporate co-culture cell models. Such models are more conducive to replicating physiological conditions and responses observed *in vivo*, thereby providing a more accurate portrayal of the cellular environment. In more detail, investigating the

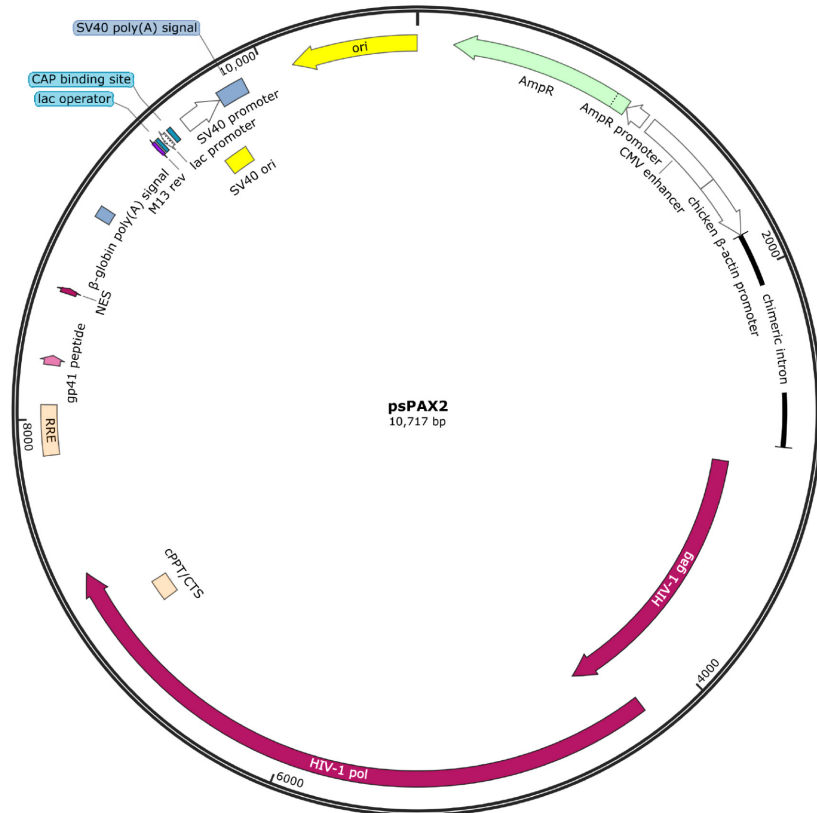
interaction between melanoma cell lines with upregulation or downregulation of *ENSG00000287723* and fibroblasts in a co-culture setup could elucidate how the expression of *ENSG00000287723* affects melanoma invasiveness²²⁸. Also, how such a cell-cell interaction affects the expression of the lncRNA. The same experimental design could be employed utilizing endothelial cells instead of fibroblasts, which form the lining of blood vessels and play significant role in angiogenesis during metastasis²²⁹. Leveraging the innovative technologies developed for molecular and cell biology, the project exhibits tremendous potential for growth and success.

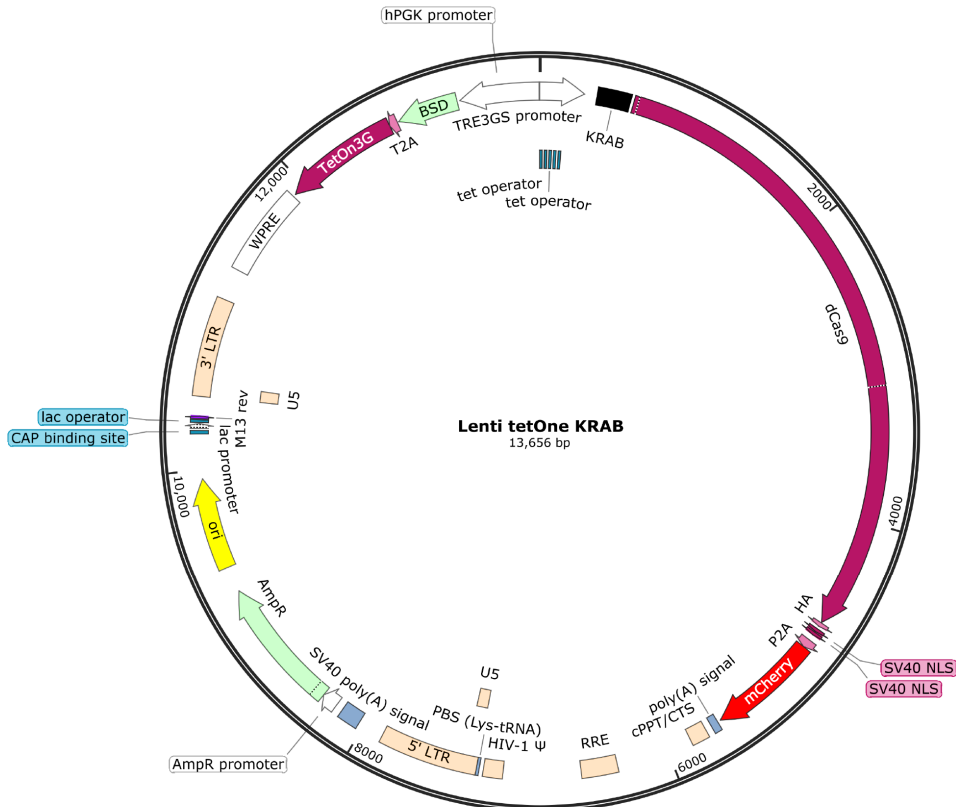
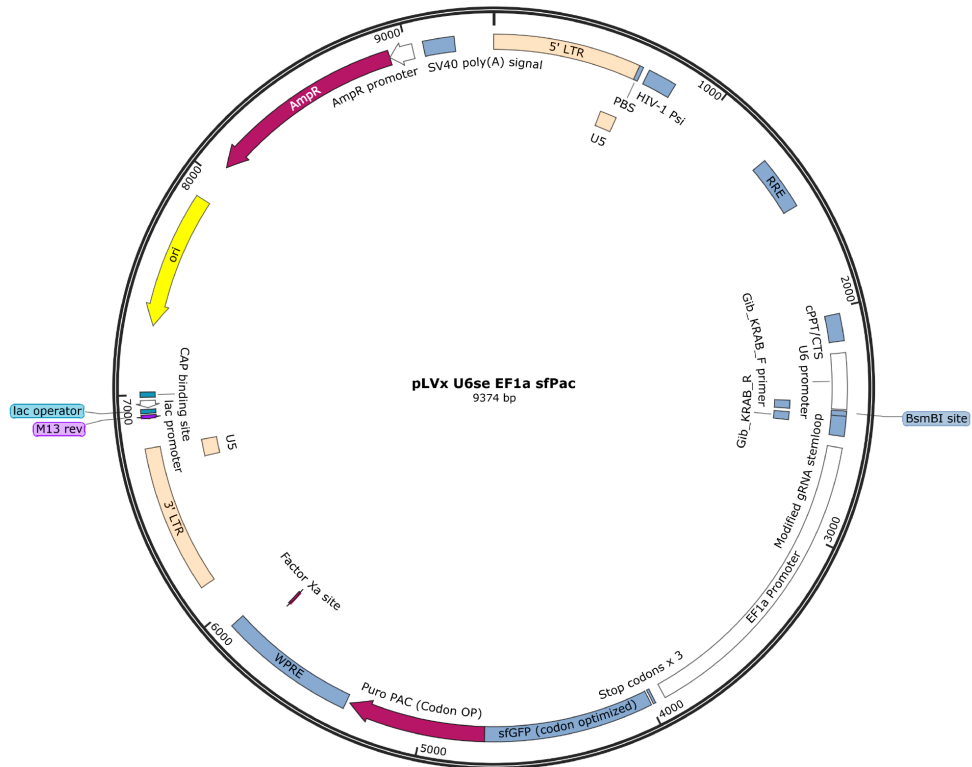
8. Supplementary Figures

Created by SnapGene



Created by SnapGene





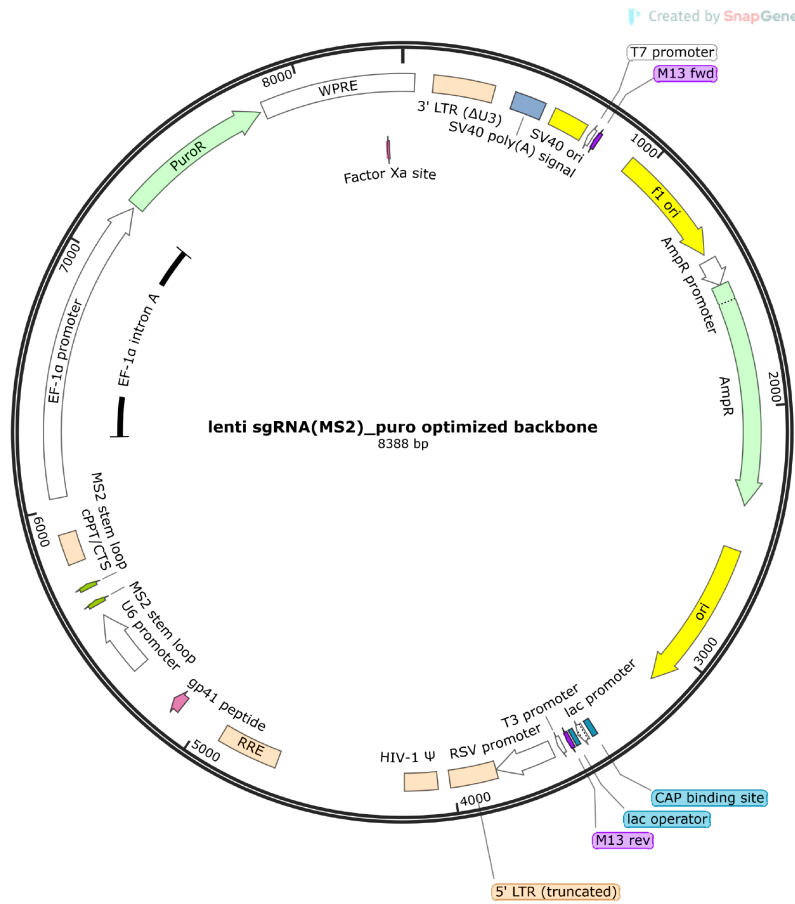


Figure 31. Vector Maps acquired from Addgene (<https://www.addgene.org/>) made on SnapGene (<https://www.snapgene.com/>) of plasmids pMD2.G, psPAX2, pLVx-U6se-EF1a-sfPac, Lenti_tetON-dCas9-KRAB, and Lenti_sgRNA-(MS2)-puro backbone, showcasing their main features.

9. Bibliography

1. Volkovova, K., Bilanicova, D., Bartonova, A., Letaiová, S. & Dusinska, M. Associations between environmental factors and incidence of cutaneous melanoma. Review. *Environ Health* **11**, 1–13 (2012).
2. Rastrelli, M., Tropea, S., Rossi, C. R. & Alaibac, M. Melanoma: Epidemiology, risk factors, pathogenesis, diagnosis and classification. *In Vivo (Brooklyn)* **28**, 1005–1012 (2014).
3. Dzwierzynski, W. W. Melanoma Risk Factors and Prevention. *Clinics in Plastic Surgery* vol. 48 543–550 Preprint at <https://doi.org/10.1016/j.cps.2021.05.001> (2021).
4. Erdmann, F. *et al.* International trends in the incidence of malignant melanoma 1953–2008—are recent generations at higher or lower risk? *Int J Cancer* **132**, 385–400 (2013).
5. Arnold, M. *et al.* Trends in incidence and predictions of cutaneous melanoma across Europe up to 2015. *Journal of the European Academy of Dermatology and Venereology* **28**, 1170–1178 (2014).
6. Arnold, M. *et al.* Global Burden of Cutaneous Melanoma in 2020 and Projections to 2040. *JAMA Dermatol* **158**, 495–503 (2022).
7. Williams, M. L. & Sagebiel, R. W. Melanoma risk factors and atypical moles. *Western Journal of Medicine* **160**, 343–350 (1994).
8. Gandini, S. *et al.* Meta-analysis of risk factors for cutaneous melanoma: II. Sun exposure. *Eur J Cancer* **41**, 45–60 (2005).
9. Gerber, B., Mathys, P., Moser, M., Bressoud, D. & Braun-Fahrländer, C. Ultraviolet Emission Spectra of Sunbeds[†]. *Photochem Photobiol* **76**, 664–668 (2002).
10. Bevona, C. *et al.* Cutaneous Melanomas Associated With Nevi. *Arch Dermatol* **139**, 1620–1624 (2003).
11. Šerman, N., Vranić, S., Glibo, M., Šerman, L. & Mokos, Z. B. Genetic risk factors in melanoma etiopathogenesis and the role of genetic counseling: A concise review. *Bosnian Journal of Basic Medical Sciences* vol. 22 673–682 Preprint at <https://doi.org/10.17305/bjbms.2021.7378> (2022).
12. Baxter, A. J. *et al.* The Queensland Study of Melanoma: Environmental and Genetic Associations (Q-MEGA); Study Design, Baseline Characteristics, and Repeatability of Phenotype and Sun Exposure Measures. *Twin Research and Human Genetics* **11**, 183–196 (2008).
13. Amos, C. I. *et al.* Genome-wide association study identifies novel loci predisposing to cutaneous melanoma. *Hum Mol Genet* **20**, 5012–5023 (2011).
14. Law, M. H., MacGregor, S. & Hayward, N. K. Melanoma genetics: Recent findings take us beyond well-traveled pathways. *Journal of Investigative Dermatology* **132**, 1763–1774 (2012).
15. Tímár, J. & Ladányi, A. Molecular Pathology of Skin Melanoma: Epidemiology, Differential Diagnostics, Prognosis and Therapy Prediction. *International Journal of Molecular Sciences* vol. 23 Preprint at <https://doi.org/10.3390/ijms23105384> (2022).
16. Akbani, R. *et al.* Genomic Classification of Cutaneous Melanoma. *Cell* **161**, 1681–1696 (2015).
17. Alexandrov, L. B. *et al.* Signatures of mutational processes in human cancer. *Nature* **500**:7463 **500**, 415–421 (2013).
18. Moran, B., Silva, R., Perry, A. S. & Gallagher, W. M. Epigenetics of malignant melanoma. *Semin Cancer Biol* **51**, 80–88 (2018).
19. Edlundh-Rose, E. *et al.* NRAS and BRAF mutations in melanoma tumours in relation to clinical characteristics: A study based on mutation screening by pyrosequencing. *Melanoma Res* **16**, 471–478 (2006).

20. Platz, A., Egyhazi, S., Ringborg, U. & Hansson, J. Human cutaneous melanoma; a review of NRAS and BRAF mutation frequencies in relation to histogenetic subclass and body site. *Mol Oncol* **1**, 395–405 (2008).
21. Goel, V. K., Lazar, A. J. F., Warneke, C. L., Redston, M. S. & Haluska, F. G. Examination of Mutations in BRAF, NRAS, and PTEN in Primary Cutaneous Melanoma. *Journal of Investigative Dermatology* **126**, 154–160 (2006).
22. Davies, M. A. *et al.* Integrated molecular and clinical analysis of AKT activation in metastatic melanoma. *Clinical Cancer Research* **15**, 7538–7546 (2009).
23. Rönstrand, L. Signal transduction via the stem cell factor receptor/c-Kit. *Cellular and Molecular Life Sciences* **61**, 2535–2548 (2004).
24. Lennartsson, J., Jelacic, T., Linnekin, D. & Shivakrupa, R. Normal and Oncogenic Forms of the Receptor Tyrosine Kinase Kit. *Stem Cells* **23**, 16–43 (2005).
25. Kim, K. B. & Alrwas, A. Treatment of KIT -mutated metastatic mucosal melanoma. *Chin Clin Oncol* **3**, 35–35 (2014).
26. Carvajal, R. D. *et al.* Phase II Study of Nilotinib in Melanoma Harboring KIT Alterations Following Progression to Prior KIT Inhibition. *Clin Cancer Res* **21**, 2289–2296 (2015).
27. Pham, D. M., Guhan, S. & Tsao, H. KIT and Melanoma: Biological Insights and Clinical Implications. *Yonsei Med J* **61**, 562–571 (2020).
28. Lennartsson, J. *et al.* Phosphorylation of Shc by Src family kinases is necessary for stem cell factor receptor/c-kit mediated activation of the Ras/MAP kinase pathway and c-fos induction. *Oncogene* **18**, 5546–5553 (1999).
29. Mort, R. L., Jackson, I. J. & Elizabeth Patton, E. The melanocyte lineage in development and disease. *Development* **142**, 620–632 (2015).
30. Braig, M. & Schmitt, C. A. Oncogene-Induced Senescence: Putting the Brakes on Tumor Development. *Cancer Res* **66**, 2881–2884 (2006).
31. Miller, A. J. & Mihm, M. C. Jr. Melanoma. <https://doi.org/10.1056/NEJMra052166> **355**, 51–65 (2006).
32. Greene, M. H. *et al.* A study of tumor progression: The precursor lesions of superficial spreading and nodular melanoma. *Hum Pathol* **15**, 1147–1165 (1984).
33. Damsky, W. E., Theodosakis, N. & Bosenberg, M. Melanoma metastasis: new concepts and evolving paradigms. *Oncogene* **33**, 2413–2422 (2013).
34. Rahmati, M., Ebrahim, S., Hashemi, S., Motamedi, M. & Moosavi, M. A. New insights on the role of autophagy in the pathogenesis and treatment of melanoma. *Molecular Biology Reports* **47**, 9021–9032 (2020).
35. Damsky, W. E., Theodosakis, N. & Bosenberg, M. Melanoma metastasis: new concepts and evolving paradigms. *Oncogene* **33**, 2413–2422 (2013).
36. Batus, M. *et al.* Optimal Management of Metastatic Melanoma: Current Strategies and Future Directions. *American Journal of Clinical Dermatology* **14**, 179–194 (2013).
37. van Zeijl, M. C. T., van den Eertwegh, A. J., Haanen, J. B. & Wouters, M. W. J. M. (Neo)adjuvant systemic therapy for melanoma. *European Journal of Surgical Oncology (EJSO)* **43**, 534–543 (2017).
38. Santamaria-Barria, J. A. & Mammen, J. M. V. Surgical Management of Melanoma: Advances and Updates. *Curr Oncol Rep* **24**, 1425–1432 (2022).
39. Balch, C. M. *et al.* Final version of 2009 AJCC melanoma staging and classification. *Journal of Clinical Oncology* **27**, 6199–6206 (2009).

40. Moncrieff, M. D. *et al.* 1 Versus 2-cm Excision Margins for pT2-pT4 Primary Cutaneous Melanoma (MelMarT): A Feasibility Study. *Ann Surg Oncol* **25**, 2541–2549 (2018).
41. Faries, M. B. *et al.* Completion Dissection or Observation for Sentinel-Node Metastasis in Melanoma. *New England Journal of Medicine* **376**, 2211–2222 (2017).
42. Wong, S. L. *et al.* Sentinel lymph node biopsy and management of regional lymph nodes in Melanoma: American society of clinical oncology and society of surgical oncology clinical practice guideline update. *Journal of Clinical Oncology* **36**, 399–413 (2018).
43. Atkins, M. B. *et al.* High-dose recombinant interleukin 2 therapy for patients with metastatic melanoma: Analysis of 270 patients treated between 1985 and 1993. *Journal of Clinical Oncology* **17**, 2105–2116 (1999).
44. Eggermont, A. M. *et al.* Adjuvant therapy with pegylated interferon alfa-2b versus observation alone in resected stage III melanoma: final results of EORTC 18991, a randomised phase III trial. *The Lancet* **372**, 117–126 (2008).
45. Parkinson, D. R. *et al.* Interleukin-2 therapy in patients with metastatic malignant melanoma: a phase II study. <https://doi.org/10.1200/JCO.1990.8.10.1650> **8**, 1650–1656 (2016).
46. Kwak, M. *et al.* Updates in adjuvant systemic therapy for melanoma. *J Surg Oncol* **119**, 222–231 (2019).
47. Bruce, W. J., Koljonen, J. L., Romanelli, M. R., Khan, A. U. & Neumeister, M. W. Adjuvant and Neoadjuvant Therapeutics for the Treatment of Cutaneous Melanoma. *Clin Plast Surg* **48**, 651–658 (2021).
48. Cohen, J. V. & Buchbinder, E. I. The Evolution of Adjuvant Therapy for Melanoma. *Curr Oncol Rep* **21**, 1–7 (2019).
49. Skudalski, L., Waldman, R., Kerr, P. E. & Grant-Kels, J. M. Melanoma: An update on systemic therapies. *J Am Acad Dermatol* **86**, 515–524 (2022).
50. Villani, A. *et al.* The Treatment of Advanced Melanoma: Therapeutic Update. *International Journal of Molecular Sciences* **2022**, Vol. 23, Page 6388 **23**, 6388 (2022).
51. Lee, J. B., Kim, H. R. & Ha, S. J. Immune Checkpoint Inhibitors in 10 Years: Contribution of Basic Research and Clinical Application in Cancer Immunotherapy. *Immune Netw* **22**, (2022).
52. DeRogatis, J. M. *et al.* Targeting the PSGL-1 Immune Checkpoint Promotes Immunity to PD-1-Resistant Melanoma. *Cancer Immunol Res* **10**, 612–625 (2022).
53. Volpe, V. O., Klufas, D. M., Hegde, U. & Grant-Kels, J. M. The new paradigm of systemic therapies for metastatic melanoma. *J Am Acad Dermatol* **77**, 356–368 (2017).
54. Ribas, A. & Wolchok, J. D. Cancer immunotherapy using checkpoint blockade. *Science (1979)* **359**, 1350–1355 (2018).
55. Nguyen, A. *et al.* Current and emerging treatment options for metastatic melanoma: A focused review. *Dermatol Online J* **26**, 1–1 (2020).
56. Villani, A., Scalvenzi, M., Fabbrocini, G., Ocampo-Candiani, J. & Ocampo-Garza, S. S. Looking into a Better Future: Novel Therapies for Metastatic Melanoma. *Dermatol Ther (Heidelb)* **11**, 751–767 (2021).
57. Jenkins, R. W. & Fisher, D. E. Treatment of Advanced Melanoma in 2020 and Beyond. *Journal of Investigative Dermatology* **141**, 23–31 (2021).
58. Skudalski, L., Waldman, R., Kerr, P. E. & Grant-Kels, J. M. Melanoma: An update on systemic therapies. *J Am Acad Dermatol* **86**, 515–524 (2022).
59. Schadendorf, D. *et al.* Pooled analysis of long-term survival data from phase II and phase III trials of ipilimumab in unresectable or metastatic melanoma. *Journal of Clinical Oncology* **33**, 1889–1894 (2015).

60. Larkin, J. *et al.* Combined Nivolumab and Ipilimumab or Monotherapy in Untreated Melanoma. *New England Journal of Medicine* **373**, 23–34 (2015).
61. PONTI, G. *et al.* BRAF, NRAS and C-KIT Advanced Melanoma: Clinico-pathological Features, Targeted-Therapy Strategies and Survival. *Anticancer Res* **37**, (2017).
62. Davies, H. *et al.* Mutations of the BRAF gene in human cancer. *Nature* **417**, 949–954 (2002).
63. Chapman, P. B. *et al.* Improved Survival with Vemurafenib in Melanoma with BRAF V600E Mutation. *New England Journal of Medicine* **364**, 2507–2516 (2011).
64. McArthur, G. A. *et al.* Safety and efficacy of vemurafenib in BRAFV600E and BRAFV600K mutation-positive melanoma (BRIM-3): extended follow-up of a phase 3, randomised, open-label study. *Lancet Oncol* **15**, 323–332 (2014).
65. Skudalski, L., Waldman, R., Kerr, P. E. & Grant-Kels, J. M. Melanoma: An update on systemic therapies. *J Am Acad Dermatol* **86**, 515–524 (2022).
66. Wyman, K. *et al.* Multicenter Phase II trial of high-dose imatinib mesylate in metastatic melanoma. *Cancer* **106**, 2005–2011 (2006).
67. Ugurel, S. *et al.* Lack of clinical efficacy of imatinib in metastatic melanoma. *British Journal of Cancer* **92**:8, 1398–1405 (2005).
68. Kim, K. B. *et al.* Phase II trial of imatinib mesylate in patients with metastatic melanoma. *British Journal of Cancer* **99**:5, 734–740 (2008).
69. Kim, K. B. & Alrwas, A. Treatment of KIT -mutated metastatic mucosal melanoma. *Chin Clin Oncol* **3**, 35–35 (2014).
70. Wilusz, J. E., Sunwoo, H. & Spector, D. L. Long noncoding RNAs: Functional surprises from the RNA world. *Genes and Development* vol. 23 1494–1504 Preprint at <https://doi.org/10.1101/gad.1800909> (2009).
71. Djebali, S. *et al.* Landscape of transcription in human cells. *Nature* **489**, 101–108 (2012).
72. Hangauer, M. J., Vaughn, I. W. & McManus, M. T. Pervasive Transcription of the Human Genome Produces Thousands of Previously Unidentified Long Intergenic Noncoding RNAs. *PLoS Genet* **9**, (2013).
73. Wu, H., Yang, L. & Chen, L. L. The Diversity of Long Noncoding RNAs and Their Generation. *Trends in Genetics* vol. 33 540–552 Preprint at <https://doi.org/10.1016/j.tig.2017.05.004> (2017).
74. Mercer, T. R., Dinger, M. E. & Mattick, J. S. Long non-coding RNAs: Insights into functions. *Nature Reviews Genetics* vol. 10 Preprint at <https://doi.org/10.1038/nrg2521> (2009).
75. Ponting, C. P., Oliver, P. L. & Reik, W. Evolution and Functions of Long Noncoding RNAs. *Cell* vol. 136 Preprint at <https://doi.org/10.1016/j.cell.2009.02.006> (2009).
76. Wang, K. C. & Chang, H. Y. Molecular Mechanisms of Long Noncoding RNAs. *Molecular Cell* vol. 43 904–914 Preprint at <https://doi.org/10.1016/j.molcel.2011.08.018> (2011).
77. Rinn, J. L. & Chang, H. Y. Genome regulation by long noncoding RNAs. *Annu Rev Biochem* **81**, (2012).
78. Batista, P. J. & Chang, H. Y. Long noncoding RNAs: Cellular address codes in development and disease. *Cell* vol. 152 1298–1307 Preprint at <https://doi.org/10.1016/j.cell.2013.02.012> (2013).
79. Statello, L., Guo, C. J., Chen, L. L. & Huarte, M. Gene regulation by long non-coding RNAs and its biological functions. *Nature Reviews Molecular Cell Biology* vol. 22 96–118 Preprint at <https://doi.org/10.1038/s41580-020-00315-9> (2021).
80. Ravasi, T. *et al.* Experimental validation of the regulated expression of large numbers of non-coding RNAs from the mouse genome. *Genome Res* **16**, (2006).

81. Cabili, M. *et al.* Integrative annotation of human large intergenic noncoding RNAs reveals global properties and specific subclasses. *Genes Dev* **25**, (2011).
82. Brown, J. A., Valenstein, M. L., Yario, T. A., Tycowski, K. T. & Steitz, J. A. Formation of triple-helical structures by the 3'-end sequences of MALAT1 and MEN β noncoding RNAs. *Proc Natl Acad Sci U S A* **109**, (2012).
83. Bridges, M. C., Daulagala, A. C. & Kourtidis, A. LNCcation: lncRNA localization and function. *Journal of Cell Biology* vol. 220 Preprint at <https://doi.org/10.1083/JCB.202009045> (2021).
84. Ma, L., Bajic, V. B. & Zhang, Z. On the classification of long non-coding RNAs. *RNA Biology* vol. 10 924–933 Preprint at <https://doi.org/10.4161/rna.24604> (2013).
85. Chen, H. & Shan, G. The physiological function of long-noncoding RNAs. *Non-coding RNA Research* vol. 5 178–184 Preprint at <https://doi.org/10.1016/j.ncrna.2020.09.003> (2020).
86. Dykes, I. M. & Emanuelli, C. Transcriptional and Post-transcriptional Gene Regulation by Long Non-coding RNA. *Genomics, Proteomics and Bioinformatics* vol. 15 Preprint at <https://doi.org/10.1016/j.gpb.2016.12.005> (2017).
87. Wilusz, J. E., Freier, S. M. & Spector, D. L. 3' End Processing of a Long Nuclear-Retained Noncoding RNA Yields a tRNA-like Cytoplasmic RNA. *Cell* **135**, (2008).
88. Dhir, A., Dhir, S., Proudfoot, N. J. & Jopling, C. L. Microprocessor mediates transcriptional termination of long noncoding RNA transcripts hosting microRNAs. *Nature Structural & Molecular Biology* **22**, 319–327 (2015).
89. Chen, L. L. Linking Long Noncoding RNA Localization and Function. *Trends in Biochemical Sciences* vol. 41 761–772 Preprint at <https://doi.org/10.1016/j.tibs.2016.07.003> (2016).
90. Preker, P. *et al.* RNA exosome depletion reveals transcription upstream of active human promoters. *Science (1979)* **322**, 1851–1854 (2008).
91. Preker, P. *et al.* PROMoter uPstream Transcripts share characteristics with mRNAs and are produced upstream of all three major types of mammalian promoters. *Nucleic Acids Res* **39**, 7179–7193 (2011).
92. Kim, T. K. *et al.* Widespread transcription at neuronal activity-regulated enhancers. *Nature* **465**, 182–187 (2010).
93. Lloret-Llinares, M., Mapendano, C. K., Martlev, L. H., Lykke-Andersen, S. & Jensen, T. H. Relationships between PROMPT and gene expression. <https://doi.org/10.1080/15476286.2015.1109769> **13**, 6–14 (2016).
94. de Santa, F. *et al.* A Large Fraction of Extragenic RNA Pol II Transcription Sites Overlap Enhancers. *PLoS Biol* **8**, e1000384 (2010).
95. Lam, M. T. Y. *et al.* Rev-Erbs repress macrophage gene expression by inhibiting enhancer-directed transcription. *Nature* **498**, 511–515 (2013).
96. Melo, C. A. *et al.* eRNAs Are Required for p53-Dependent Enhancer Activity and Gene Transcription. *Mol Cell* **49**, 524–535 (2013).
97. Yin, Q. F. *et al.* Long Noncoding RNAs with snoRNA Ends. *Mol Cell* **48**, 219–230 (2012).
98. Wu, H. *et al.* Unusual Processing Generates SPA lncRNAs that Sequester Multiple RNA Binding Proteins. *Mol Cell* **64**, 534–548 (2016).
99. Statello, L., Guo, C. J., Chen, L. L. & Huarte, M. Gene regulation by long non-coding RNAs and its biological functions. *Nature Reviews Molecular Cell Biology* **22**, 96–118 (2020).
100. Lasda, E. & Parker, R. Circular RNAs: Diversity of form and function. *RNA* vol. 20 1829–1842 Preprint at <https://doi.org/10.1261/rna.047126.114> (2014).

101. Groff, A. F. *et al.* In Vivo Characterization of Linc-p21 Reveals Functional cis-Regulatory DNA Elements. *Cell Rep* **16**, 2178–2186 (2016).
102. Kopp, F. & Mendell, J. T. Functional Classification and Experimental Dissection of Long Noncoding RNAs. *Cell* vol. 172 393–407 Preprint at <https://doi.org/10.1016/j.cell.2018.01.011> (2018).
103. Latos, P. A. *et al.* Airn transcriptional overlap, but not its lncRNA products, induces imprinted Igf2r silencing. *Science (1979)* **338**, 1469–1472 (2012).
104. Paralkar, V. R. *et al.* Unlinking an lncRNA from Its Associated cis Element. *Mol Cell* **62**, 104–110 (2016).
105. Núñez-Martínez, H. N. & Recillas-Targa, F. Emerging Functions of lncRNA Loci beyond the Transcript Itself. *International Journal of Molecular Sciences 2022, Vol. 23, Page 6258* **23**, 6258 (2022).
106. Atianand, M. K. *et al.* A Long Noncoding RNA lincRNA-EP5 Acts as a Transcriptional Brake to Restrain Inflammation. *Cell* **165**, 1672–1685 (2016).
107. Hutchinson, J. N. *et al.* A screen for nuclear transcripts identifies two linked noncoding RNAs associated with SC35 splicing domains. *BMC Genomics* **8**, (2007).
108. Fox, A. H. & Lamond, A. I. Paraspeckles. *Cold Spring Harb Perspect Biol* **2**, a000687 (2010).
109. Clemson, C. M. *et al.* An Architectural Role for a Nuclear Noncoding RNA: NEAT1 RNA Is Essential for the Structure of Paraspeckles. *Mol Cell* **33**, 717–726 (2009).
110. Tichon, A. *et al.* A conserved abundant cytoplasmic long noncoding RNA modulates repression by Pumilio proteins in human cells. *Nat Commun* **7**, (2016).
111. Lee, S. *et al.* Noncoding RNA NORAD Regulates Genomic Stability by Sequestering PUMILIO Proteins. *Cell* **164**, 69–80 (2016).
112. Wang, B. *et al.* lncRNA NORAD accelerates the progression and doxorubicin resistance of neuroblastoma through up-regulating HDAC8 via sponging miR-144-3p. *Biomedicine & Pharmacotherapy* **129**, 110268 (2020).
113. Ghafouri-Fard, S. *et al.* Non-coding RNA Activated by DNA Damage: Review of Its Roles in the Carcinogenesis. *Front Cell Dev Biol* **9**, 714787 (2021).
114. Schmitt, A. M. & Chang, H. Y. Long Noncoding RNAs in Cancer Pathways. *Cancer Cell* **29**, 452–463 (2016).
115. Bhan, A. & Mandal, S. S. lncRNA HOTAIR: A master regulator of chromatin dynamics and cancer. *Biochimica et Biophysica Acta (BBA) - Reviews on Cancer* **1856**, 151–164 (2015).
116. Camacho, C. V., Choudhari, R. & Gadad, S. S. Long noncoding RNAs and cancer, an overview. *Steroids* **133**, 93–95 (2018).
117. Gupta, R. A. *et al.* Long non-coding RNA HOTAIR reprograms chromatin state to promote cancer metastasis. *Nature* **464**, 1071–1076 (2010).
118. Tseng, Y. Y. *et al.* PVT1 dependence in cancer with MYC copy-number increase. *Nature* **512**, 82–86 (2014).
119. Wu, J. *et al.* Long non-coding RNA Fer-1-like protein 4 acts as a tumor suppressor via miR-106a-5p and predicts good prognosis in hepatocellular carcinoma. *Cancer Biomark* **20**, 55–65 (2017).
120. Zhou, Y. *et al.* Activation of p53 by MEG3 non-coding RNA. *J Biol Chem* **282**, 24731–24742 (2007).
121. Uroda, T. *et al.* Conserved Pseudoknots in lncRNA MEG3 Are Essential for Stimulation of the p53 Pathway. *Mol Cell* **75**, 982–995.e9 (2019).
122. Pandey, G. K. & Kanduri, C. Long Non-Coding RNAs: Tools for Understanding and Targeting Cancer Pathways. *Cancers (Basel)* **14**, (2022).

123. Sun, H., Huang, Z., Sheng, W. & Xu, M. D. Emerging roles of long non-coding RNAs in tumor metabolism. *Journal of Hematology & Oncology* 2018 11:1 **11**, 1–16 (2018).
124. Hu, Q. *et al.* Oncogenic lncRNA downregulates cancer cell antigen presentation and intrinsic tumor suppression. *Nat Immunol* **20**, 835–851 (2019).
125. Pasmant, E. *et al.* Characterization of a Germ-Line Deletion, Including the Entire INK4/ARF Locus, in a Melanoma-Neural System Tumor Family: Identification of ANRIL, an Antisense Noncoding RNA Whose Expression Coclusters with ARF. *Cancer Res* **67**, 3963–3969 (2007).
126. Morlando, M. & Fatica, A. Alteration of Epigenetic Regulation by Long Noncoding RNAs in Cancer. *International Journal of Molecular Sciences* 2018, Vol. 19, Page 570 **19**, 570 (2018).
127. Wozniak, M. & Czyz, M. The Functional Role of Long Non-Coding RNAs in Melanoma. *Cancers* 2021, Vol. 13, Page 4848 **13**, 4848 (2021).
128. Sarkar, D. *et al.* Multiple Isoforms of ANRIL in Melanoma Cells: Structural Complexity Suggests Variations in Processing. *International Journal of Molecular Sciences* 2017, Vol. 18, Page 1378 **18**, 1378 (2017).
129. Li, R. *et al.* Long Non-Coding RNA BANCR Promotes Proliferation in Malignant Melanoma by Regulating MAPK Pathway Activation. *PLoS One* **9**, e100893 (2014).
130. Massi, D. *et al.* Evidence for differential expression of Notch receptors and their ligands in melanocytic nevi and cutaneous malignant melanoma. *Modern Pathology* **19**, 246–254 (2006).
131. Galasso, M. *et al.* Loss of miR-204 expression is a key event in melanoma. *Mol Cancer* **17**, 1–6 (2018).
132. Yin, Y., Zhao, B., Li, D. & Yin, G. Long non-coding RNA CASC15 promotes melanoma progression by epigenetically regulating PDCD4. *Cell Biosci* **8**, 1–13 (2018).
133. Richtig, G. *et al.* Function and Clinical Implications of Long Non-Coding RNAs in Melanoma. *International Journal of Molecular Sciences* 2017, Vol. 18, Page 715 **18**, 715 (2017).
134. Lessard, L. *et al.* The CASC15 Long Intergenic Noncoding RNA Locus Is Involved in Melanoma Progression and Phenotype Switching. *Journal of Investigative Dermatology* **135**, 2464–2474 (2015).
135. Smith, C. M. & Steitz, J. A. Classification of gas5 as a Multi-Small-Nucleolar-RNA (snoRNA) Host Gene and a Member of the 5'-Terminal Oligopyrimidine Gene Family Reveals Common Features of snoRNA Host Genes. <https://doi.org/10.1128/MCB.18.12.6897> **18**, 6897–6909 (2023).
136. Jacob, A. & Prekeris, R. The regulation of MMP targeting to invadopodia during cancer metastasis. *Front Cell Dev Biol* **3**, 127875 (2015).
137. Chen, L. *et al.* Lentiviral-mediated overexpression of long non-coding RNA GAS5 reduces invasion by mediating MMP2 expression and activity in human melanoma cells. *Int J Oncol* **48**, 1509–1518 (2016).
138. Luo, C. *et al.* MiR-137 inhibits the invasion of melanoma cells through downregulation of multiple oncogenic target genes. *Journal of Investigative Dermatology* **133**, 768–775 (2013).
139. Gupta, R. A. *et al.* Long non-coding RNA HOTAIR reprograms chromatin state to promote cancer metastasis. *Nature* 2010 464:7291 **464**, 1071–1076 (2010).
140. Gonzalez, D. M. & Medici, D. Signaling mechanisms of the epithelial-mesenchymal transition. *Sci Signal* **7**, re8 (2014).
141. Luan, W. *et al.* Long non-coding RNA HOTAIR acts as a competing endogenous RNA to promote malignant melanoma progression by sponging miR-152-3p. *Oncotarget* **8**, 85401–85414 (2017).
142. Wu, C. F., Tan, G. H., Ma, C. C. & Li, L. The Non-Coding RNA linc23 Drives the Malignant Property of Human Melanoma Cells. *Journal of Genetics and Genomics* **40**, 179–188 (2013).

143. Moreno-Traspas, R., Vujic, I., Sanlorenzo, M. & Ortiz-Urda, S. New insights in melanoma biomarkers: long-noncoding RNAs. <http://dx.doi.org/10.2217/mmt-2016-0008> **3**, 195–205 (2016).
144. Luan, W. *et al.* Long non-coding RNA MALAT1 acts as a competing endogenous RNA to promote malignant melanoma growth and metastasis by sponging miR-22. *Oncotarget* **7**, 63901–63912 (2016).
145. Li, F. *et al.* MALAT1 regulates miR-34a expression in melanoma cells. *Cell Death & Disease* **2019 10:6** **10**, 1–11 (2019).
146. Sun, Y. *et al.* Deregulation of miR-183 promotes melanoma development via lncRNA MALAT1 regulation and ITGB1 signal activation. *Oncotarget* **8**, 3509–3518 (2016).
147. Bond, C. S. & Fox, A. H. Paraspeckles: nuclear bodies built on long noncoding RNA. *Journal of Cell Biology* **186**, 637–644 (2009).
148. Dong, P. *et al.* Long Non-coding RNA NEAT1: A Novel Target for Diagnosis and Therapy in Human Tumors. *Front Genet* **9**, 471 (2018).
149. Xia, Y. *et al.* lncRNA NEAT1 facilitates melanoma cell proliferation, migration, and invasion via regulating miR-495-3p and E2F3. *J Cell Physiol* **234**, 19592–19601 (2019).
150. Feng, Z. *et al.* E2F3 promotes cancer growth and is overexpressed through copy number variation in human melanoma. *Onco Targets Ther* **11**, 5303–5313 (2018).
151. Goding, C. R. Targeting the lncRNA SAMMSON Reveals Metabolic Vulnerability in Melanoma. *Cancer Cell* **29**, 619–621 (2016).
152. Yang, L. *et al.* Long Noncoding RNA SAMMSON Promotes Melanoma Progression by Inhibiting FOXA2 Expression. *Stem Cells Int* **2023**, (2023).
153. Khaitan, D. *et al.* The melanoma-upregulated long noncoding RNA SPRY4-IT1 modulates apoptosis and invasion. *Cancer Res* **71**, 3852–3862 (2011).
154. Mazar, J. *et al.* The functional characterization of long noncoding RNA SPRY4-IT1 in human melanoma cells. *Oncotarget* **5**, 8959–8969 (2014).
155. Wei, Y. *et al.* lncRNA UCA1-miR-507-FOXM1 axis is involved in cell proliferation, invasion and G0/G1 cell cycle arrest in melanoma. *Medical Oncology* **33**, 1–9 (2016).
156. Han, C. *et al.* Knockdown of lncRNA-UCA1 inhibits the proliferation and migration of melanoma cells through modulating the miR-28-5p/HOXB3 axis. *Exp Ther Med* **17**, 4294–4302 (2019).
157. Tuschl, T., Zamore, P. D., Lehmann, R., Bartel, D. P. & Sharp, P. A. Targeted mRNA degradation by double-stranded RNA in vitro. *Genes Dev* **13**, 3191 (1999).
158. Zamore, P. D., Tuschl, T., Sharp, P. A. & Bartel, D. P. RNAi: Double-stranded RNA directs the ATP-dependent cleavage of mRNA at 21 to 23 nucleotide intervals. *Cell* **101**, 25–33 (2000).
159. Awwad, D. A. Beyond classic editing: innovative CRISPR approaches for functional studies of long non-coding RNA. *Biol Methods Protoc* **4**, (2019).
160. Lennox, K. A. & Behlke, M. A. Cellular localization of long non-coding RNAs affects silencing by RNAi more than by antisense oligonucleotides. *Nucleic Acids Res* **44**, 863–877 (2016).
161. Lucere, K. M., O'malley, M. M. R. & Diermeier, S. D. Functional Screening Techniques to Identify Long Non-Coding RNAs as Therapeutic Targets in Cancer. *Cancers* **2020, Vol. 12, Page 3695** **12**, 3695 (2020).
162. Wiedenheft, B., Sternberg, S. H. & Doudna, J. A. RNA-guided genetic silencing systems in bacteria and archaea. *Nature* **2012 482:7385** **482**, 331–338 (2012).

163. Bhaya, D., Davison, M. & Barrangou, R. CRISPR-Cas Systems in Bacteria and Archaea: Versatile Small RNAs for Adaptive Defense and Regulation. <https://doi.org/10.1146/annurev-genet-110410-132430> **45**, 273–297 (2011).
164. Koonin, E. V. & Makarova, K. S. Origins and evolution of CRISPR-Cas systems. *Philosophical Transactions of the Royal Society B* **374**, (2019).
165. Makarova, K. S. *et al.* Evolution and classification of the CRISPR–Cas systems. *Nature Reviews Microbiology* **2011** 9:6 **9**, 467–477 (2011).
166. Jinek, M. *et al.* A programmable dual-RNA-guided DNA endonuclease in adaptive bacterial immunity. *Science* (1979) **337**, 816–821 (2012).
167. Cong, L. *et al.* Multiplex genome engineering using CRISPR/Cas systems. *Science* (1979) **339**, 819–823 (2013).
168. Mali, P. *et al.* RNA-guided human genome engineering via Cas9. *Science* (1979) **339**, 823–826 (2013).
169. Hazan, J. & Bester, A. C. CRISPR-Based Approaches for the High-Throughput Characterization of Long Non-Coding RNAs. *Non-Coding RNA* **2021**, Vol. 7, Page 79 **7**, 79 (2021).
170. Jiang, W., Bikard, D., Cox, D., Zhang, F. & Marraffini, L. A. RNA-guided editing of bacterial genomes using CRISPR-Cas systems. *Nat Biotechnol* **31**, 233–239 (2013).
171. Cong, L. *et al.* Multiplex genome engineering using CRISPR/Cas systems. *Science* (1979) **339**, 819–823 (2013).
172. Bikard, D. *et al.* Programmable repression and activation of bacterial gene expression using an engineered CRISPR-Cas system. *Nucleic Acids Res* **41**, 7429–7437 (2013).
173. Perez-Pinera, P. *et al.* RNA-guided gene activation by CRISPR-Cas9–based transcription factors. *Nature Methods* **2013** 10:10 **10**, 973–976 (2013).
174. Kiani, S. *et al.* CRISPR transcriptional repression devices and layered circuits in mammalian cells. *Nature Methods* **2014** 11:7 **11**, 723–726 (2014).
175. Parsi, K. M., Hennessey, E., Kearns, N. & Maehr, R. Using an Inducible CRISPR-dCas9-KRAB Effector System to Dissect Transcriptional Regulation in Human Embryonic Stem Cells. *Methods Mol Biol* **1507**, 221–233 (2017).
176. So, R. W. L. *et al.* Application of CRISPR genetic screens to investigate neurological diseases. *Molecular Neurodegeneration* **2019** 14:1 **14**, 1–16 (2019).
177. le Sage, C., Lawo, S. & Cross, B. C. S. CRISPR: A Screener’s Guide. *SLAS Discovery* **25**, 233–240 (2020).
178. Bock, C. *et al.* High-content CRISPR screening. *Nature Reviews Methods Primers* **2022** 2:1 **2**, 1–23 (2022).
179. Pulido-Quetglas, C. & Johnson, R. Designing libraries for pooled CRISPR functional screens of long noncoding RNAs. *Mammalian Genome* **2021** 33:2 **33**, 312–327 (2021).
180. Radzisheskaya, A., Shlyueva, D., Müller, I. & Helin, K. Optimizing sgRNA position markedly improves the efficiency of CRISPR/dCas9-mediated transcriptional repression. *Nucleic Acids Res* **44**, e141–e141 (2016).
181. Bergadà-Pijuan, J., Pulido-Quetglas, C., Vancura, A. & Johnson, R. CASPR, an analysis pipeline for single and paired guide RNA CRISPR screens, reveals optimal target selection for long non-coding RNAs. *Bioinformatics* **36**, 1673–1680 (2020).
182. Miles, L. A., Garippa, R. J. & Poirier, J. T. Design, execution, and analysis of pooled in vitro CRISPR/Cas9 screens. *FEBS J* **283**, 3170–3180 (2016).
183. Hartenian, E. & Doench, J. G. Genetic screens and functional genomics using CRISPR/Cas9 technology. *FEBS J* **282**, 1383–1393 (2015).
184. Cuellar, T. L. *et al.* Application of CRISPR for Pooled, Vector-based Functional Genomic Screening in Mammalian Cell Lines. *Genome Editing and Engineering: From TALENs, ZFNs and CRISPRs to Molecular Surgery* 209–222 (2018) doi:10.1017/9781316756300.016.

185. Yu, X., Zhang, Y. & Chen, H. LPA receptor 1 mediates LPA-induced ovarian cancer metastasis: An in vitro and in vivo study. *BMC Cancer* **16**, 1–9 (2016).
186. Hanniford, D. *et al.* Epigenetic Silencing of CDR1as Drives IGF2BP3-Mediated Melanoma Invasion and Metastasis. *Cancer Cell* **37**, 55–70.e15 (2020).
187. Sanber, K. S. *et al.* Construction of stable packaging cell lines for clinical lentiviral vector production. *Scientific Reports 2015 5:1* **5**, 1–10 (2015).
188. Labisch, J. J., Philip Wiese, G., Barnes, K., Bollmann, F. & Pflanz, K. Infectious titer determination of lentiviral vectors using a temporal immunological real-time imaging approach. *PLoS One* **16**, e0254739 (2021).
189. Katsantoni, M. *et al.* ZARP: An automated workflow for processing of RNA-seq data. (2021) doi:10.1101/2021.11.18.469017.
190. Babraham Bioinformatics - FastQC A Quality Control tool for High Throughput Sequence Data. <https://www.bioinformatics.babraham.ac.uk/projects/fastqc/>.
191. Martin, M. Cutadapt removes adapter sequences from high-throughput sequencing reads. *EMBnet J* **17**, 10–12 (2011).
192. GitHub - zavolanlab/zpca: PCA analysis. <https://github.com/zavolanlab/zpca>.
193. Dobin, A. *et al.* STAR: ultrafast universal RNA-seq aligner. *Bioinformatics* **29**, 15–21 (2013).
194. Patro, R., Duggal, G., Love, M. I., Irizarry, R. A. & Kingsford, C. Salmon provides fast and bias-aware quantification of transcript expression. *Nature Methods 2017 14:4* **14**, 417–419 (2017).
195. Love, M. I., Huber, W. & Anders, S. Moderated estimation of fold change and dispersion for RNA-seq data with DESeq2. *Genome Biol* **15**, 1–21 (2014).
196. Wu, T. *et al.* clusterProfiler 4.0: A universal enrichment tool for interpreting omics data. *Innovation (Cambridge (Mass.))* **2**, (2021).
197. Bioconductor - enrichplot. <https://bioconductor.org/packages/release/bioc/html/enrichplot.html>.
198. Subramanian, A. *et al.* Gene set enrichment analysis: A knowledge-based approach for interpreting genome-wide expression profiles. *Proc Natl Acad Sci U S A* **102**, 15545–15550 (2005).
199. Unfried, J. P. & Ulitsky, I. Substoichiometric action of long noncoding RNAs. *Nature Cell Biology 2022 24:5* **24**, 608–615 (2022).
200. Wong, R. S. Y. Apoptosis in cancer: from pathogenesis to treatment. *J Exp Clin Cancer Res* **30**, 87 (2011).
201. Stallaert, W. *et al.* The structure of the human cell cycle. *Cell Syst* **13**, 230–240.e3 (2022).
202. Pijuan, J. *et al.* In vitro cell migration, invasion, and adhesion assays: From cell imaging to data analysis. *Front Cell Dev Biol* **7**, 449183 (2019).
203. Justus, C. R., Marie, M. A., Sanderlin, E. J. & Yang, L. V. Transwell In Vitro Cell Migration and Invasion Assays. *Methods in Molecular Biology* **2644**, 349–359 (2023).
204. Effect of long non-coding RNA PVT1 on cell proliferation and migration in melanoma. <https://www.spandidos-publications.com/10.3892/ijmm.2017.3335>.
205. Mattick, J. S. *et al.* Long non-coding RNAs: definitions, functions, challenges and recommendations. *Nat Rev Mol Cell Biol* **24**, 430–447 (2023).
206. Jiang, C. *et al.* Identifying and functionally characterizing tissue-specific and ubiquitously expressed human lncRNAs. *Oncotarget* **7**, 7120–7133 (2016).

207. Zhang, B. *et al.* The lncRNA Malat1 is dispensable for mouse development but its transcription plays a cis-regulatory role in the adult. *Cell Rep* **2**, 111–123 (2012).
208. Nakagawa, S. *et al.* Malat1 is not an essential component of nuclear speckles in mice. *RNA* **18**, 1487 (2012).
209. Abbas, T. & Dutta, A. p21 in cancer: intricate networks and multiple activities. *Nature Reviews Cancer* **9**:6, 400–414 (2009).
210. Yeh, C. H., Bellon, M. & Nicot, C. FBXW7: a critical tumor suppressor of human cancers. *Molecular Cancer* **17**:1, 1–19 (2018).
211. Alasady, M. J. & Mendillo, M. L. The Multifaceted Role of HSF1 in Tumorigenesis. *Adv Exp Med Biol* **1243**, 69–85 (2020).
212. Dai, C. & Sampson, S. B. HSF1: Guardian of Proteostasis in Cancer. *Trends Cell Biol* **26**, 17–28 (2016).
213. Śmiech, M., Leszczyński, P., Kono, H., Wardell, C. & Taniguchi, H. Emerging BRAF Mutations in Cancer Progression and Their Possible Effects on Transcriptional Networks. *Genes* **2020**, Vol. 11, Page 1342 **11**, 1342 (2020).
214. Pastwińska, J., Karaś, K., Karwaciak, I. & Ratajewski, M. Targeting EGFR in melanoma – The sea of possibilities to overcome drug resistance. *Biochimica et Biophysica Acta (BBA) - Reviews on Cancer* **1877**, 188754 (2022).
215. Hartman, M. L. & Czyz, M. MITF in melanoma: Mechanisms behind its expression and activity. *Cellular and Molecular Life Sciences* **72**, 1249–1260 (2015).
216. Ennen, M. *et al.* MITF-high and MITF-low cells and a novel subpopulation expressing genes of both cell states contribute to intra- and intertumoral heterogeneity of primary melanoma. *Clinical Cancer Research* **23**, 7097–7107 (2017).
217. Vlčková, K., Vachtenheim, J., Réda, J., Horák, P. & Ondrušová, L. Inducibly decreased MITF levels do not affect proliferation and phenotype switching but reduce differentiation of melanoma cells. *J Cell Mol Med* **22**, 2240–2251 (2018).
218. Caldwell, C. C. & Spies, M. Dynamic elements of replication protein A at the crossroads of DNA replication, recombination, and repair. *Crit Rev Biochem Mol Biol* **55**, 482–507 (2020).
219. Ghafouri-Fard, S., Khoshbakht, T., Taheri, M. & Ghanbari, M. A concise review on the role of BDNF-AS in human disorders. *Biomedicine & Pharmacotherapy* **142**, 112051 (2021).
220. Peng, W. *et al.* lncRNA GMDS-AS1 restrains lung adenocarcinoma progression via recruiting TAF15 protein to stabilize SIRT1 mRNA. <https://doi.org/10.2217/epi-2022-0432> **15**, 417–434 (2023).
221. Ye, D. *et al.* lncGMDS-AS1 promotes the tumorigenesis of colorectal cancer through HuR-STAT3/Wnt axis. *Cell Death Dis* **14**, 1–13 (2023).
222. Huang, J., Zhong, T., Li, G., Wang, S. & Qin, R. Epigenetic inhibition of lncRNA GMDS-AS1 by methyltransferase ESET promoted cell viability and metastasis of hepatocellular carcinoma. *Clinical and Translational Oncology* **25**, 1793–1804 (2023).
223. AP005901.6 expression in human. <https://www.bgee.org/gene/ENSG00000287723>.
224. Pucci, B., Kasten, M. & Giordano, A. Cell Cycle and Apoptosis. *Neoplasia* **2**, 291 (2000).
225. Plesca, D., Mazumder, S. & Almasan, A. Chapter 6 DNA Damage Response and Apoptosis. *Methods Enzymol* **446**, 107–122 (2008).
226. Van Zijl, F., Krupitza, G. & Mikulits, W. Initial steps of metastasis: Cell invasion and endothelial transmigration. *Mutation Research/Reviews in Mutation Research* **728**, 23–34 (2011).
227. Hafner, M. *et al.* CLIP and complementary methods. *Nature Reviews Methods Primers* **2021** 1:1, 1–23 (2021).

228. Wu, M. *et al.* Evaluation of the Effect of Fibroblasts on Melanoma Metastasis Using a Biomimetic Co-Culture Model. *ACS Biomater Sci Eng* **9**, 2347–2361 (2023).
229. Ghislin, S. *et al.* LFA-1 and ICAM-1 expression induced during melanoma-endothelial cell co-culture favors the transendothelial migration of melanoma cell lines in vitro. *BMC Cancer* **12**, 1–11 (2012).
230. Yao, R. W., Wang, Y. & Chen, L. L. Cellular functions of long noncoding RNAs. *Nature Cell Biology* *2019* **21**:5, 542–551 (2019).
231. Bodapati, S., Daley, T. P., Lin, X., Zou, J. & Qi, L. S. A benchmark of algorithms for the analysis of pooled CRISPR screens. *Genome Biol* **21**, 1–13 (2020).
232. Heberle, H., Meirelles, V. G., da Silva, F. R., Telles, G. P. & Minghim, R. InteractiVenn: A web-based tool for the analysis of sets through Venn diagrams. *BMC Bioinformatics* **16**, 1–7 (2015).

Eidesstattliche Versicherung (Affidavit)

Name, Vorname
(Surname, first name)

Matrikel-Nr.
(Enrolment number)

Belehrung:

Wer vorsätzlich gegen eine die Täuschung über Prüfungsleistungen betreffende Regelung einer Hochschulprüfungsordnung verstößt, handelt ordnungswidrig. Die Ordnungswidrigkeit kann mit einer Geldbuße von bis zu 50.000,00 € geahndet werden. Zuständige Verwaltungsbehörde für die Verfolgung und Ahndung von Ordnungswidrigkeiten ist der Kanzler/die Kanzlerin der Technischen Universität Dortmund. Im Falle eines mehrfachen oder sonstigen schwerwiegenden Täuschungsversuches kann der Prüfling zudem exmatrikuliert werden, § 63 Abs. 5 Hochschulgesetz NRW.

Die Abgabe einer falschen Versicherung an Eides statt ist strafbar.

Wer vorsätzlich eine falsche Versicherung an Eides statt abgibt, kann mit einer Freiheitsstrafe bis zu drei Jahren oder mit Geldstrafe bestraft werden, § 156 StGB. Die fahrlässige Abgabe einer falschen Versicherung an Eides statt kann mit einer Freiheitsstrafe bis zu einem Jahr oder Geldstrafe bestraft werden, § 161 StGB.

Die oben stehende Belehrung habe ich zur Kenntnis genommen:

Official notification:

Any person who intentionally breaches any regulation of university examination regulations relating to deception in examination performance is acting improperly. This offence can be punished with a fine of up to EUR 50,000.00. The competent administrative authority for the pursuit and prosecution of offences of this type is the chancellor of the TU Dortmund University. In the case of multiple or other serious attempts at deception, the candidate can also be unenrolled, Section 63, paragraph 5 of the Universities Act of North Rhine-Westphalia.

The submission of a false affidavit is punishable.

Any person who intentionally submits a false affidavit can be punished with a prison sentence of up to three years or a fine, Section 156 of the Criminal Code. The negligent submission of a false affidavit can be punished with a prison sentence of up to one year or a fine, Section 161 of the Criminal Code.

I have taken note of the above official notification.

Ort, Datum
(Place, date)

Unterschrift
(Signature)

Titel der Dissertation:
(Title of the thesis):

Ich versichere hiermit an Eides statt, dass ich die vorliegende Dissertation mit dem Titel selbstständig und ohne unzulässige fremde Hilfe angefertigt habe. Ich habe keine anderen als die angegebenen Quellen und Hilfsmittel benutzt sowie wörtliche und sinngemäße Zitate kenntlich gemacht.

Die Arbeit hat in gegenwärtiger oder in einer anderen Fassung weder der TU Dortmund noch einer anderen Hochschule im Zusammenhang mit einer staatlichen oder akademischen Prüfung vorgelegen.

I hereby swear that I have completed the present dissertation independently and without inadmissible external support. I have not used any sources or tools other than those indicated and have identified literal and analogous quotations.

The thesis in its current version or another version has not been presented to the TU Dortmund University or another university in connection with a state or academic examination.*

*Please be aware that solely the German version of the affidavit ("Eidesstattliche Versicherung") for the PhD thesis is the official and legally binding version.

Ort, Datum
(Place, date)

Unterschrift
(Signature)